Electro-acoustic heart interface for mapping 3D cardiac electro-mechanical coupling in Arrhythmia

Design and Fabrication of a Device for Simultaneous Recording of Electrograms and Mechanical Properties of the Atria

Cecília Molnár

Delft University of Technology

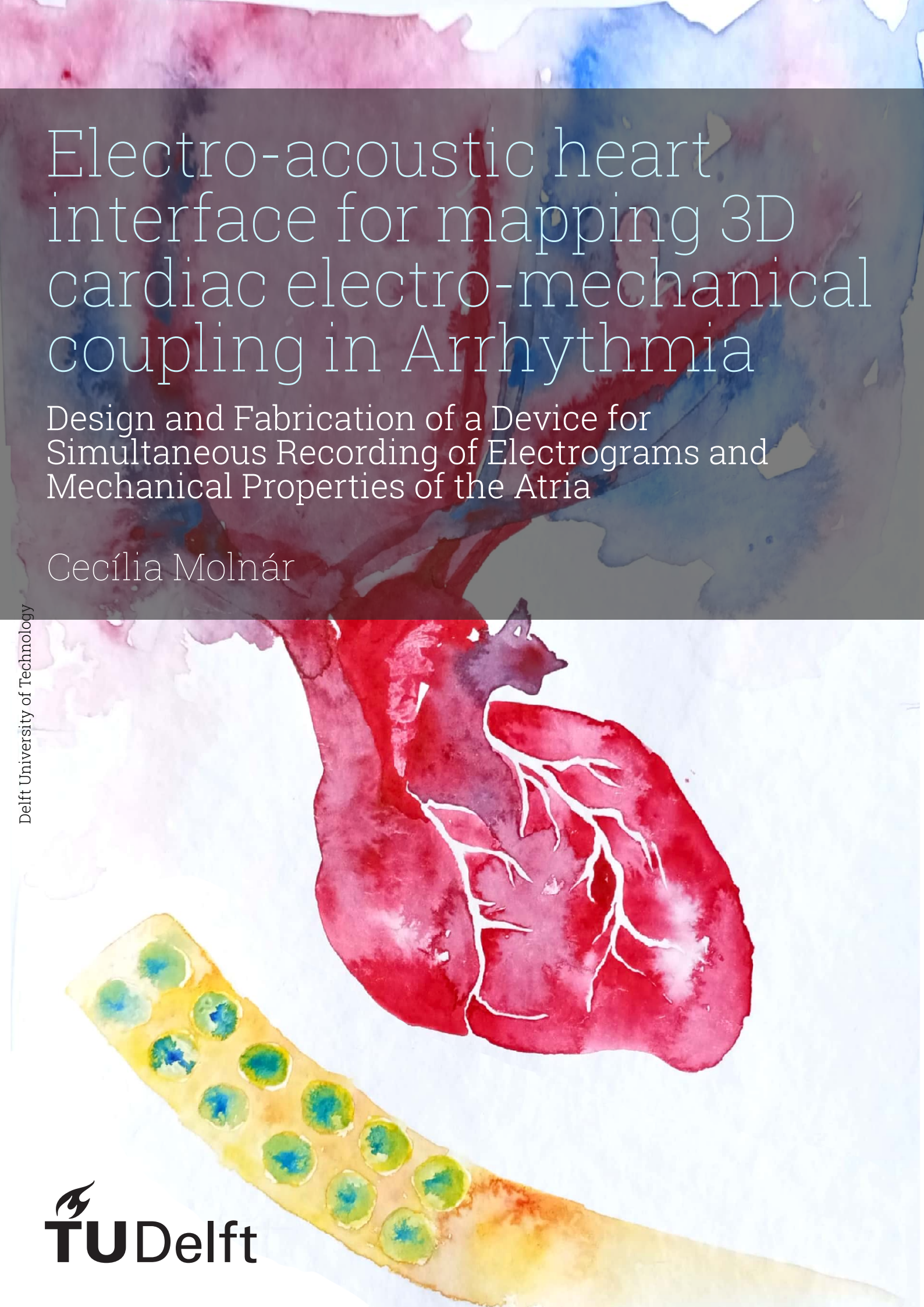

TU Delft

Electro-acoustic heart interface for mapping 3D cardiac electro-mechanical coupling in Arrhythmia

Design and Fabrication of a Device for Simultaneous Recording of Electrograms and Mechanical Properties of the Atria

by

Cecília Molnár

to obtain the degree of Master of Science
at the Delft University of Technology,
to be defended publicly on Monday August 26, 2024 at 9:00 AM.

Student number:	5690188	
Project duration:	November 1, 2023 – August 26, 2024	
Thesis committee:	Dr. T. Costa	TU Delft, supervisor
	Dr. ir. R. C. Hendriks	TU Delft, supervisor
	Dr. M. Mastrangeli	TU Delft
	Dr. M. S. van Schie	Erasmus Medical Center

Style: TU Delft Report Style, with modifications by Daan Zwaneveld

An electronic version of this thesis is available at http://repository.tudelft.nl/.

TU Delft

Preface

I would like to invite you on a journey of my master thesis, a journey full of engineering challenges and way more. I am thankful for the opportunity to work under the supervision of Tiago da Costa and Richard Hendriks. In addition to sharing their extensive knowledge, they guided me with both efficiency and thoughtfulness. I am honored to work in collaboration with Erasmus Medical Center broadening my horizons. Moreover, I would like to thank my friends and family for their support. Lastly, I want to give a special thanks to Pradnya for keeping me on track.

Cecília Molnár
Delft, August 2024

Contents

1 Introduction

1.1. Background

Cardiac arrhythmia in general refers to any abnormal activity of the heart such as abnormalities in the heart rate or heart rhythm [22, 2]. The range of cardiac arrhythmias is wide, from harmless disorders to even fatal problems such as stroke or cardiac arrest. Atrial fibrillation (AF) is a common type of arrhythmia characterized by rapid, chaotic electrical impulses in the atria (upper chambers) of the heart [1]. In AF, the atria lose their coordinated contraction, resulting in a quivering or irregular heartbeat. This irregular electrical activity can lead to inefficient pumping of blood and disrupt the normal flow of blood through the heart. AF is associated with an increased risk of blood clot formation, which can potentially cause a stroke or other complications.

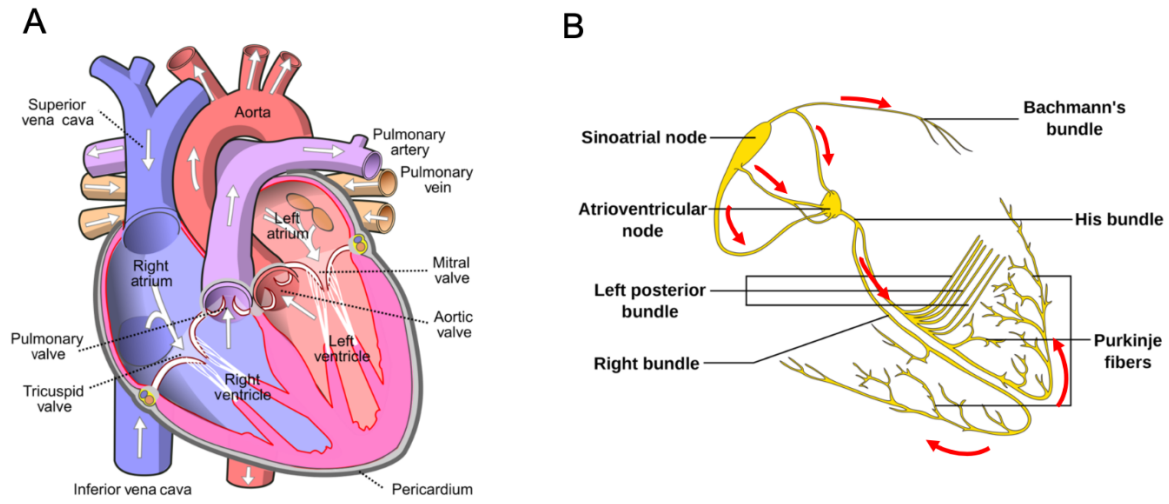

Figure 1.1: (A) The diagram of the heart as well as (B) the cardiac conduction system. The red arrows shows the direction of electrical wave propagation in normal heart [1].

In order to sufficiently treat atrial fibrillation it is important to know the underlying causes. Several studies focused on the responsible pathological mechanisms, however, the main causes are not yet completely discovered [2, 17, 8]. Some studies showed that electropathology of the atrial tissue plays an important role in the development and progression of AF [22]. Thus investigating the electrical activity of the atrial tissue and the cardiac conduction system (shown in Figure 1.1) may be beneficial in order to gain more information on heart diseases. The most common way to record this activity is by placing electrodes on a patient's body surface. The measured electrical activity of the heart over time at the electrode location is called an electrocardiogram (ECG or EKG) which is the spatial average activity of all heart cells [1]. In order to get more detailed information about the electrical activity of

the atrial tissue, the electrodes can also be placed directly on the heart tissue to record the electrical activity and wave propagation of the heart. This process can be done during open chest or open heart surgeries, or by using a catheter inside the heart. The signals obtained are called atrial or ventricular electrograms (EGMs). These signals provide more detailed information with a higher spatial resolution of the depolarization wave propagation through the heart tissue. Moreover, they are less affected by the surrounding structures of the heart than electrocardiograms, thus providing a less noisy signal.

Atrial mapping is the procedure of recording electrograms at several locations of the atrial tissue in order to create a detailed three-dimensional map of the electrical activity within the heart's atria [8]. Electrograms and atrial mapping can be helpful in localization and quantification of the degree of electropathology and may provide useful information on the stage of cardiac arrhythmia [67]. By providing a detailed map of the atrial electrical activity, atrial mapping allows physicians to identify and target the sources of arrhythmia with greater precision, improving the effectiveness of treatment and reducing the risk of complications. Epicardial mapping is a form of atrial mapping, during which the electrical activity of the epicardium is collected. The epicardial mapping is done during open heart surgeries, prior to the start of extra-corporal circulation. A temporary bipolar epicardial pacemaker wire is stitched to the right atrial free wall in order to create a reference electrode. The epicardial mapping in Erasmus Medical Center is performed during sinus rhythm and (induced) AF with a custom-made flexible 192-unipolar electrode mapping array, mounted on a custom-made spatula in order to ease the correct placing of the electrode as it provides stability and can be bent to match the atrial curvature.

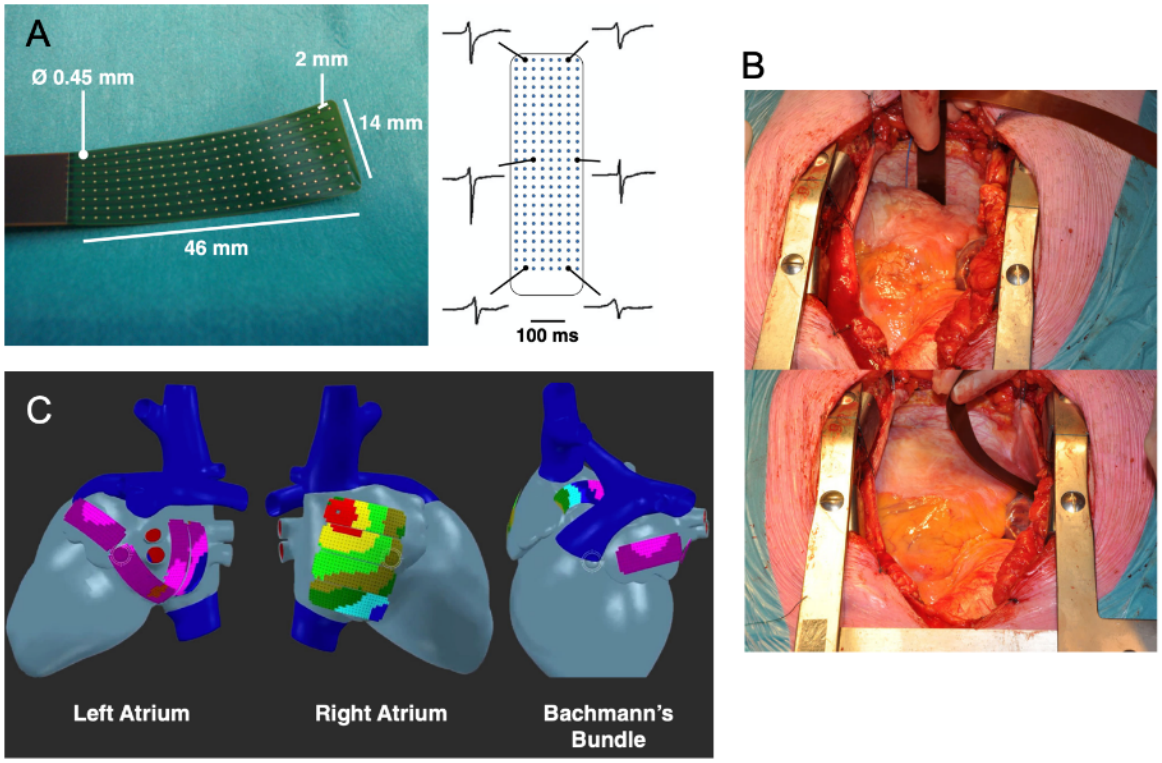

Figure 1.2: (A) Previously used electrode array and some sample electrogram recordings in Erasmus Medical Center. (B) The positioning of the electrogram on atria during open chest surgeries. (C) The 9 successive locations where the electrode array is positioned in order to achieve sufficient mapping [67].

Cardiac electro-mechanical coupling is a fundamental process in the function of the heart [19]. It refers to the tight coordination between the electrical activity of cardiac cells and the mechanical contraction of the heart muscle that results in the pumping of blood. The process occurs in the cardiac muscle cells in response to electrical stimulus. Firstly, the electrical stimulation occurs due to the electrical signal generated by the sinoatrial node, which action potential spreads rapidly throughout the heart via specialized conduction pathways, triggering the contraction of the cardiac muscle cells. Then a calcium influx occurs though the voltage gated calcium channels in the cardiomyocyte membrane,

increasing the intracellular calcium levels rapidly. Due to this, more calcium ions are released from the sarcoplasmic reticulum leading to the amplification of the calcium signal within the cell, creating a greater force of contraction. The calcium ions bind to specific proteins in the cardiomyocyte called troponin and tropomyosin, leading to a conformational change in the actin and myosin filaments of the cardiac muscle cells. This conformational change allows the actin and myosin filaments to interact, generating the force necessary for contraction. Afterwards, the intracellular calcium levels are lowered due to the calcium reuptake into the sarcoplasmic reticulum and the extrusion of calcium out of the cell, thus leading to the relaxation of the cardiac muscle cells. As the electro-mechanical coupling is a complex and tightly regulated process, the disruption of any of these steps can lead to several different cardiac disorders [22]. Therefore it may be beneficial to investigate not only the electrical activity, but the deformations of the atrial tissue [19]. Gaining more information on the behaviour of atrial tissue from patients with arrhythmia may help us understand the underlying causes of the development of such disease, thus more efficient treatments could be introduced.

Therefore, the visualization of atrial tissue would be beneficial as then the structure of the tissue would be revealed additionally to the electrograms. This would allow a more detailed understanding of the atrial tissue, which may be beneficial in further improvements regarding treatment of atrial fibrillation. The behaviour of atrial tissue can be observed with many techniques, however previous research showed that ultrasound would be the most beneficial as it can provide a detailed image of the deformations of the tissue in vivo, relatively simple and widely accessible [46, 11, 41]. Ultrasound is used in a wide range of medical applications in both diagnostic and therapeutic settings, including obstetrics and gynecology, cardiology, oncology, neurology and musculoskeletal imaging [28]. It has several benefits, which makes it a favorable choice in many medical applications. One of the biggest advantages of ultrasound is its ability to produce images in real-time, allowing doctors to see internal structures and organs as they function in real-time. Additionally, it is relatively low-cost, widely available. Moreover, it can be used to characterize the tissue as the acoustic reflectivity can imply the tissue content of the myocardium [9]. Several clinical studies have confirmed a good correlation between the amplitude of the echo and biochemically assessed collagen content [9]. Gaining more information of the content of the tissue may be beneficial in the diagnosis and treatment of arrhythmia.

However, there are several challenges that need to be overcome when a device is designed for simultaneous visualization of the atrial tissue during atrial mapping as previous research showed [41]. The upcoming guidelines should be followed based on technical limitations and considerations of the environment:

1. **Possible to integrate with Electrode Array** - As the current design of the electrode array is optimal for this application, any further imaging devices should be able to be integrated with it. According to the research of Booijink and Porte, simply placing an IVUS in the middle of the electrode array or imaging through the array is suboptimal [3, 48]. Mechanical and electrical integrity should be considered.
2. **Sufficient Resolution** - The lateral resolution of the electrode array is 2 mm (interelectrode distance being 2 mm). In order to sufficiently image the structure of the tissue, sub-millimeter axial and millimeter lateral resolution is desired.
3. **Size** - the current electrode array is 46 mm x 16 mm, with a thickness of 180 μm. Due to the limited space during mapping, it is desirable to keep the size of the device around this size.
4. **Portability** - Due to the convenience for the surgeons and staff the device should be portable. The recorder of the current electrode array is being stored on a moveable trolley. A similar setup for further development is desirable, if not better portability is achievable.
5. **Biocompatibility** - As the device is in direct contact with the tissue, the coating materials shall be biocompatible due to safety regulations [36].
6. **Compatible with Sterilization** - Currently the electrode array is sterilized with ethylene oxide [20], thus the raw materials with the new device shall be compatible with ethylene oxide and the diffusion properties should be optimized.
7. **Penetration Depth** - In case the tissue below the surface is desired to be imaged, the imaging technique must have the sufficient penetration depth. As the atrial tissue is around 5-7 mm, not high penetration depth is needed.

8. **Focus** – It is important that the focal point of the imaging device is around the area of interest for the highest resolution. As the electrode array is placed on the surface of the tissue, for future developments it would be desired that the focal point is in the range of millimeters.
9. **Conformable** - The current electrode array is highly conformable in order to ensure minimum signal loss, this feature should be preserved.
10. **Sufficient SNR** – The signal-to-noise ratio (SNR) should be as large as possible. The SNR of the electrode array is between 10 dB and 34 dB as the atrial signals are in the range of 1 - 15 mV and the noise levels are 0.3 mV. The minimal SNR for any sensing equipment is 5 dB, however the higher the better.
11. **Satisfies the Safety Regulations** - There are several regulations that should be considered, such as the medical electronic device (IEC 60601, [44]) and the local regulations [36].
12. **Mechanically Robust** - Mechanical robustness should be ensured due to possible deformations.

1.2. Problem Statement

Recording elecrocardiograms on the surface of the heart is a special environment with unique challenges that limit the usage of other additional devices. Thus the recording of any mechanical activity of atrial tissue simultaneously with atrial mapping is a challenging process, which has only vaguely been described in the literature before. According to the current state-of-art, there has not been any device reported, which has been designed to simultaneously record electrical and mechanical activity of the same area of the heart tissue in vivo. Therefore it would be beneficial to explore the design process of such a device and create a prototype.

1.3. Goals and Objectives

The primary objective of this thesis is to design, fabricate, and evaluate a prototype device where an ultrasound transducer and an electrode array are integrated. This prototype is envisioned for in vivo application during open heart surgeries in order to further enhance the data collection of the atrial tissue, thus allowing for further research on cardiac arrhythmia. Such a concept has not been commercialized and remains sparsely studied in current research. The key design objective is to integrate an ultrasound transducer and an electrode array in a way that the data loss and cross-talk are minimal. Through proper algorithm implementation, the device will be able to simultaneously record the electrical and mechanical activity of the same area of the heart tissue. This research will analyze the design and optimization of the conformal ultrasound transducers for cardiac applications, and the means of integration with electrode arrays. Emphasis will be placed on addressing the optimal design parameters and the final design.

A prototype has been designed, fabricated, and tested. This prototype consists of two parts, a device with ultrasound transducers and a flexible electrode array. Considering the limitations of the environment and the purpose of the device, 1-3 piezocomposite rings have been chosen as ultrasound transducers, of which 12 have been placed on a two-layer flexible PCB. The electrode array consists of 36 electrodes, of which 12 have a special cutout to allow better transmission of the ultrasound waves. The two parts have been mounted together, forming the final device.

In order to investigate the performance of the device several experiments have been conducted. The pressure field created by the transducers was analyzed, with and without the electrode array to see how the electrode array affects the performance of the transducers. Moreover, the impedance of the electrode array was measured with and without the ultrasound transducers, in order to see how it affects the performance of the electrode array.

1.4. Thesis Structure

Chapter 1 presents the background and relevancy of the current work. It outlines the problem statement and the goals and objectives of the study.

Chapter 2 explores the theoretical background of the proposed device, namely electrode arrays, and ultrasound transducers.

Chapter 3 presents previous works where the subject of this thesis was studied previously. Moreover, it provides an overview of recent advances in conformal ultrasound arrays for cardiac applications.

Chapter 4 presents the different phases of device development, comparing the several concepts, and analyzing the simulations conducted in order to retrieve optimal design parameters. The final design is presented in great detail, along with a detailed explanation of intended usage. Furthermore, the assembly procedure is explored detailing the steps, struggles and recommendations.

Chapter 5 outlines the characterization process for both components of the final device. The impedance of the ultrasound transducer and the electrode array has been analyzed individually. The pressure fields of the ultrasound transducer have been obtained with and without the presence of the electrode array. Preliminary pulse-echo measurements have been conducted of the ultrasound transducer with the electrode array.

Chapter 6 discusses the relevance, the results, and the limitations of this work.

Chapter 7 concludes by summarizing the findings of this study. Potential points of improvement of the current work are suggested as future work.

2

Theoretical Background

2.1. Electrode Arrays

2.1.1. Basics of Electrode Arrays

In principle, multi-electrode Arrays (MEAs) are two-dimensional arrangements of voltage probes designed for extracellular stimulation and monitoring of electrical activity of electrogenic cells [63]. These cells can be either isolated or in muscle, neuronal, or cardiac tissue. To analyze the performance and the transfer properties of the probes the entire system has to be considered. The entire system consists of (1) the cellular signal sources and the tissue allowing the spread of ionic current, (2) the contact between the cells and the electrodes and the contact between the tissue and the electrodes, (3) the substrate and the embedded microelectrodes and (4) the external hardware consisting of simulators and filter amplifiers connected to the electrodes. As in this study, the focus is on cardiac tissue recording, this process will be detailed further. The electrical activity of the tissue spreads within the cellular compartments from cells-to-cells via synaptic connections, which spread is always accompanied by the flow of ionic current through the extracellular fluid. The current flow indicates an extracellular voltage gradient that varies in time and space according to the time course of the activity of the tissue as well as the spatial distribution and orientation of the cells. This voltage gradient can be measured with the recording electrodes using read-out circuits. The measurement setup of extracellular recording of a single cell activity is shown in Figure 2.1. The cell body is partially covering the electrode surface, and the free electrode area is in contact with the external saline and connected to the ground. The amplifier connected to the conducting lane records the sum of the potentials at the surface of the free electrode and the surface of the electrode covered by the membrane.

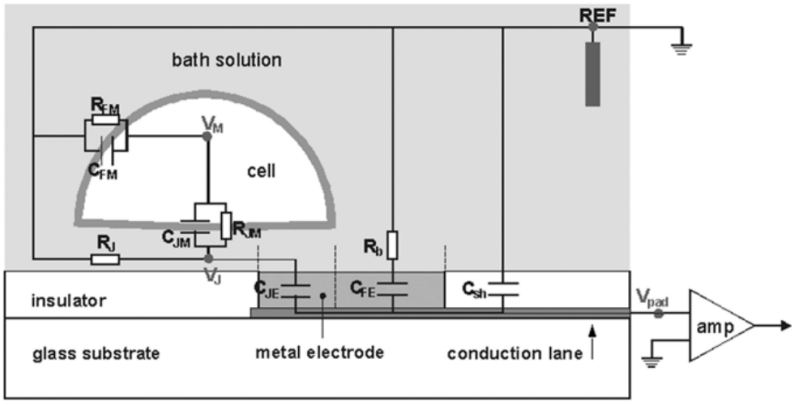

Figure 2.1: Working principle of an extracellular recording of single-cell activity with planar electrodes. Given the electrical circuit, the voltage picked up by the amplifier between the contact pads and the reference electrode can be calculated [63].

Generally, the MEAs have several advantages which make them favorable for several applications in the medical field [59]. Firstly, they have a sufficiently high spatial resolution as they enable the simultaneous recording or stimulating of electrical signals from multiple sites, providing detailed spatial information about the activity within tissues or cell cultures. Additionally, the stimulation recording and stimulation of electrical activity facilitates high-throughput data acquisition and analysis. Secondly, they are easily adaptable to various applications in the field of researching different excitable tissues. Moreover, they are suitable for long-term recordings of electrical activity, allowing for the study of dynamic processes and the assessment of chronic effects of drugs or interventions. When micro-electrode arrays were first developed in the early 1970s, mainly Au was used for the electrode material [63]. Au planar electrodes have a relatively high impedance in the range of a few hundred ohms to several kilohms, thus the common practice was to platinize the electrodes in order to reduce the impedance R_o in the range of a few ohms, thus improving the SNR. However, due to the degradation of Pt-layer, this type of electrode was not stable in the long term, therefore new technologies were introduced. Nowadays the standard electrode is made of TiN by plasma-enhanced chemical vapor deposition with the insulator layer being silicon nitride [63]. The surface area of the TiN electrode created by this process is high, which leads to increased capacitance, thus providing a reduced noise level. In general, a noise level less than $\pm 10\ \mu V$ can be observed, measured with a $30 \mu m$ MEA electrode at a cut-off frequency of 1 Hz to 3 kHz, with a sampling rate of 25 kHz [63]. However, more specific MEA designs exist for different applications.

The standard line of MEA consists of a pattern of 8 x 8 or 6 x 10 electrodes and is generally used for measuring acute brain slices, single cell cultures, and organotypic preparations [63]. Thin MEAs are only $180 \mu m$ thick and they are constructed using cover slip glass in order to allow microscopy imaging through it [10]. Another design, the 2 x 30 MEA aims to study the local responses at a high spatial resolution in parallel with studying the functional connectivity of two organotypic slices placed next to each other [52]. These technologies are mostly used in vitro measurement, for example, to record multi-unit activity of retina slices. In the case of precise measurement of conduction velocity or synaptic delays over long distances, spatial resolution is especially important. Hence high-density MEAs were developed in which 256 electrodes in a square grid pattern utilize a $100 \mu m$ interelectrode distance in the center and $200 \mu m$ in the periphery, yielding a total recording area of about 2.8 × 2.8 mm [37]. However, all of the previously presented designs are mostly used for in vitro measurements.

2.1.2. Flexible Electrode Arrays

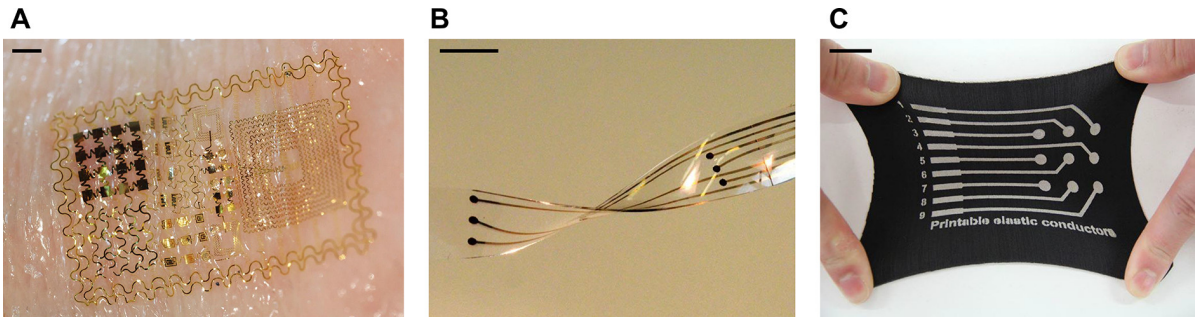

Figure 2.2: Recent flexible multielectrode arrays presented in the review of Lee et al. [26]. (A) Epidermal electronics with good adhesion to human skin. Scale bar: 1 mm. (B) Electronic dura meter with biocompatible substrate. Scale bar: 3 mm. (C) Electronic textile with stretchability. Scale bar: 25 mm.

To perform measurements in vivo and semi-intact preparations a different approach is needed for multi-channel recordings. The attachment between the tissue and the array has to be tight in order to maximize SNR. High conformity can be achieved with flexible MEAs as the recent development in thin film electronics allows the fabrication of ultrathin substrates, biocompatible substrates and/or stretchable textiles (Figure 2.2) [26, 45]. The flexible MEA can be combined with an active matrix to minimize the number of wires and to increase SNR [27]. In order to perform atrial mapping, a flexible MEA is needed to ensure the attachment between the tissue and the device, thus the flexible structures will be detailed further.

The simplest flexible MEA consists of a patterned electrode and an electrical passivation layer which

exposes only the target area [63]. It is favorable to use in many cases as it is easy to fabricate. The voltage measurement of such structure happens between the sensing pad and the inactive part of the living cell as a reference. The functionality of a passive MEA can be increased by adding active components in each cell of the array, creating an active array [26, 27]. The voltage measurement in such an active array is generally performed by a transistor. The bioelectric signals at the gate electrode of the transistor are amplified to the current modulation between the source and the drain. Combining two transistors in each cell (one for sensing and one for multiplexing) an active matrix can be created to reduce the number of wires, thus increasing the spatial resolution. Moreover, by using transistors as sensors, the active MEAs achieved scalable design and signal amplification. Additionally, low power consumption and low crosstalk can be achieved by using specific multiple-addressing transistors.

In order to be applicable for medical applications, active flexible meas have to possess several attributes, such as high spatiotemporal resolution, high conformability, flexibility, transparency, and biocompatibility [26]. The conformal contact between the tissue and the device is important to achieve sufficiently high SNR. This can be ensured by further increasing the flexibility of the device by decreasing the thickness of the entire device. In some cases, optical transparency is required to perform microscopy or modulation of ion imaging. However, for atrial mapping, this is not a criterion. Furthermore, biocompatibility is essential for all devices that have to be in contact with the body for a long period. As the atrial mapping occurs during open-heart surgeries and the device is not implanted in the body, this requirement does not have to be fulfilled.

2.1.3. Some Applications of Electrode Arrays

Considering the several advantages of MEAs, they are favorable in many application areas [59]. Firstly, in neurophysiology they are used to research the electrical activity of neurons and neural networks as they enable simultaneous recordings from multiple neurons, providing insights into neural communication, synaptic plasticity, and brain function with possible developments in the field of brain-computer interfaces and neural prosthetics [13, 54, 61]. Secondly, they are widely used in drug screening and toxicity testing as they are useful for researching the effects of drugs on electrical activity [60, 23]. By measuring changes in electrical signals from cultured cells or tissue slices, MEAs can help identify potential cardiotoxicity or neurotoxicity of drug candidates. Furthermore, they play a crucial role in tissue engineering as they aid the development of functionally engineered tissues by monitoring cell behavior and optimizing tissue growth and integration [29]. Lastly, they are widely used in the field of cardiac electrophysiology as they are employed in cardiac research to investigate the electrical behavior of cardiac cells and tissue [11, 34]. They allow for the study of arrhythmias, drug effects on the heart, and tissue engineering approaches for regenerative medicine. MEAs can provide valuable data on action potentials, conduction velocity, and synchronization of cardiac cells.

2.1.4. Electrode Array of Erasmus Medical Center for Electrophysiological Mapping

One of the research methods of electrophysiology is the mapping of the atria. During atrial mapping, the electrical signals of the heart are measured directly on the surface of the heart during open-heart surgeries creating electrocardiograms. Atrial mapping aims to retrieve more information on unhealthy heart tissue, thus facilitating the unraveling of the mysteries of atrial fibrillation mechanisms, which can have a significant effect on strategies for the prevention or therapy of AF. The atrial mapping is done during open heart surgeries, before the start of extra-corporal circulation. A temporary bipolar epicardial pacemaker wire is stitched to the right atrial free wall in order to create a reference electrode. The epicardial mapping is performed during sinus rhythm and (induced) AF with a custom-made flexible 192-unipolar electrode mapping array, mounted on a custom-made spatula to ease the correct placing of the electrode as it provides stability and can be bent to match the atrial curvature. Recordings of real-time epicardial electrograms from Bachmann's bundle are used to confirm the atrial capture. The mapping is conducted sequentially along several imaginary lines between anatomical borders in order to cover the entire left and right atria. The mapping array is shifted along these imaginary lines with a fixed orientation. The surgeon visually tries to avoid the omission of areas, however this comes with the cost of possible overlaps between successive mapping sites. The mapping lines and the correct positioning of the 192-electrode array are presented in Figure 1.2. The array is held in place with light manual pressure exerted by the surgeon. The mean duration of the entire mapping procedure including preparation time is approximately 10 minutes [67]. The risk of complication related to the

mapping procedure during or after the cardiac surgery is minimal [67].

The epicardial electrograms are recorded with a thin custom-made flexible 8 x 24 unipolar electrode mapping array with the size of 46 mm x 16 mm shown in Figures 2.3 and 2.4. The array consists of an electroless nickel immersion gold-plated electrode array, which is mounted on a thin flexible copper-clad polyimide laminate (kapton) and overlay composite film. Sterilization is performed by an outside party with ethylene oxide, according to the NEN-EN-ISO 11135:2014 standard [20]. The sterilized array is connected to the 3-meter-long, shielded flat cables via the connectors shown in Figure 2.4, which is delivered to the surgeon in a sterile sack. The flat cables are connected to a battery-driven, custom computerized mapping system with 256 channels and $\pm 8mV$ input range, 16-bit ADC, filter between 0.5 Hz and 400 Hz. The Recorder is connected to a laptop computer via USB 2.0, where all the recorded electrograms are visualized real-time with a custom-made software. Three channels are designated to display the surface ECG, reference signals, and a calibration signal of 1 mV and 1000 ms pulse-width. The sampling rate is 1 kHz.

Figure 2.3: Currently used electrode array for atrial mapping in Erasmus MEdical Center.

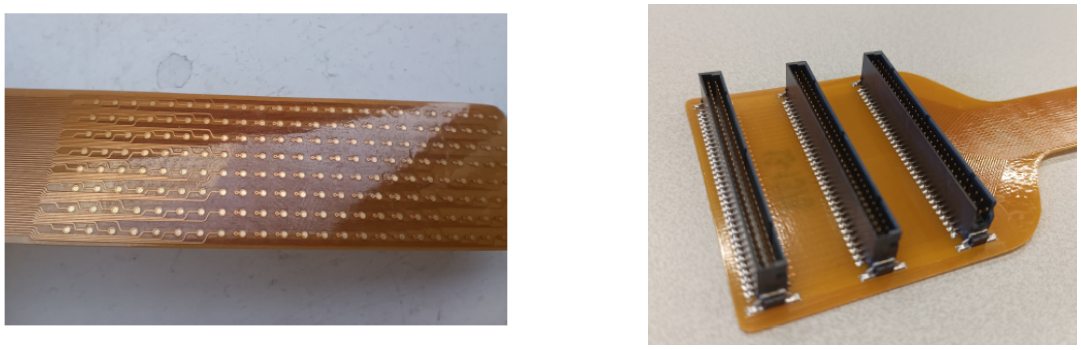

(a) **(b)**

Figure 2.4: (a) A close-up and (b) the connectors of the currently used electrode array for atrial mapping in Erasmus Medical Center.

2.2. Ultrasound Transducers

2.2.1. Basics of Ultrasound

Sound waves are the mechanical vibrations of an object and a form of energy propagation. Sound frequency, measured in hertz (Hz), refers to the number of vibrations per second. The human ear can perceive sound waves between 20Hz and 20kHz. Frequencies above 20kHz are classified as ultrasonic waves.

Ultrasound has distinct advantages in medicine due to its higher energy levels, frequencies, and shorter wavelengths, which result in minimal diffraction. This allows ultrasound to travel in straight lines with good beam formation and directionality over a distance. Sound waves can be described by their frequency, wavelength, and wave speed according to the following equation.

$$f = \frac{v}{\lambda}, \tag{2.1}$$

where f is frequency in MHz, v is the speed of sound in the medium, λ is the wavelength. In medical ultrasound, wavelength determines the image's resolution, while frequency affects the depth of tissue that can be imaged as the attenuation of the waves depends on the frequency. The attenuation can be calculated using the following equation.

$$A = \alpha \cdot l \cdot f, \tag{2.2}$$

where A is the attenuation in dB, α is the attenuation coefficient of the material in $\frac{dB}{MHz \cdot cm}$, l is the travelled distance of the sound waves in cm.

One of the important physical characteristics relating to the propagation of ultrasound is the acoustic impedance of the medium in which the sound wave travels. It is given with the following equation.

$$Z = \frac{p}{U}, \tag{2.3}$$

where Z is acoustic impedance in MRayl, p is the acoustic pressure of the wave in Pa, and U is the volume velocity in $\frac{m}{s}$. In general, different media in which the speed of sound is different has different acoustic impedance. Therefore, when the sound wave travels through different media it encounters impedance mismatch, which results in some reflections of the wave leading to energy loss. For this reason, the use of matching layer is advised, which matching layer has the acoustic impedance with the geometrical mean of the two neighboring media, and a thickness of $\lambda/4$, which ensures that the energy loss and the reflections will be minimalized when the ultrasound waves propagate through the other media.

An important principle in ultrasound theory is the pulse-echo principle. As pulse waves propagate through body tissues with varying acoustic impedances, some parts of the waves are reflected back to the transducer as echo signals, while others continue to penetrate deeper into the tissue. When these returning echo signals strike the transducer, deformation is induced in the piezoelectric material, generating electrical signals. These signals are then processed and can be combined to produce an image. The transducer thus functions dually as a transmitter, emitting pulse waves, and as a receiver, detecting the returning echoes. The pulse-echo principle is employed to achieve the necessary depth resolution for diagnostic imaging. By precisely measuring the time interval between the emission of a pulse and the reception of its corresponding echo, the imaging system can calculate the distance between the transducer and the structure that generated the echo.

Moreover, it is important to consider the axial resolution of the ultrasound waves as it determines the ability to discern two separate objects with are longitudinally adjacent to each other in the ultrasound image. It is defined by the following equation:

$$r_{ax} = \frac{1}{2} \cdot l_{sp}, \tag{2.4}$$

where r_{ax} is the axial resolution in mm, l_{sp} is the spatial pulse length in mm. The latter is determined by the product of the wavelength of the wave and the number of cycles (periods) within a pulse.

2.2.2. Piezoelectric Transducer

The core element of the ultrasound system is the ultrasound transducer, which is able to convert mechanical energy into electrical energy and vice versa [30]. In order to produce a piezoelectric transducer piezoelectric materials are used, which contain lead-content materials and lead-free materials [30]. The performance of the transducer is determined by the material properties, such as the piezoelectric coefficient (d_{33}), dielectric properties, electromechanical coupling coefficient (k_t), and acoustic impedance (Z). The piezoelectric coefficient quantifies the volume change when a piezoelectric material is subject to an electric field. The dielectric properties determine the storage and dissipation of electric and magnetic energy in insulators. The electromechanical coupling coefficient is a numerical measure of the conversion efficiency between electrical and acoustic energy in piezoelectric materials.

The most commonly used lead-content piezoelectric material is Lead Zirconate Titanate (PZT), which has low mechanical losses and great dielectric properties [30]. It is flexible, thus it is applicable for high-conformity applications. Another lead-content piezoelectric material is Relaxor-PT, which has low dielectric loss, and great performance in dielectric permittivity, electromechanical coupling coefficient, and piezoelectric coefficient [30]. There are several lead-free piezoelectric ceramics, such as (K,Na)NbO3 (KNN) with stable piezoelectric properties and high Curie temperature, or BaTiO3 (BT) and (Bi, Na)TiO3 (NBT) with stable electrical properties, good electromechanical coupling, low dielectric loss, but low piezoelectric coefficient, which limits its application areas [30]. Moreover, ZnO is a commonly used piezoelectric ceramic due to its ultrahigh frequency, excellent uniformity on a substrate, low density, high flexibility, and low acoustic impedance [30]. Organic piezoelectric transducers

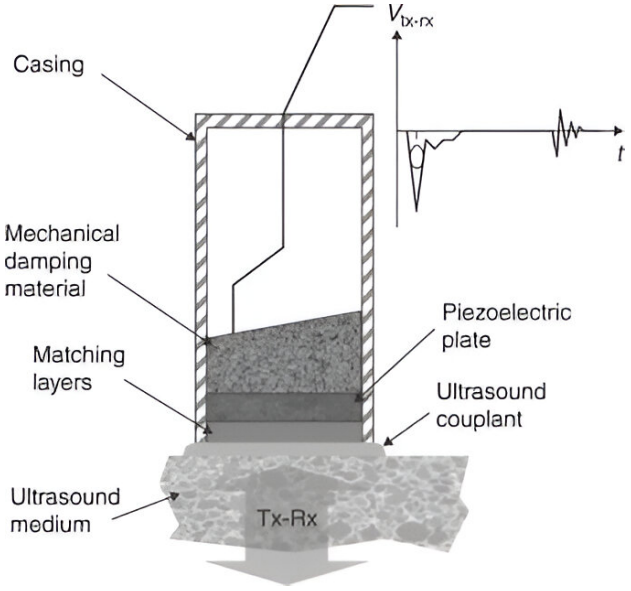

Figure 2.5: A single element transducer and its structure [7].

are also researched, for example, polyvinylidene difluoride (PVDF) is a beneficial ceramic as its low acoustic impedance is matched to tissues, and has good broadband receiving performance even on a smaller area [30]. Moreover, recently piezoelectric composites have been researched as they have enhanced electromechanical coupling, which allows the broadening of the bandwidth, thus improving the SNR. Piezoelectric composites generally have an acoustic impedance closer to human tissue, thus the matching layer can be eliminated.

Usually, there is a significant mismatch in acoustic impedance between the piezoelectric transducer (around $Z = 30MRayl$) and the media to be imaged (around $Z = 1.6MRayl$ for tissue), thus in order to minimize energy loss the use of a matching layer is needed with the acoustic impedance of the geometrical mean of the two media to be matched [7]. Commonly used materials are polymers, glasses, ceramics, and metals, lately composites of gold and silver -polymers have been thoroughly researched [51]. Choosing the thickness of the matching layer to be $\frac{\lambda}{4}$ ensures that the waves that were reflected remain in phase. Furthermore, a backing layer is used at the non-imaging side of the transducer in order to prevent the backward emitted sound waves to echo and cause back ringing into the transducer. Frequently used materials are alumina or tungsten-loaded epoxy [42].

Generally, ultrasound transducers have two main types: single-element transducer and array (linear, circular, and 2D array) shown in Figure 2.6 [30]. The structure of the single-element transducer is shown in Figure 2.5. Compared to the simpler single-element transducer, the arrays are capable of dynamic focusing, high frame rate, and real-time measurements. The 2D arrangement in the array enables various imaging and sensing techniques, such as beamforming and spatial focusing. By controlling the timing and amplitude of electrical signals applied to each element, the array can steer and focus the ultrasound beam in different directions, allowing for real-time imaging with high spatial resolution and sensitivity. The conventionally fabricated bulk piezoelectric transducers are often designed as solid structures made from the formerly mentioned piezoelectric materials, usually in the form of plates, discs, or beams. Electrodes are placed on the surfaces of the material to apply electric fields and measure the generated charges. Bulk piezoelectric transducers are found in most biomedical applications due to their high power handling capacity, simplicity, wide frequency range, high sensitivity, and great reliability [47]. Their high SNR is due to the high-quality piezoelectric materials that exhibit strong and consistent piezoelectric properties [47]. As they can be constructed with larger physical dimensions, larger apertures, and improved beamforming capabilities are possible. This can result in better lateral resolution and the ability to focus and steer ultrasound beams electronically. Moreover, they are generally more robust and less susceptible to mechanical damage or wear compared to delicate microfabricated structures used in MEMS transducers. However, they have some limitations as well, as they are not able to be miniaturized, thus not allowing the integration of electronic circuits.

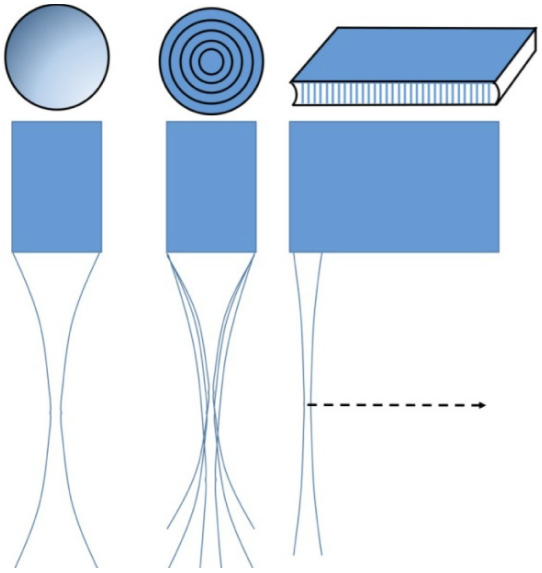

Figure 2.6: Different types of ultrasound transducers [56].

An ultrasound transducer can be either focused or unfocused, depending on whether the ultrasound waves are focused or not. For single-element transducers, focusing is typically achieved using acoustic lenses. Focused transducers are generally preferred for imaging applications as they produce pulses with small diameters, which gives better visibility of image details. Specifically, the best detail and therefore resolution is obtained for structures within the focal zone. An unfocused ultrasound transducer generates a beam with two distinct regions: the near field (Fresnel zone) and the far field (Fraunhofer zone). In the near field, the beam maintains a relatively constant diameter, which is useful for imaging. The beam diameter is determined by the transducer's diameter, while the length of the near field ($l_{near\ field}$ depends on both the transducer's diameter (D) and the wavelength (λ) of the ultrasound beam, as described by the following expression:

$$l_{near\ field} = \frac{D^2}{4\lambda} \tag{2.5}$$

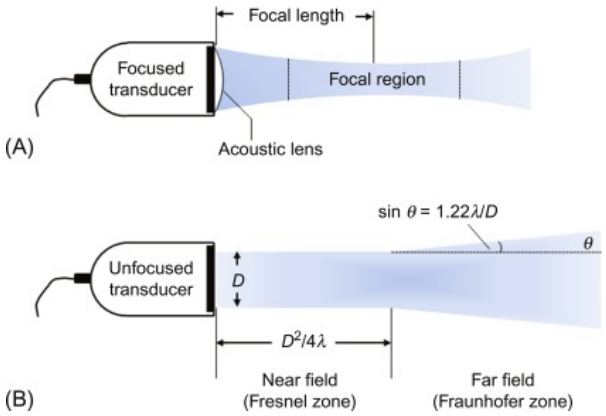

Figure 2.7: Focused and unfocused ultrasound transducer [55].

Since wavelength is inversely related to frequency, the near field length increases with frequency for a given transducer size. In contrast, the far field is characterized by beam divergence, causing the ultrasound pulses to expand in diameter while reducing the intensity along the central axis. Due to the inverse relationship between wavelength and frequency, higher ultrasound frequencies, corresponding to shorter wavelengths result in less beam divergence. This is a significant advantage of using higher frequencies, as they produce less blur and better image detail. Although ultrasound beams are often

idealized in theory, in practice, unfocused transducers can produce beams with side lobes—secondary beams that spread out around the primary beam. These side lobes can generate echoes, potentially introducing artifacts into the image and compromising its quality.

In order to achieve high conformity during direct ultrasound imaging of the heart, ultrasound transducers mounted on a flexible substrate are preferred. High conformity reduces the signal loss during monitoring, thus the SNR is improved. Recently several devices have been introduced with such properties [66]. The technology of piezoelectric ultrasound transducers on flexible substrate demonstrated to have the most benefits for biomedical applications [58]. Recently several fabrication strategies have employed rigid bulk piezoelectric materials and packaged them onto flexible substrates or assemblies. Fabrication methods have included attaching bulk piezoelectrics onto flexible printed circuits [49], transferring bulk piezoelectrics from polydimethylsiloxane (PDMS) templates to flexible substrates with adhesive films [50], and mounting transducers onto spring loaded probe matrices [68]. Some of these bulk piezoelectric fabrication strategies have yielded fully-packaged flexible devices, but with limitations in uniformity and scalability [57]. Recently, transducers made out of flexible substrates are being researched, as they provide high conformity and the materials used are lead-free [43].

2.2.3. Some Application of Ultrasound

Ultrasound has several applications in the medical field, from diagnostic to therapy. The most common application is diagnostic imaging, including obstetrics and gynecology, cardiology, oncology, neurology, and musculoskeletal imaging [28]. For example, in obstetrics and gynecology, it is used for prenatal imaging to monitor fetal development, detect abnormalities, and determine the position of the fetus [15]. Moreover, it is widely used in cardiology to evaluate the structure and function of the heart, including the assessment of heart valves, blood flow, and the overall cardiac performance [46]. Furthermore, it is favorable for image-guided procedures to get real-time information during specific medical procedures such as needle insertions, biopsies, and catheter placements as it allows the surgeons to achieve higher accuracy and safety [35]. For therapeutic purposes, it is widely used for tumor ablation, drainage of fluid collections, or guided injections of medications, offering a minimally invasive approach with precise targeting [5].

3

Literature Review

Considering the limitations of the working environment as detailed in Chapter 1, the preferred method of simultaneously measuring the mechanical and electrical properties of the heart in vivo is using piezoelectric transducers mounted on flexible substrate and electrode arrays, as previously presented in Chapter 2. Therefore a literature review has been conducted on previous works integrating the two systems, and recent development of conformal ultrasound transducers on cardiac applications.

3.1. Previous Works on Integration of Cardiac Electrodes and Ultrasound Transducers

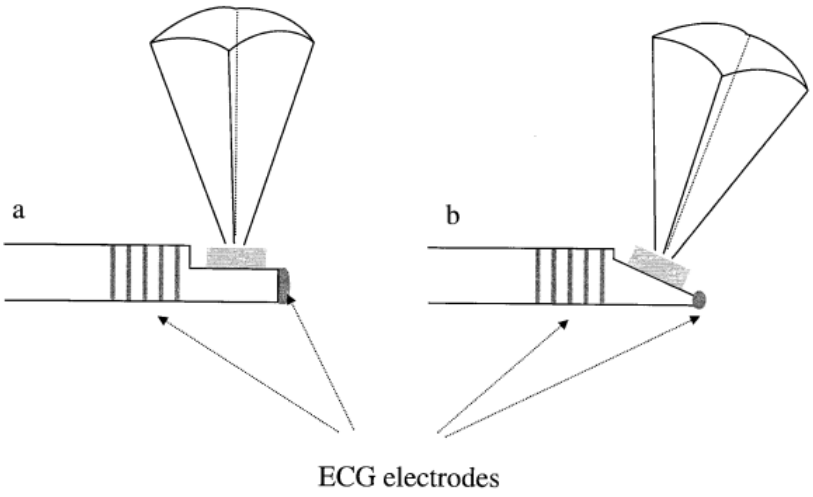

Figure 3.1: Schematic showing the two transducer orientations designed by [32]. (A) Side-scanning and (B) beveled with the five ring electrodes and the tip electrode on each.

Previously few studies from a group examined integrating ultrasound transducers and ECG electrodes in the same probe. [32, 33]. Light et al. designed a catheter-mounted 2-D array transducer in order to obtain real-time 3-D intracardiac ultrasound images [32]. They have constructed a device containing several transducers with 64 channels inside a 12 French catheter lumen operating at 5 MHz and six electrodes to acquire simultaneous electrocardiograms. Two configurations have been designed for the device, a side-scanning and a beveled concerning the long axis of the catheter lumen. Both configurations are presented in Figure 3.1, with the tip ECG electrode and the five-ring electrodes. All of their transducers were built on a 6-layer polyimide substrate with thin film patterning. An open-chest sheep subject has been used to study the utility of the device in vivo intracardiac 3-D scanning. It has been demonstrated that the device was able to image the major anatomical landmarks of the heart

while collecting electrocardiogram signals from the tissue, showing that the two technologies can be integrated. The integration did not seem to have a significant effect on the quality of the acquired data from either the electrodes or the ultrasound transducer. The limitation of the device is that the electric signals and the mechanical properties of the heart are not collected from the same location. Moreover, the field of view of the electrodes is relatively low as the device contains five ECG electrodes.

3.2. Conformal Ultrasound Arrays for Cardiac Applications

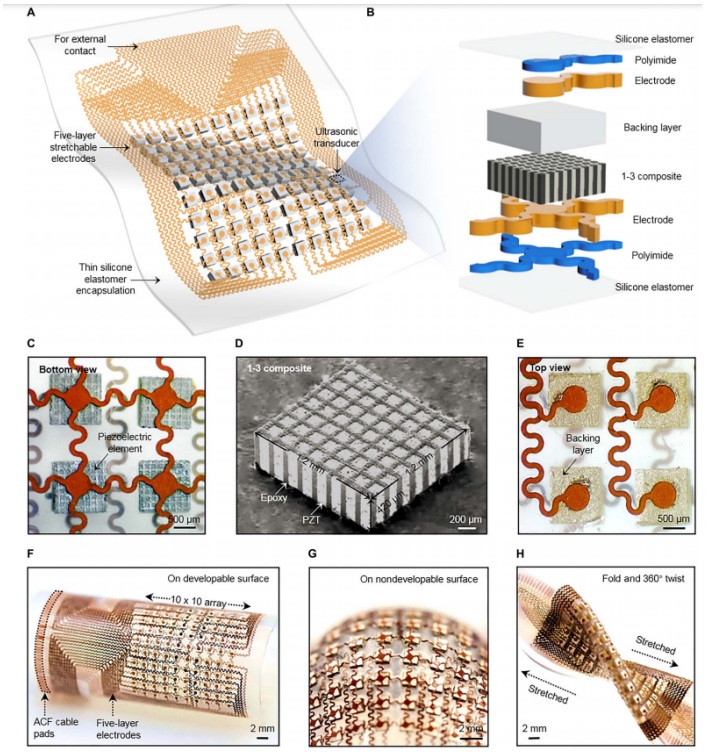

Figure 3.2: Schematics and design of the stretchable ultrasonic transducer array designed by [18]. (A) Schematics showing the device structure. (B) Exploded view to illustrate each component in an element. (C) The optical image (bottom view) of four elements, shows the morphology of the piezoelectric material and bottom electrodes. (D) The tilted scanning electron microscopy image of a 1-3 piezoelectric composite. (E) The optical image (top view) of four elements, shows the morphology of the backing layer and top electrodes. (F)-(H) shows flexibility in different directions.

Recently several studies were conducted in the field of conformal ultrasound transducers for cardiac imaging [18, 16, 64, 65, 39]. Hu et al. designed and fabricated a stretchable conformal ultrasound robe that can detect nonplanar complex surfaces [18]. The probe consists of a 10 x 10 array of piezoelectric transducers with an island-bridge layout multilayer electrode array (Figure 3.2). Their innovative structure featured islands, each with a rigid element, and undulating bridges that unfold to accommodate external strain while maintaining limited strain in the components. The matrix was locally rigid but globally soft, and each element in the array was individually controllable. The flexible probe could reconstruct the morphology of the target through multisection images. The frequency of the device was 3.5 MHz with a fractional bandwidth of 47%. The substrate and superstrate consisted of silicone elastomer thin films, providing a highly compliant platform for various building blocks. Piezoelectric 1-3 composites were fabricated by the group to serve as transducer materials, offering superior electromechanical coupling coefficients. An Ag-epoxy composite backing layer was used to dampen piezoelectric vibrations, improving image resolution. The design included a small pitch between transducer elements for artifact reduction and sufficient space for stretchability. The biggest challenge in the design was the need for numerous electrical connections in the 10 × 10 array. Thus, a multilayered electrode design based on the transfer printing method was presented to tackle this problem. Accord-

ing to their findings, the array showed a high electromechanical coupling coefficient ($k_{eff} \sim 0.60$), a high signal-to-noise ratio ($SNR \sim 20.28dB$), a wide bandwidth ($\sim 47.11\%$), a negligible cross-talk level between adjacent elements ($\sim -70dB$), and a high spatial resolution ($\sim 610mm$) at different depths. The "island-bridge" layout offered biaxial stretchability of more than 50% with minimal impact on the transducer performance, which allowed the device to work on nonplanar complex surfaces. With these unique properties, the device could obtain three-dimensional (3D) images of complex defects under flat, concave, and convex surfaces.

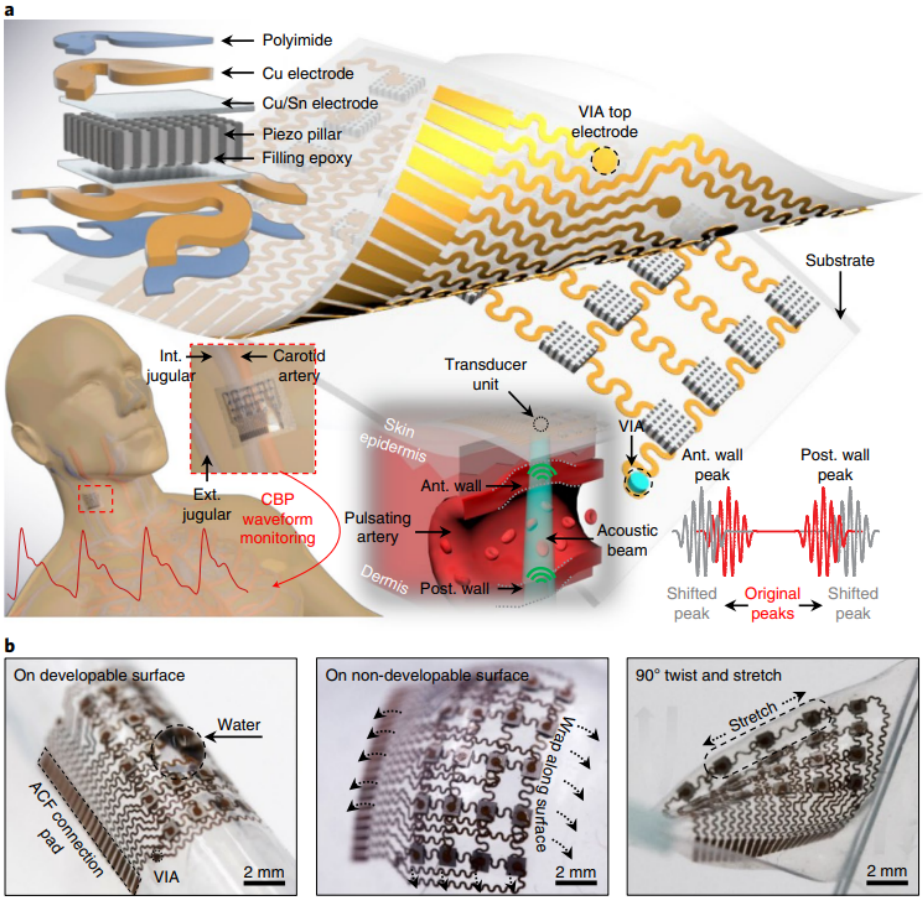

Figure 3.3: (Schematics and design of the stretchable ultrasonic transducer array designed by [64]. (A) The high-performance 1–3 composite with periodic piezoelectric rods embedded in an epoxy matrix (B) The device conforms to complex surfaces and under mixed modes of stretching and twisting, demonstrating the mechanical compliance and robustness of the device.

Later on, the same group developed a conformal ultrasound device to capture blood pressure waveforms at deeply embedded atrial and venous sites [64]. Their device was ultrathin ($240\mu m$) and stretchable (with strains up to 60%), and enabled the non-invasive, continuous, and accurate monitoring of cardiovascular events from multiple body locations, which should facilitate its use in a variety of clinical environments. The device itself consisted of high-performance rigid 1–3 piezoelectric composites (Smart Material Corp.) with soft structural components, resulting in an ultrathin ($24\mu m$) and highly elastic medical ultrasonic probe (Figure 3.3). The anisotropic 1–3 composite, with improved acoustic coupling to tissue, achieved a $400\mu m$ axial resolution at a working frequency of 7.5MHz. The piezoelectric composite design enhanced longitudinal coupling, and the rigid transducer elements were thin (0.9×$0.9mm^2$) for deep tissue penetration with minimal skin loading. Stretchable electrodes, fabricated through bilayer stacking of polyimide (PI) and copper (Cu), connected a 4×5 array of transducers. The array, designed for vessel mapping, included 20 stimulating electrodes for individual transducer addressing. The elements of the device, softly laminated on the skin, could be individually activated with low power consumption (23.6 mW). It captured pulsating blood vessel diameter dynamically with high

spatial (axial resolution of $0.77\mu m$) and temporal ($500\mu s$) resolution. Encapsulated in a thin silicone elastomer with a skin-like modulus, the device was hydrophobic, protecting it from sweat corrosion. The ultrasound patch was flexible and robust, conforming to both developable and non-developable surfaces, making it highly suitable for skin integration applications.

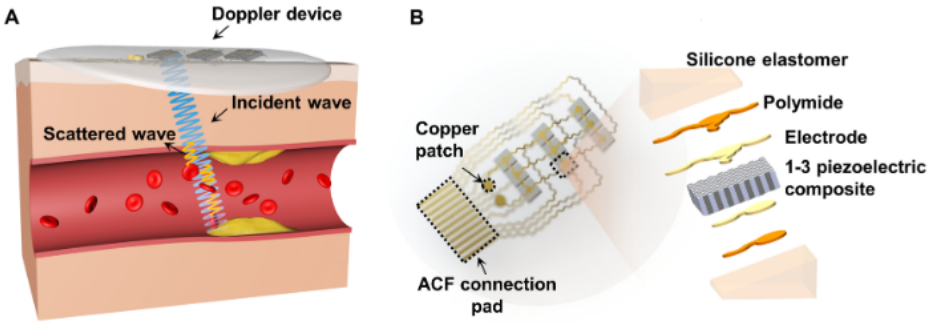

Figure 3.4: (Schematics and design of the Doppler ultrasonic transducer array designed by [65]. (A) The device continuously transmits ultrasound waves and receives echoes from a moving scatterer (such as red blood cells). (B) Schematics (left) and exploded view (right) of the device structure. ACF, Anisotropic Conductive Film.

Wang et al. introduced a flexible Doppler ultrasound device for the continuous monitoring of the absolute velocity of blood flow in deeply embedded arteries based on the Doppler effect [65]. Their device was thin (1 mm), lightweight (0.75 g), and skin-conforming fabricated with microfabrication technologies (Figure 3.4). The fabrication process of the device began by spin coating a $10\mu m$ thick polyimide (PI) film on a silicon wafer, followed by curing and deposition of a $400nm$ thick copper (Cu) layer. The Cu layer was etched into desired patterns using photolithography. Soft substrates were created using machined Cu molds filled with Ecoflex, resulting in top and bottom substrates. The PI film with a shaped Cu conductor was transferred to these substrates. Two films with top and bottom electrodes were patterned by dry etching, and 1-3 piezocomposite transducers (Baoding Xinwei Dianzi Technology Co. Ltd.) were bonded to the bottom electrode. The top electrode was then bonded, and the device was encapsulated in Ecoflex within a designed mold and vacuumized to eliminate interfacial gaps and later cured at room temperature for 3 hours. Compared to the clinical ultrasound machine, their device avoided complex imaging (for Doppler angle measuring), required no experienced operator, and applied much smaller pressure, thus helping with long-term monitoring. Compared to other blood flow monitoring technologies, it could provide the absolute velocities of all moving scatterers in the sample range. The penetration performance of ultrasound made detecting arterial blood flow velocity possible at a depth of at least 25 mm. The frequency of the device was 5 MHz.

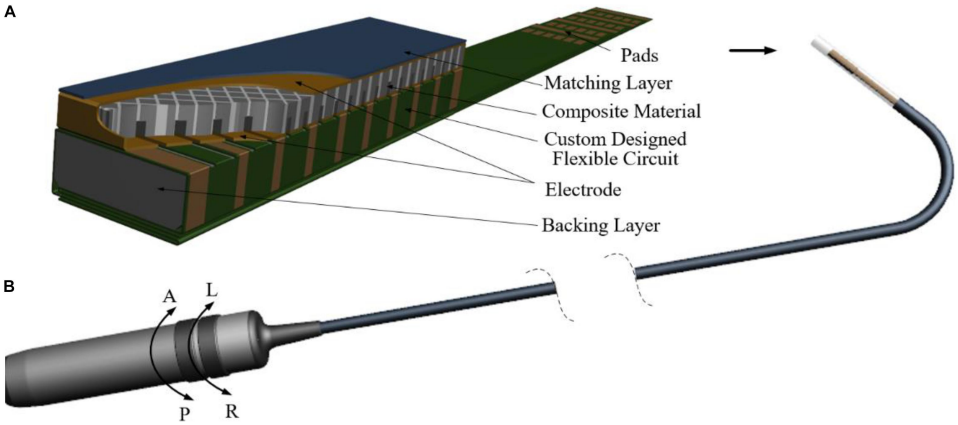

Figure 3.5: Schematics and design of the ultrasonic transducer array designed by [16]. Model of (A) the phased-array transducer and (B) the ICE catheter.

Han et al. designed and fabricated a phased-array ultrasonic transducer using 1-3 piezocomposite with minimal transducer size for intracardiac echocardiography [16]. The piezocomposite was fabri-

cated by the group using PZT and epoxy, with a pitch of $70\mu m$, kerf of $20\mu m$, and thickness of $170\mu m$. The phased-array transducer had 64 elements, the size of each element was $85\mu m \times 1.3mm$, the pitch of the transducer was $100\mu m$, and the kerf between the elements was only $15\mu m$. In order to minimize the transducer size, an encasing structure was used for the 1-3 piezocomposite, which connected the upper surface of the composite directly to the flexible circuit board bonded to the lower surface as the ground electrode (Figure 3.5). The size of the final fabricated transducer was 2 mm × 7.4 mm, and the transducer was mounted on a 9 F (3 mm diameter) catheter, which could bend in four directions and was primarily used for intracardiac echocardiography. According to their findings, the fabricated transducer had a center frequency of 9 MHz with a bandwidth of 55%, an electromechanical coupling coefficient of 0.66, and a peak-to-peak sensitivity of $150mV$. The crosstalk levels were analyzed as well. It was found that the maximum cross-talk values at the center frequency were -34.5, -36.4, and $-38.9dB$ for the first, second, and third adjacent elements respectively, which was said to be sufficient. The penetration depth of the transducer was 100 mm. Lastly, the spatial resolutions and imaging performance were demonstrated with wire-phantom measurements. According to the results, the axial spatial resolution was $188\mu m$ and the SNR of the images of the wire phantom was higher than $30dB$. This study showed that this transducer with its compact design and construction could bring higher performance for the single-use disposable ICE catheter.

Moldovan presented the development of a miniature 1-3 connectivity piezocomposite 1D phased array for intracorporeal sonoporation, intended for incorporation into a capsule or catheter (Figure 3.6) [39]. The primary design constraint was the small size of the piezoelectric element (2.5 mm width, 12 mm length). Simulation and optimization were employed to determine specifications for phased array designs, considering resonance frequencies of 1.5 MHz and 3.0 MHz. Devices made with PZT-5H and PMN-29%PT were evaluated, and prototypes were manufactured using the dice and fill technique. The arrays were tested in vitro, inducing and controlling the sonoporation of a human cell layer. A 1.5 MHz PZT-5H array was implemented in a biocompatible capsule for in vivo operation, with scanning tank characterization showing correlation with the simulation framework. The peak negative pressure was investigated to evaluate the acoustic field of the ultrasound transducer. According to his results, the spatial resolution of the designed arrays was 0.2 mm and the penetration depth was 7 mm. However the application was slightly different from the desired application of this work as Moldovan aimed for a therapeutic ultrasound, the design considerations are useful. Considering the formerly presented devices, it is advised to use similar materials and methods for the ultrasound transducer of the current study.

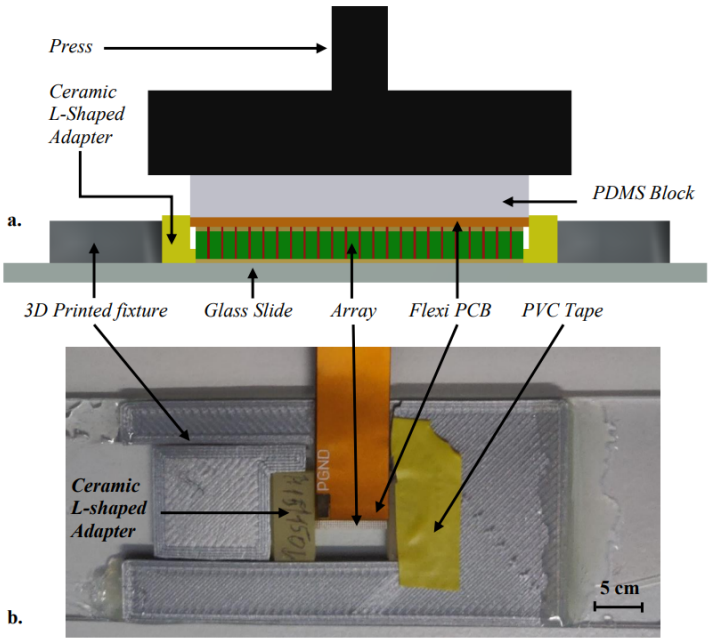

Figure 3.6: Schematics and fixture for flexible PCB bonding of the ultrasonic transducer array designed by [39]. (A) Schematic Side View; (B) Top View .

4

Device Development

4.1. Concepts

A key design objective was to prioritize simplicity in order to effectively demonstrate the proof-of-concept of a device that is simultaneously able to collect electrical and mechanical signals from the same location of the atrial tissue. For this reason, bulk piezoelectric transducers were selected as ultrasound transducers. For the electrode array of this study, the previously designed electrode array (EGM array) for the atrial mapping was taken as the base as the concept has been demonstrated to work for this application [67]. The integration of the two devices comes with several challenges if the goal is to simultaneously record with both devices from the same area of interest. It is desired to position the devices beneath each other to be able to visualize the same area of interest. This way the electrodes will record the electrical activity on the surface of the heart where the electrode touches the atrial tissue, while the ultrasound transducer will focus on the whole depth of the atrial tissue. However, it is important to consider that the electrode array has to be in contact with the tissue to properly collect data. Therefore, the ultrasound transducer can only be placed underneath. This raises the issue of propagating ultrasound through the electrode array. It has been demonstrated before that imaging through the electrode array with a standard high-frequency transducer does not provide the desired results [3]. As outlined before, if the ultrasound passes several media with different acoustic impedances, the attenuation will lead to losses in the ultrasound, and reflections from other media than the field of interest will cause unwanted echoes (Chapter 2). As fully ultrasound transparent electrodes are not commercialized, it would be beneficial to find a solution that would minimize the attenuation [4]. For this reason, it is proposed to use piezoelectric rings in a way that the rings and the electrodes are centered, and that the size of the inner diameter of the ring is slightly larger than the electrode, thus the placement of the electrodes does not lead to ultrasound loss.

One of the proposed solutions to this problem is to create holes in the polyimide substrate around the electrodes in a way that the polyimide does not interfere with the propagation of ultrasound. The transducer chosen for this concept is ring-shaped for which the cavity in the transducer annular ring is slightly larger than the electrode being concentrical to each other with an acoustic impedance for the transducer close to the human tissue. Considering the literature, an acoustic impedance of 4 MRayl is achievable with 1-3 piezocomposite made out of PZT 5H and epoxy [6]. This way the attenuation of the acoustic waves is expected to be minimal as there is no obstacle between the tissue and the transducer. This configuration is referred to as Idea I. further on, its concept is presented in Figure 4.1. The advantage of this concept is that no matching layer is needed, thus the fabrication is less complex. The disadvantage is that 1-3 piezocomposite transducers have lower efficiency than ceramic transducers due to high dielectric and mechanical energy losses.

Another proposed solution to minimize the loss of ultrasound is to use the polyimide of the electrode array as a matching layer between the transducer and the tissue by choosing its thickness accordingly. Polyimide is a suitable material for a matching layer as its acoustic impedance is 3.6 MRayl, as the acoustic impedance of the matching layer should be the geometrical mean of the tissue (1.6 MRayl) and the transducer as outlined before in Chapter2. Therefore, choosing a transducer with a relatively low acoustic impedance, such as a 1-3 piezocomposite with an acoustic impedance of 8.4 MRayl

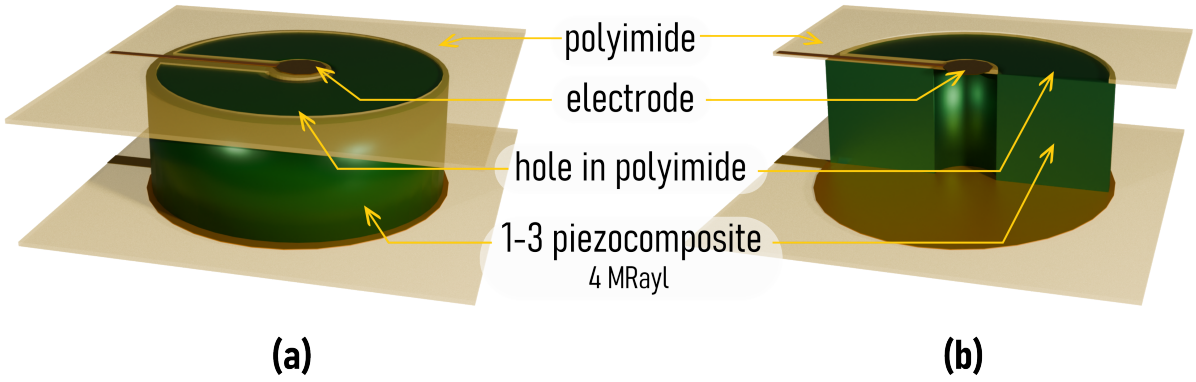

Figure 4.1: Idea I. Preliminary concept of the integration of ultrasound transducers and electrode arrays using 1-3 piezocomposite as ultrasound transducer and holes in the polyimide of the electrode array. The holes ensure that there is no media between the tissue and the transducer which would affect the quality of the ultrasound. (a) presents the 3D view of the concept, (b) is a cross-section by the diameter of the transducer.

would be sufficient for this solution. This concept differs from Idea I. in a way that there are no holes in the polyimide of the electrode array and the intact polyimide is used as a matching layer between the tissue and the 1-3 piezocomposite ring leveraging existing resources and converting obstacles into opportunities. This concept is referred to as Idea II. further on, and it is illustrated in Figure 4.2. The advantage of this concept is that it integrates the existing resources, the polyimide substrate of the electrode array into the ultrasound transducer, and the mechanical robustness of the electrode array is higher as there are no holes in it. The disadvantage is that the fabrication of a matching layer is a complex procedure and 1-3 piezocomposite transducers have lower efficiency than ceramic transducers.

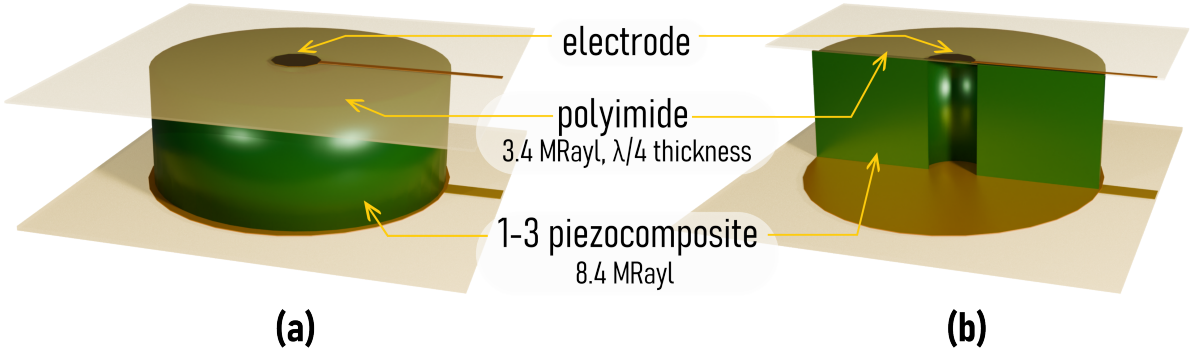

Figure 4.2: Idea II. Preliminary concept of the integration of ultrasound transducers and electrode arrays using 1-3 piezocomposite as ultrasound transducer and the polyimide of the electrode array as a matching layer between the transducer and the tissue. This ensures that the energy loss is minimal for the ultrasound while using the existing resources, the polyimide of the electrode array. (a) presents the 3D view of the concept, (b) is a cross-section by the diameter of the transducer.

The third proposed concept for optimal transducer design for this problem is using conventional piezoelectric transducers with a matching layer and similarly to Idea I., holes in the electrode array. PZT 5H with an acoustic impedance of 34.2 MRayl is proposed to be used for the ultrasound transducer with a corresponding matching layer with an acoustic impedance of 7.16 MRayl to ensure that the acoustic impedance of the matching layer is the geometrical mean of the transducer and the tissue (1.6 MRayl). The holes in the polyimide of the electrode array aim to ensure that the electrode array does not attenuate the ultrasound significantly. This concept is similar to Idea I. as it aims to eliminate the obstacles of the electrode array by extracting the material in the locations where ultrasound is supposed to propagate. However, it uses conventional PZT 5H material for the transducer as it is more accessible. This concept is referred to as Idea III. further on, and it is illustrated in Figure 4.3. The advantage of this concept is using conventional piezoelectric transducers, which are more accessible

and have higher efficiency than 1-3 piezocopmosites to low dielectric and mechanical energy losses. The disadvantages are that fabricating matching layers is a complex procedure and the mechanical robustness of the electrode array is lower due to the presence of holes in the polyimide substrate.

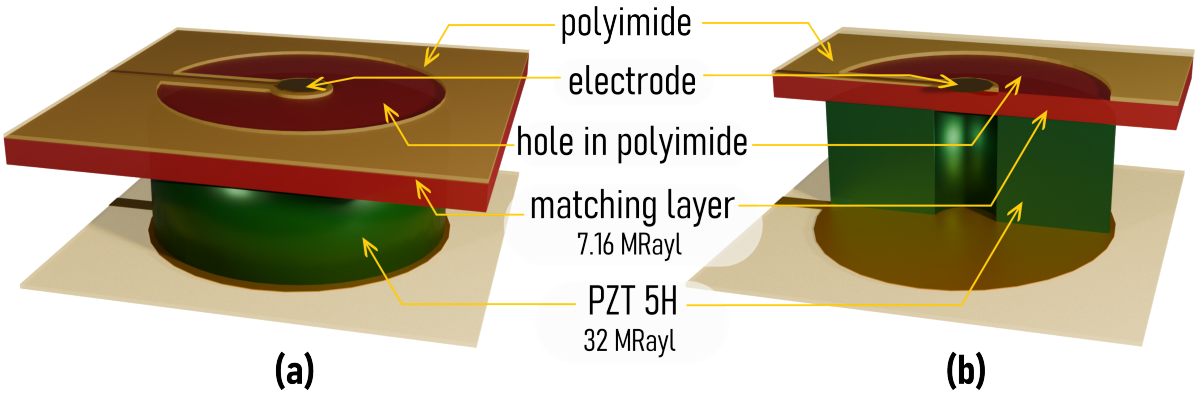

Figure 4.3: Idea III. Preliminary concept of the integration of ultrasound transducers and electrode arrays using PZT 5H as ultrasound transducer with a matching layer and holes in the polyimide of the electrode array. This ensures that the energy loss is minimal for the ultrasound while using conventional ultrasound transducers. (a) presents the 3D view of the concept, (b) is a cross-section by the diameter of the transducer.

4.2. Simulations for Optimal Design Parameters

4.2.1. Design Considerations

The viability of the ideas has to be considered by examining the behavior of the different configurations. This was done by analyzing the pressure field created by the transducer by examining the acoustic intensity and the total acoustic pressure in the field of interest. Moreover, the fabrication limitations have to be considered regarding the scope of the project. The geometrical constraints need to be considered as well as the working environment is limited. The currently used electrode array is 46 mm x 16 mm, thus it is favorable to keep the size of the designed device around this size while minimizing the thickness to maintain flexibility and to ensure that the device fits appropriately within the confined area of interest. In order to maximize the field of view both in the electrical and mechanical domains, the number of ultrasound transducers and electrodes should be maximized as much as the size allows. As the goal is to image the atrial tissue, it is important to choose the transducer parameters accordingly. The atrial tissue is approximately 5-7 mm thick, thus aiming for this length for the near-field is ideal. The diameter and resonance frequency of the piezoelectric ring will determine the length of the near-field (Equation 2.5). Furthermore, the resonance frequency will determine the axial resolution of the transducer as highlighted before (Equation 2.4). However, choosing too high frequencies will result in high attenuation as presented before (Equation 2.2).

The electrical interference of the electrode array and ultrasound transducer should be considered. Conductive coupling can be avoided by using different grounding for the separate circuits. Capacitive coupling on the other hand has to be considered, as there are two individual circuits. The interference will depend on the impedance of the measurement system (Z_i), the wiring (Z_g), the capacitance between the measuring system and the aggressor (C_c), the aggressor signal itself (U_n) based on the equation presented on Figure 4.4. In the case of integration of the ultrasound system and the electrode array, there are two sensitive measurement systems, suggesting that the following configurations should be considered. Firstly, considering the electrograms as the signals and the ultrasound signals are the interference. In this case, U_g is max 80 mV and in the range of 0.5 - 400 Hz [67], C_c depends on the layout of the PCB, U_n is max 600 mV [62] in the range of 40 MHz, Z_g is impedance of wiring and the electrode itself, Z_i is the impedance of the electrogram measuring system. Secondly, the electrograms are considered to be the signals, and the ultrasound pulser is the interference. This case is quite similar to the previous one, except for the interfering signal U_n, which can be around 100 V [62] and in the range of 40 MHz. Lastly, considering the ultrasound signals as the signals and the record electrograms as the interference. In this case, U_g is max 600 mV and in the range of 40MHz, C_c depends on the layout of the PCB similarly to the first two cases, U_n is max 80 mV in the range of 0.5 - 400 Hz, Z_g =

impedance of ultrasound transducer and wiring itself, Z_i is the impedance of the ultrasound measuring system. It can be seen that in every case the signal and interference are in a different frequency range, thus the interference should not be a significant problem providing that there is sufficient filtering for the ultrasound receiver and the electrogram receiver as well.

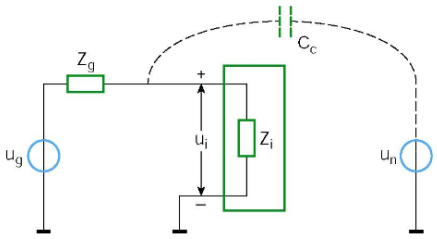

$$u_{i,g} = \frac{Z_i}{Z_g + Z_i} u_g$$

$$u_{i,n} = \frac{Z_g // Z_i}{Z_g // Z_i + \frac{1}{j\omega C_c}} u_n$$

Figure 4.4: Capacitive coupling is a type of electrical interference, which needs to be considered for this device [**pertis 2022**]. The effect of the noise on the signal is presented.

4.2.2. COMSOL Simulations

In order to achieve optimal parameters for the ultrasound transducer several finite element model simulations were conducted in COMSOL Multiphysics. Three different 2D axisymmetric models were built for ideas shown in Figure 4.5. Figure 4.5 (a) illustrates Idea I., where the 1-3 piezocomposite transducer has a low acoustic impedance and there are holes in the polyimide substrate around the electrodes. Figure 4.5 (b) presents Idea II., where the polyimide of the electrode array is used as a matching layer between the tissue and the transducer, thus the 1-3 piezocomposite transducers are chosen to have an acoustic impedance of 8.4 MRayl. Figure 4.5 (c) depicts Idea III., where traditional PZT 5H is used with a matching layer and holes fabricated in the polyimide substrate similarly to Idea I. The material properties were set according to literature values. Solid mechanics physics was used to model the mechanical behavior of the transducer. A roller boundary condition has been applied on the bottom of the transducer. Piezoelectric material boundary condition has been applied to the transducer. Electrostatic physics has been used to simulate the stimulation of the transducer. The ground has been set on the top electrode, while an electric potential of 10 V has been set on the bottom electrode. Piezoelectric charge conservation boundary condition has been applied to the transducer. Pressure acoustics physics in the frequency domain has been used to determine the behavior of the pressure field in the tissue. A spherical wave radiation boundary was set on the outer edge of the tissue. Symmetry has been applied along the axis of the symmetry. The attenuation coefficient of the tissue was set to literature values. Out of the multiphysics modules, Acoustic-Structure Boundary has been applied to the surface where the tissue meets the device. A Piezoelectric Effect module has been applied to the transducer.

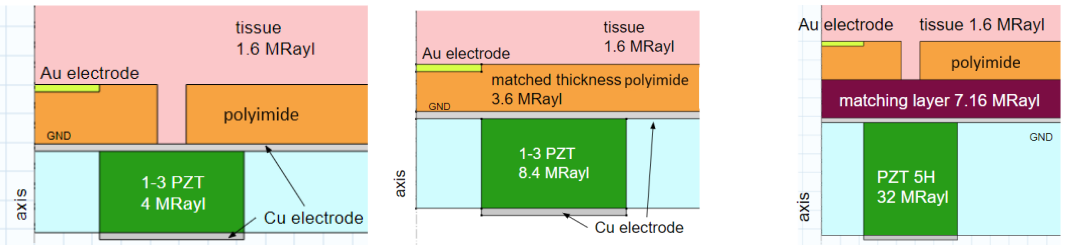

Figure 4.5: The different design ideas for integrating the electrode array and the ultrasound transducer.

In order to obtain the optimal frequency, a parametric sweep was done in the frequency domain. Based on the values of the literature, the chosen frequencies were between 3 MHz and 9 MHz (Chapter 3), with 1 MHz step considering the commercially available transducers. As the thickness of the transducer depends on the resonance frequency, it was set to be parametric in accordance with the

resonance frequency. The total pressure fields and the intensity magnitude of the pressure field have been analyzed in order to obtain information about the performance of the transducers. For example, Figure 4.6 and 4.7 present the simulation results for Idea I. with a diameter of 5 mm for two different resonance frequencies. Figure 4.6 shows the intensity magnitude of the pressure field. It can be seen that the 9 MHz transducer has two higher-intensity areas, suggesting that echo signals from that area will be stronger. Considering the intensity magnitudes, the 4 MHz transducer presents a more coherent pressure field, suggesting that the echo signals would be more coherent than those from the 9 MHz transducer. Moreover, the 9 MHz transducer has more distinguished side lobes, causing strong reflections from unwanted areas. Figure 4.7 shows the total acoustic pressure of the pressure field. Its intensity correlates with the intensity magnitude, moreover, the wave behavior can be observed by the alternating pressure values.

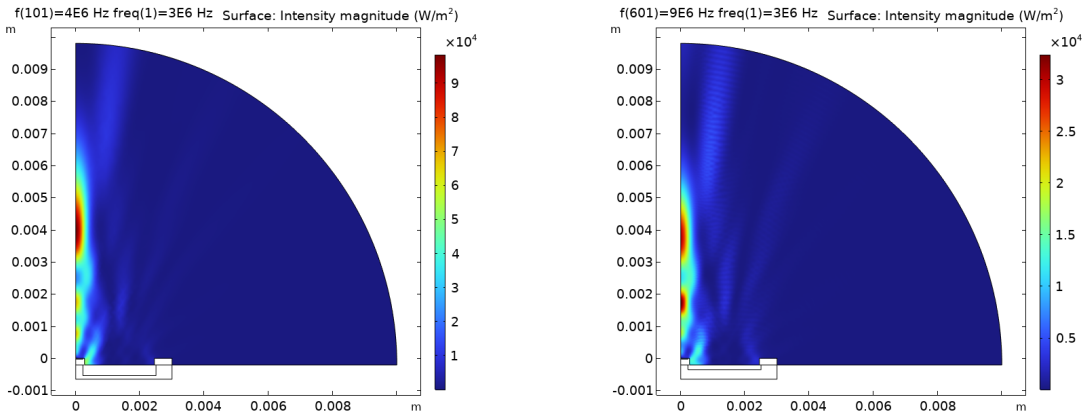

(a) 4 MHz transducer **(b)** 9 MHz transducer

Figure 4.6: Intensity magnitude of the pressure field for Idea I. with 5 mm aperture size.

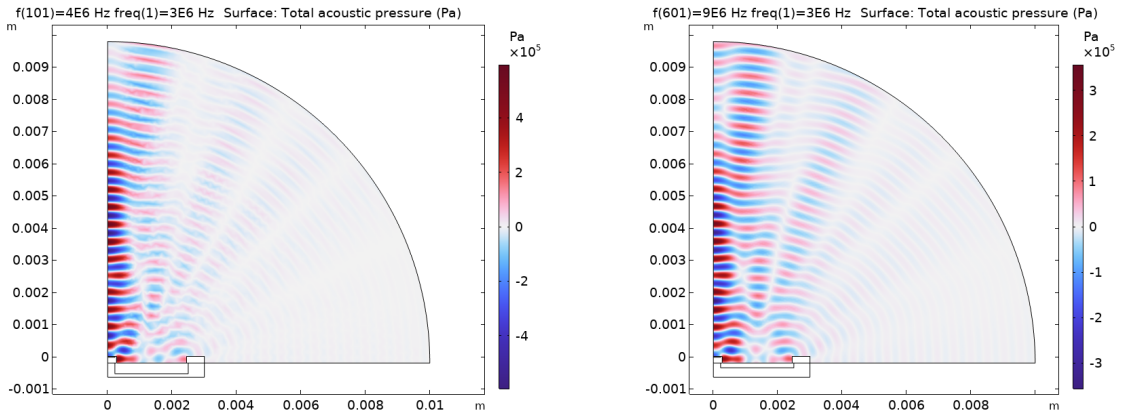

(a) 4 MHz transducer **(b)** 9 MHz transducer

Figure 4.7: Total acoustic pressure of the pressure field for Idea I. with 5 mm aperture size.

In order to compare the results from all frequencies, the acoustic intensity values had been extracted along the centerline of the transducer via the whole depth of the tissue, shown on Figure 4.8. The preferred intensity magnitude has a coherent uniform shape, with higher intensity at the area of interest (between arc lengths 0 and 7 mm).

Moreover, it is important to consider the axial resolution of the transducer. It can be calculated by using the previously presented Equation 2.4, given that the speed of sound in tissue is $c = 1480\frac{m}{s}$ and the number of pulses is $n = 3$. Additionally, using the formula given in Equation 2.2 the attenuation can be calculated for the examined frequencies. As the total traveled distance is twice the tissue thickness $l = 2 \cdot 7mm$, the attenuation coefficient in muscle $A = 1.09\frac{dB}{MHz \cdot cm}$. The attenuation and the axial

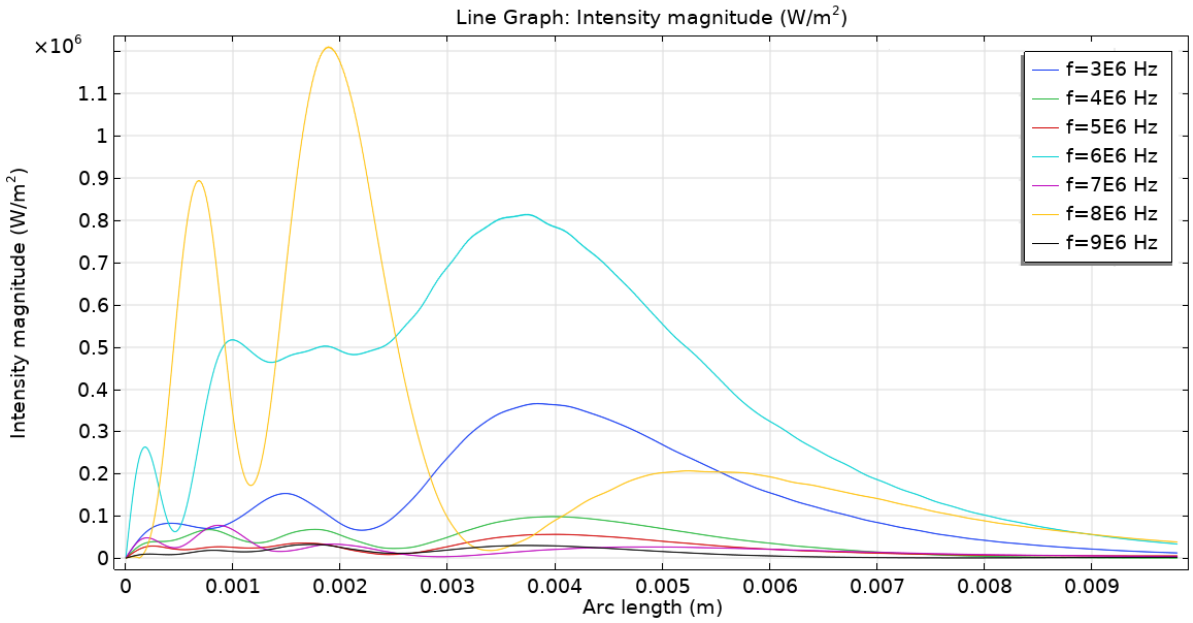

Figure 4.8: Intensity magnitude along the centerline of the transducer via the whole depth of the tissue for resonance frequencies between 3 MHz and 9 MHz. This figure is an example of Idea I. with d=5mm.

resolution in human muscle tissue are shown in Figure 4.9. The resolution should be below 1 mm and the attenuation below 10 dB [21]. Based on the simulations and the calculations, a resonance frequency of 4 MHz was chosen for the first prototype to compromise the attenuation and the axial resolution.

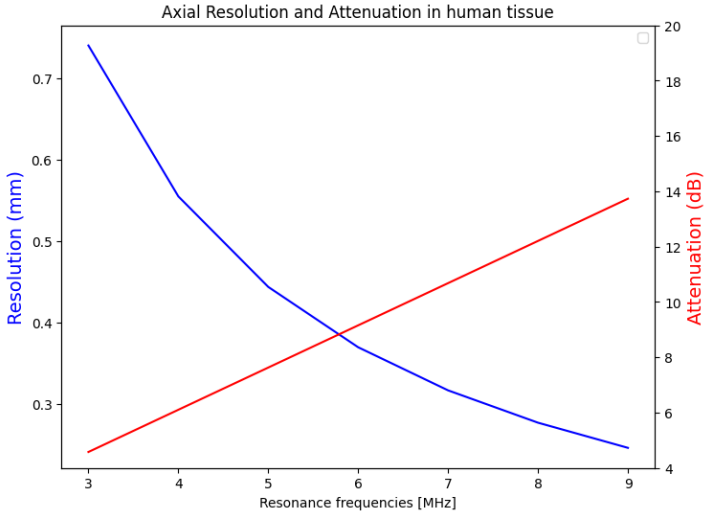

Figure 4.9: The axial resolution and attenuation in human tissue of ultrasound for different resonance frequencies.

To obtain the ideal aperture, three different aperture sizes were examined for all three ideas. Aperture sizes of 2 mm, 5 mm, and 7 mm had been considered based on the fabrication limits of the manufacturer and the size limitations of the device. As the resonance frequency can change due to mechanical load on the transducer, another parametric sweep was done with the fixed thickness correlating to the 4 MHz resonance frequency between 100 kHz and 5 MHz for all three ideas with all three aperture sizes. The corrected resonance frequency can be determined by plotting the impedance of the transducer as the minimum peak of the impedance correlates with the corrected resonance frequency, while the maximum peak corresponds to the antiresonance frequency. The difference between the nominal

and corrected resonance frequencies can be explained by the fact that the resonance frequency can decrease if there is a load on the transducer, such as an electrode array [24].

Obtaining the corrected resonance frequency, the total acoustic pressure fields were examined, as they provided information about the acoustic intensity of the pressure field and the near-field of the transducer. It can be seen in Figure 4.10, Figure 4.11, and Figure 4.12 that the intensity values are in the range of $10^1 \frac{W}{cm^2}$, which is an expected order of magnitude for these transducers [14]. Generally, it can be observed that the intensity increases as the aperture size increases. Moreover, the higher intensities represent the near field as outlined before in Chapter 2, it can be observed that as the aperture size increases the length of the near-field increases in accordance with the theory (Equation 2.5).

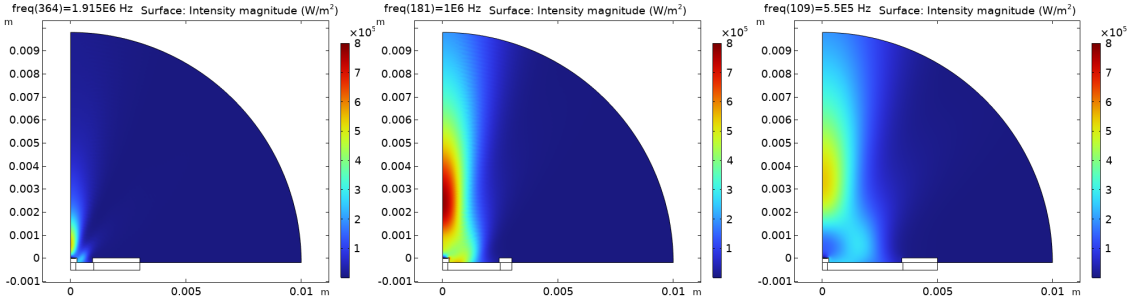

(a) Aperture size of 2 mm **(b)** Aperture size of 5 mm **(c)** Aperture size of 7 mm

Figure 4.10: Acoustic intensity plots for Idea I. with the corrected resonance frequencies.

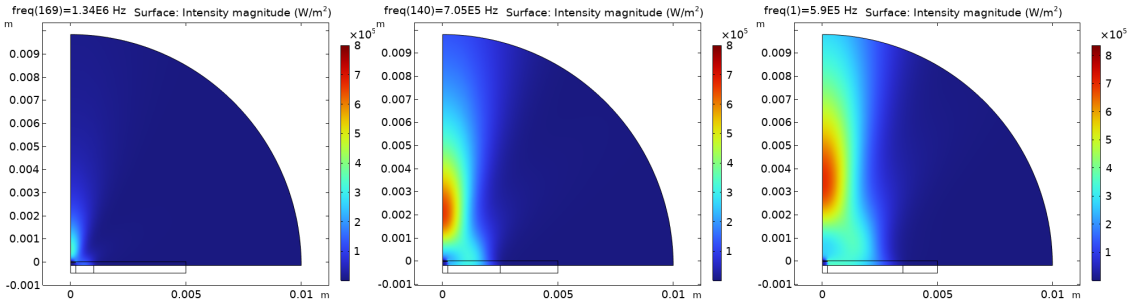

(a) Aperture size of 2 mm **(b)** Aperture size of 5 mm **(c)** Aperture size of 7 mm

Figure 4.11: Acoustic intensity plots for Idea II. with the corrected resonance frequencies.

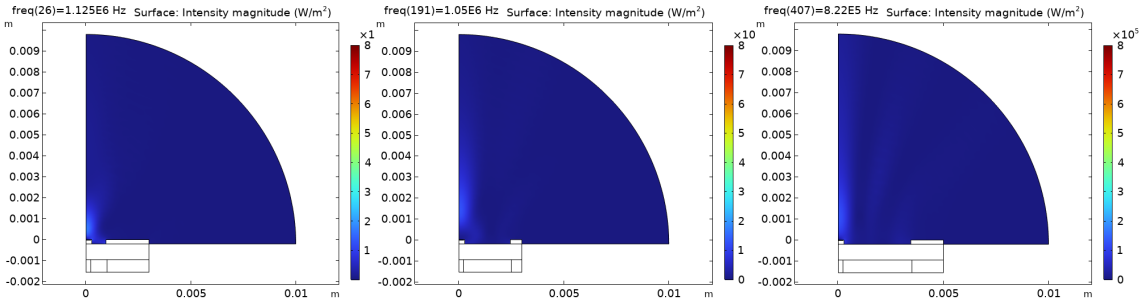

(a) Aperture size of 2 mm **(b)** Aperture size of 5 mm **(c)** Aperture size of 7 mm

Figure 4.12: Acosutic intensity plots for Idea III. with the corrected resonance frequencies.

In order to compare the different aperture sizes for all of the ideas the acoustic intensity values were extracted along the centerline of the transducer via the whole depth of the tissue, shown in Figure 4.13. It can be observed that the acoustic intensity values of Idea I. and Idea II. are comparable, while Idea III. presents significantly lower intensity values. This suggests that even with the use of the matching

layer, using simple PZT 5H is less favorable than the use of piezocomposites. Moreover, the shape of the intensity curve suggests which areas of the tissue would be imaged with higher reliability, as higher acoustic intensity values mean that with the same attenuation, the strength of the echo signals would be higher. According to Equation 2.5, the length of the near-field for a 4 MHz transducer with a diameter of 2 mm is $l = \frac{D^2}{4\lambda} = 2.7\ mm$. The length of the near-field for a 4 MHz transducer with a diameter of 5 mm and 7 mm is $16.89\ mm$ and $33.1\ mm$, respectively. This can also be observed on Figure 4.13. Considering that the atrial tissue is 5-7 mm deep, aperture size of 2 mm is not sufficient for its imaging, while aperture sizes of 5 mm and 7 mm are.

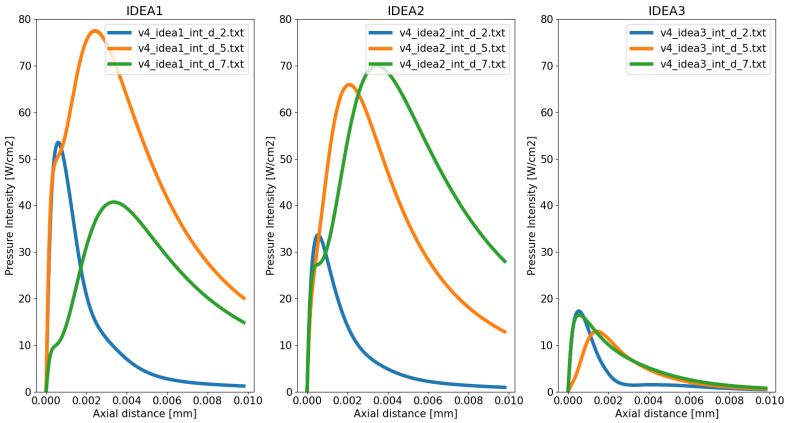

Figure 4.13: Acoustic intensities along the centerline of the transducer for Idea I., Idea II., and Idea III. with aperture sizes of 2 mm, 5 mm, and 7 mm.

Furthermore, simulations have been conducted in order to determine how far the ultrasound transducers can be placed from each other so that the interference is minimal considering the simultaneous usage of the transducers. For this reason, a 3D model has been set up with two transducers next to each other for all three ideas with similar settings and boundary conditions to the previous simulations. An example is shown in Figure 4.14, where Idea I. has been examined with a 0.1 mm distance between the transducers. The intensity magnitude is displayed on a plane perpendicular to the transducers. It can be observed that there is some interference between the transducers, approximately $0.8\frac{W}{m^2}$.

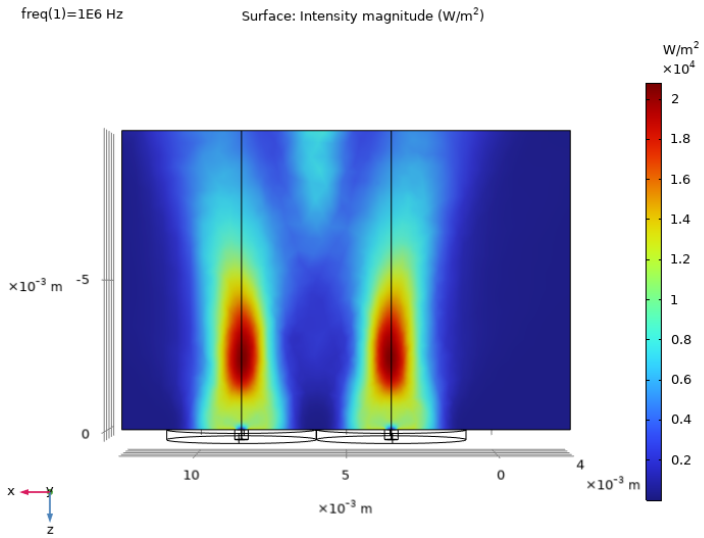

Figure 4.14: Acosutic intensities created by the two neighboring transducers for Idea I. with an aperture size of 5mm, and 0.1 mm distance between the transducers.

In order to compare the interference for different distances, a parametric sweep was conducted, where the distance between the transducers had been swept between 0.1 mm and 5.1 mm, in 0.5 mm steps. An example is shown in Figure 4.15, where the acoustic intensities along the midline between the two neighboring transducers had been plotted for Idea I. with an aperture size of 5 mm. It can be observed that the acoustic intensity values are presenting a triangular shape, which can be explained by the fact that the mesh size was not an integer multiple of the wavelength. According to the literature, the typical rejection ratio interference is 60 dB [38], thus considering that the maximum of acoustic intensity at the area of interest is $2\frac{W}{cm^2}$, the maximum allowed interference is $0.02\frac{W}{cm^2}$. Based on the results, it can be determined that 8 mm between the center of the transducers should be sufficient to minimize the interference if they are operated simultaneously.

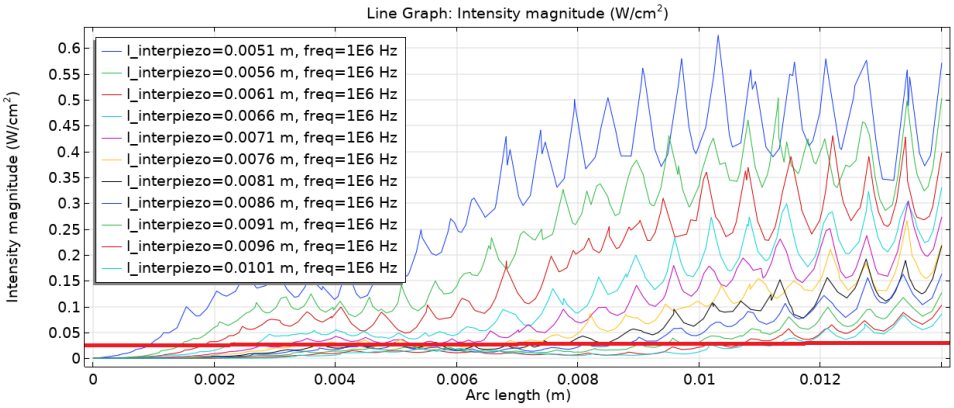

Figure 4.15: Acoustic intensities along the midline between the two neighboring transducers for Idea I. with an aperture size of 5 mm. The red line presents the maximum allowed interference according to [38].

Despite the relevant findings obtained from the COMSOL simulations regarding spatial information, it is important to also highlight its limitations. First, the acoustic intensity and pressure values obtained from the simulations may differ from actual measurements due to the omission of certain non-idealities, such as assembly imperfections, the presence of traces in the electrode array, and the lack of encapsulation. Additionally, due to the inherent nature of simulations, the results can only serve as an approximation. Therefore, it is preferable to evaluate the device design using experimental data. In summary, the COMSOL simulations offered insights into the optimal design of the transducers, including resonance frequency, aperture size, and transducer placement, which insights were incorporated into the final design.

4.3. Final Design

4.3.1. Final Choice

Based on the results of the simulation it can be concluded, that Idea I. and Idea II. are more favorable due to their better performance. Moreover, as the tolerance of the matching layer is in the range of micrometers, the fabrication process of such a matching layer can be a long, time-consuming process. Therefore, a solution without a matching layer is preferred. Thus Idea I. is the most feasible concept for the first prototype, with an electrode array with holes above the 1-3 piezocomposite transducers with the acoustic impedance of 4 MRayl. Furthermore, based on the results of the simulations, it can be concluded that a resonance frequency of 4 MHz is optimal as the trade-off between axial resolution and attenuation is acceptable.

Due to the spatial limitations, the recording components of the device have to be below 46 mm x 16 mm. In order to maximize the spatial resolution of the electrode array and the ultrasound transducer, a smaller aperture size is preferred, as more transducers can be placed on the device. Therefore, the aperture size of 5 mm has been chosen as the axial distance of the maximum acoustic intensity from the electrode array is sufficient and it is smaller than the 7 mm aperture size. Moreover, this allows for higher conformity of the device. In total, this means 12 piezocomposite rings on one device, placed in 2 rows with 6 rings in each row. The size of the electrodes has been chosen to be 0.45 mm as in the original electrode array. This allows for not only placing electrodes above the ultrasound transducers but also

placing them in between the transducers, maximizing the field of view while keeping the fabrication limitations in mind. In total, the electrode array consists of 36 electrodes, of which 12 are above the center of ultrasound transducers.

As the proposed device is a medical device, the chosen materials in contact with the tissue need to be biocompatible. For the electrode array, gold electrodes were used, which is a standard electrode material with relatively high conductivity. For the ultrasound transducer, the commercially available 1-3 piezocomposite has been chosen, consisting of PZT 5H and epoxy, with a fill factor of 11%. The rings have been fabricated by Smart Materials. Lastly, it is important to create an encapsulation layer on the device to ensure watertight insulation. A standard method for this purpose is parylene coating [31]. For the first prototype $4\mu m$ thick parylene coating was chosen as it is proposed to be sufficiently thick to ensure proper insulation and not too thick to severely affect the performance of the piezoelectric ring.

4.3.2. PCB Design

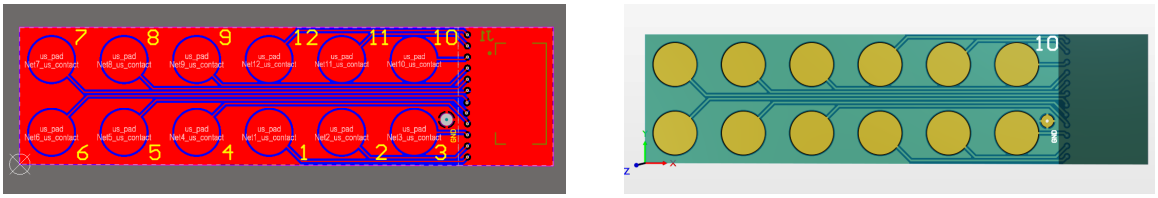

(a) All layers presented.

(b) 3D view. Note: Altium Designer has a bug, thus the coverlay numbering does not show in 3D view.

Figure 4.16: The design of the flexible PCB for the ultrasound transducer.

Two flexible PCBs have been designed for the device in Altium Designer. One PCB is for the ultrasound transducers, while another is for the electrode array. Fabrication was done by PCBWay. Both PCBs are made out of the standard flexible polyimide material, with standard copper traces and a gold finish. The PCB of the ultrasound transducers consists of 2 layers. The active area of the PCB is 46 mm x 15 mm, while the full size of the PCB is 58 mm x 15 mm, both in accordance with the guidelines. The finished board thickness is 0.18 mm. It has 12 contact pads for the transducers and a contact pad for the ground. The contact pads have a diameter of 5 mm and the distance between their center is 8 mm based on the simulation results. The ground of the transducers is chosen to be an aluminum foil on top of the transducers, thus providing shielding for the electrode array. This aluminum foil is designed to be connected to the PCB manually. An FFC/FPC connector has been used with 16 contacts. A stiffener has been placed beneath the connector. A polygon pour has been applied for the ground pour, providing shielding. The Altium Design files are shown in Figure 4.16.

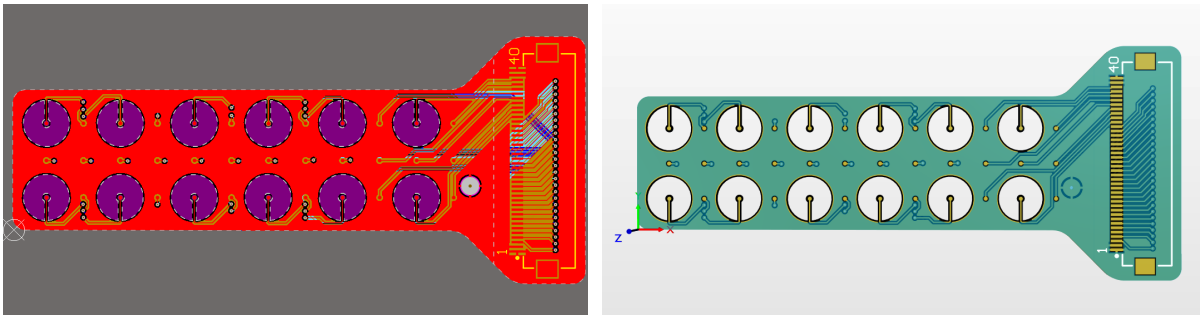

(a) All layers presented.

(b) 3D view.

Figure 4.17: The design of the flexible PCB for the electrode array.

The second PCB is for the electrode array, consisting of 4 layers. The active area of the PCB is 46 mm x 15 mm, while the full size of the device is 58 mm x 25 mm, applying the guidelines. The finished board thickness is 0.23 mm. It has 36 electrodes in total, of which 12 have a hole around them to allow the transmission of ultrasound with minimal energy loss. The electrodes have a diameter of 0.45 mm, similar to the currently used array. An FFC/FPC connector has been used with 40 contacts. A stiffener

has been placed beneath the connector. Similarly to the PCB for the ultrasound transducers, a polygon pour has been applied for the ground pour, providing shielding. The Altium Design files are shown in Figure 4.17. The fabricated PCBs had great flexibility although the copper polygon pour caused them to be less flexible than flexible PCBs without copper polygon pour. Figure 4.18 presents the fabricated flexible PCBs.

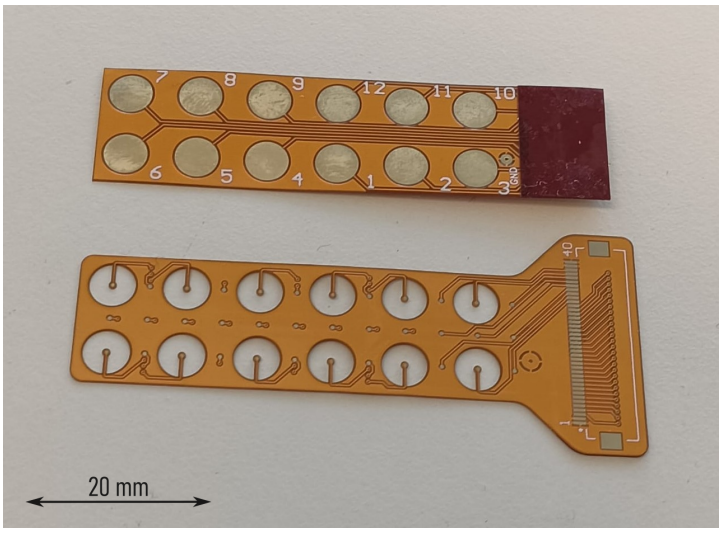

Figure 4.18: The flexible PCBs fabricated by PCBWay.

4.3.3. Overview of Device and Intended Usage

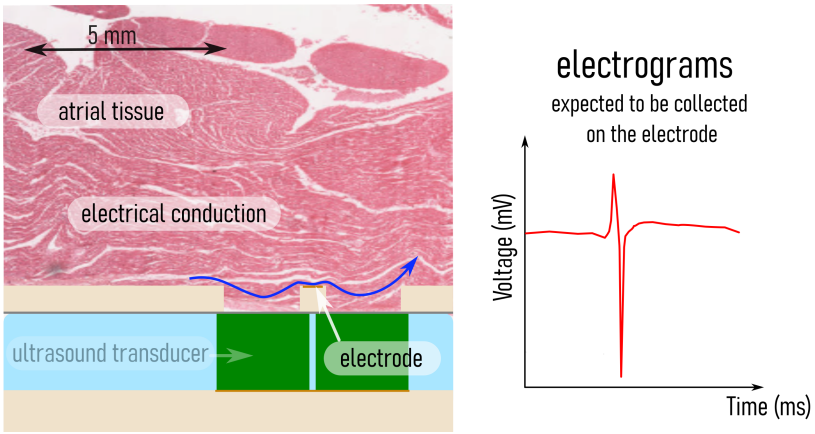

Figure 4.19: Preliminary concept of the integration of ultrasound transducers and electrode arrays using 1-3 piezocomposite as ultrasound transducer and holes in the polyimide of the electrode array. The electrical signal travels through the tissue during the contraction of the heart muscles, which are being recorded by the electrode.

The proposed device consists of two parts, an electrode array and a device with ultrasound transducers, mounted on top of each other. The electrode array is designed to be in contact with the tissue, thus it can collect the electrical signals of the atrial tissue. The ultrasound transducer rings are placed beneath them to be able to collect data from the same area of the tissue. In order for the ultrasound signals to propagate with minimal energy loss, holes are designed to be in the electrode array at the locations of the ultrasound transducers. The functions of the proposed device are shown in Figure 4.19 and Figure 4.20. These Figures are only to demonstrate the concept and the data expected to be collected based on the previous electrode array of EMC and general pulse-echo response [67, 7].

The intended usage of the device with the recording systems is shown in Figure 4.21. The electrograms can be recorded with the TDT Electrophysiology workstation of the Bioelectronics Group. The

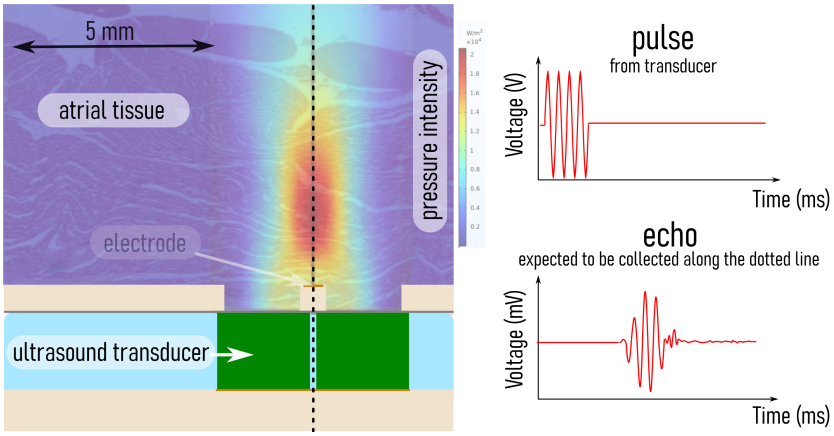

Figure 4.20: Preliminary concept of the integration of ultrasound transducers and electrode arrays using 1-3 piezocomposite as ultrasound transducer and holes in the polyimide of the electrode array. The ultrasound waves are transmitted into the tissue, and expected to be reflected due to different media, providing echo information of the structure of the tissue.

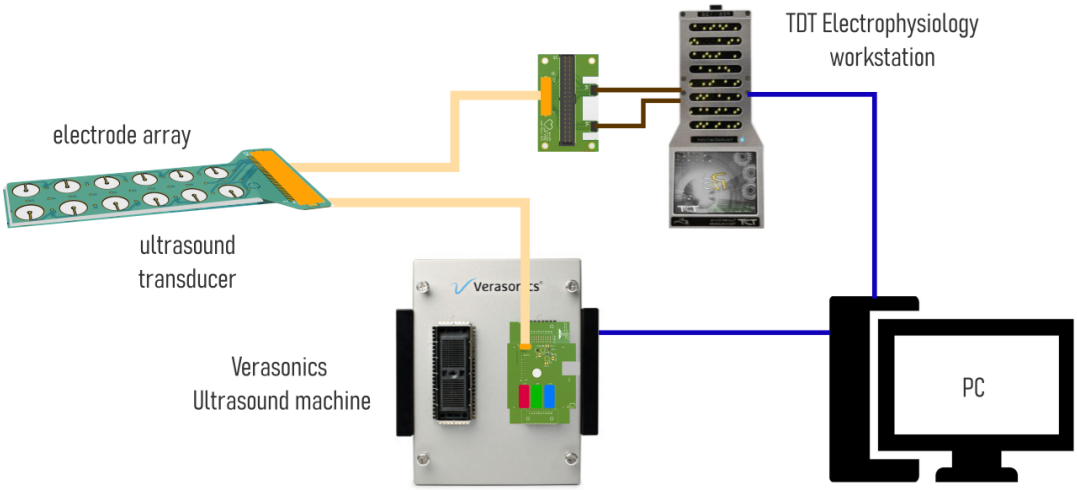

Figure 4.21: Intended usage of the proposed device.

ultrasound transmission and receiving can be controlled by the Verasonics Vantage System of the Bioelectronics Group. This setup is sufficient for measuring the signals, however as the regulations do not allow them in the operating room, it is only to be used in research settings for the first prototype. Considering the interference and cross-talk of the two devices it is advised to not receive electrograms while transmitting ultrasound at the same time as the expected electrogram signals are in the range of millivolts, while the transducers need at least 10 V to be driven, and the input range of the electrophysiology recording systems are also in the range of millivolts, potentially causing saturation. Moreover, it is advised to only operate one piezoelectric ring at a time, so that transducers do not record the pulse of their neighbors, only their own echoes. For this reason, the proposed sequence of operation is the following:

1. Transducer number 1 transmits 2 pulses $f_{transmit} = 4\ MHz$, $t_{transmit} = 0.5\ \mu s$. No electrodes are recording.
2. Transducer number 1 receives $f_{sampling,Verasonics} = 62.5MHz$. All electrodes are recording $f_{sampling,TDT} = 50kHz$.
3. Transducer number 2 transmits. No electrodes are recording.
4. Transducer number 2 receives. All electrodes are recording. The sequence continues.

This sequence allows for sufficient collection of electrical data as the speed of the conduction wave in the atrial tissue is $80 - 120\frac{cm}{s}$. This means that with the 4 mm interelectrode distance, the sampling frequency of the electrodes shall be more than 50 Hz. The TDT system has a maximum sampling frequency of 50 kHz, allowing for sufficient sampling.

4.4. Assembly

The assembly was done manually in the facilities of the Faculty of Electrical Engineering, Mathematics and Computer Science of TU Delft. The assembly was done as shown in Figure 4.22. Testing of the electrical connections was necessary after each step of the assembly. After both devices have been tested, they can be combined with superglue carefully applied avoiding the transducers. In order to measure the performance of the devices individually for reference, the devices have been assembled completely, only fixed together with polyimide tape (Figure 4.23). Two devices have been made with this method, where some of the issues of the first prototype have been avoided on the second prototype with improved technique. The first prototype is referred to as Device number 1., and the second prototype is referred to as Device number 2. further on. The steps of the assembly are the following:

1. Mount the FFC/FPC connector on the flexible PCB for the electrode array with EPO-TEK 301 conductive epoxy (Figure 4.22 a)). Cure the epoxy at $120°C$ for 5 minutes with the help of a hot plate. Check for short circuits, and ensure that the connection is proper.
2. Encapsulate the device with a $4\mu m$ parylene coating (Figure 4.22 b)). Ensure that the contact pads of the connector and the electrodes are covered in polyimide tape, thus the parylene will not coat them.
3. Mount the FFC/FPC connector on the flexible PCB for the ultrasound transducers with EPO-TEK 301 conductive epoxy (Figure 4.22 c))). Cure the epoxy at $120°C$ for 5 minutes with the help of a hot plate. Check for short circuits, and ensure that the connection is proper.
4. Mount the ultrasound transducer rings on the flexible PCB for the ultrasound transducers with EPO-TEK 301 conductive epoxy (Figure 4.22 d) - e)). Ensure that the pad is completely covered in a thin uniform layer of epoxy. Cure the epoxy at $90°C$ for 3 hours. Ensure that the transducers are stable. The piezoelectric rings used are listed in Table 4.1 and Table 4.2.
5. Mount the aluminum foil on top of the ultrasound transducer rings with conductive adhesive silver paint (Thermo Fischer Scientific, 042469.10) (Figure 4.22 f)). Ensure that the transducers are completely covered in a thin uniform layer of paint. Cure the silver paint at $96°C$ for 15 minutes. Ensure that the connection is proper.
6. Connect the aluminum foil to the ground pad with a wire and conductive epoxy (Figure 4.22 g)). Ensure that the transducers are completely covered in a thin uniform layer of paint. Cure the silver paint at $96°C$ for 15 minutes. Cure the epoxy at $120°C$ for 5 minutes. Ensure that the connection is proper.
7. Encapsulate the device with a $4\mu m$ parylene coating (Figure 4.22 h)). Ensure that the contact pads of the connector are covered in polyimide tape, thus the parylene will not coat them.

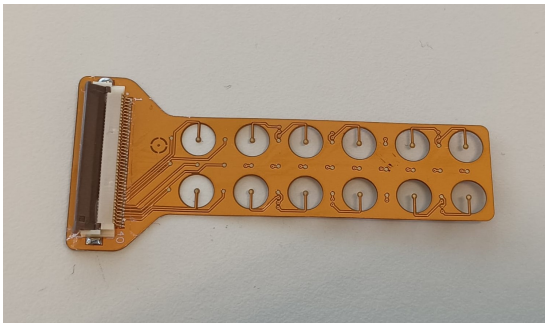

(a) Step 1. Mount the FFC/FPC connector on the flexible PCB for the electrode array with EPO-TEK 301 conductive epoxy.

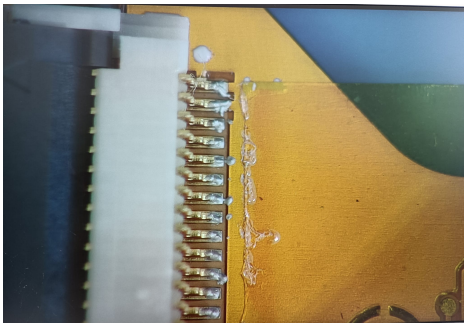

(b) Step 2. Encapsulate the device with a $4\mu m$ parylene coating.

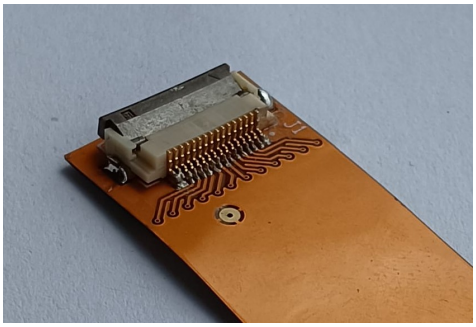

(c) Step 3. Mount the FFC/FPC connector on the flexible PCB for the ultrasound transducers with EPO-TEK 301 conductive epoxy.

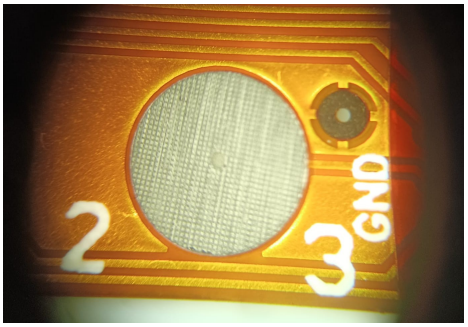

(d) Step 4. Mount the ultrasound transducer rings on the flexible PCB for the ultrasound transducers with EPO-TEK 301 conductive epoxy.

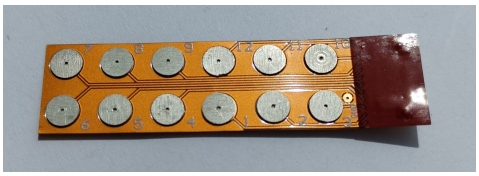

(e) Step 4. All 12 piezoelectric rings mounted on the flexible PCB.

(f) Step 5. Mount the aluminum foil on top of the ultrasound transducer rings with conductive adhesive paint.

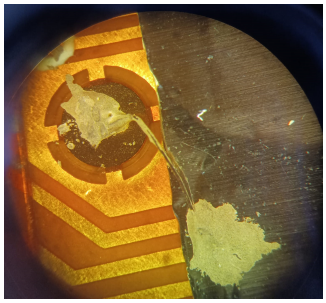

(g) Step 6. Connect the aluminum foil to the ground pad with a wire and conductive epoxy.

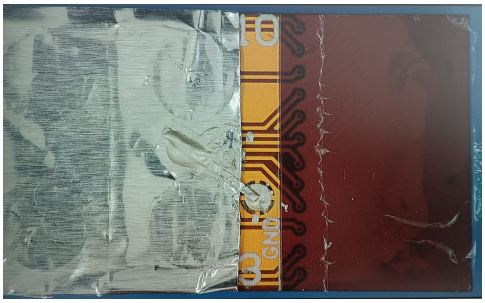

(h) Step 7. Encapsulate the device with a $4\mu m$ parylene coating. The end of the parylene can be observed at the stiffener.

Figure 4.22: Steps of assembly.

Ultrasound Channel	us1	us2	us3	us4	us5	us6	us7	us8	us9	us10	us11	us12
Piezoelectric Ring Number	p27	p26	p25	p28	p29	p30	p36	p35	p34	p31	p32	p33
Verasonics Channel	81	85	86	87	88	92	91	90	89	93	94	95

Table 4.1: The ultrasound channels, the piezoelectric ring numbers, and the Verasonics Channels of Device number one.

Ultrasound Channel	us1	us2	us3	us4	us5	us6	us7	us8	us9	us10	us11	us12
Piezoelectric Ring Number	p15	p14	p13	p16	p17	p18	p24	p23	p22	p19	p20	p21
Verasonics Channel	81	85	86	87	88	92	91	90	89	93	94	95

Table 4.2: The ultrasound channels, the piezoelectric ring numbers, and the Verasonics Channels of Device number two.

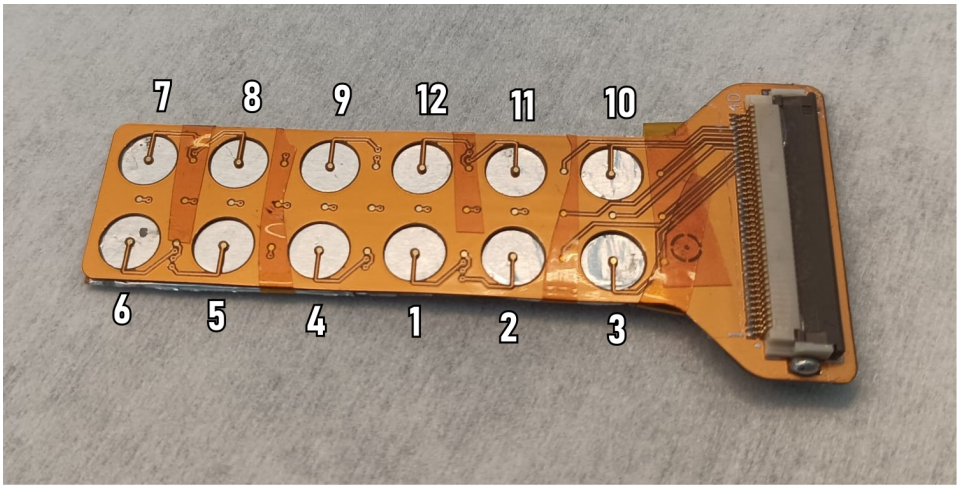

Figure 4.23: The ultrasound transducer and the electrode array fixed with polyimide tape for some measurements. The 12 ultrasound channels are labeled.

5 Results

5.1. Ultrasound Transducer Characterization

5.1.1. Impedance Measurement

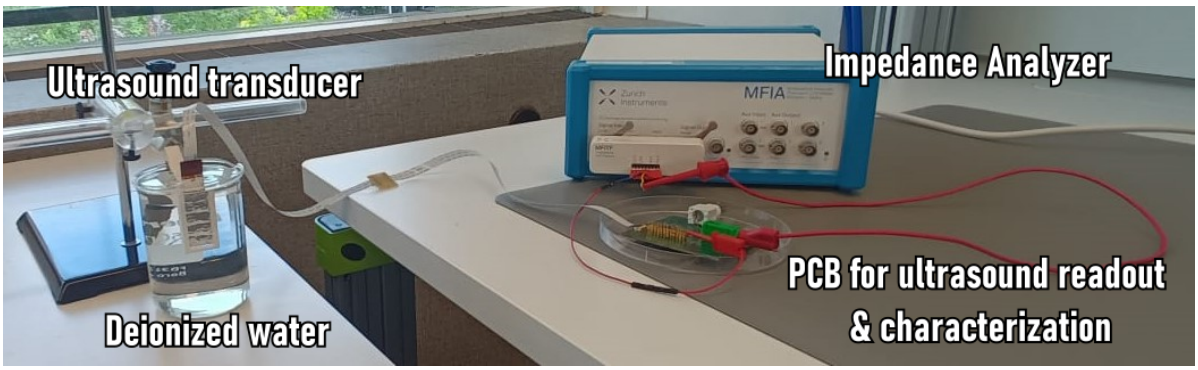

Figure 5.1: Measurement setup of impedance measurements of the piezoelectric rings.

An impedance measurement was performed on the piezoelectric rings in order to obtain information about their performance and functionality. The setup of the impedance measurement can be seen in Figure 5.1. An MFIA 500 kHz / 5 MHz Impedance Analyzer (Zürich Instruments) was used to conduct the measurement. The ultrasound transducer was placed in a beaker containing deionized water. A PCB specifically designed for this project provided an interface for connecting the Impedance Analyzer and the ultrasound transducer. Furthermore, this PCB can be used for manual transducer characterization and an interface for the Verasonics Ultrasound machine for further measurements. A frequency sweep between 1 MHz and 5 MHz has been performed with approximately 3kHz steps to acquire 500 data points. The phase and the absolute impedance of the piezoelectric transducers have been collected. This was compared with the data provided by the manufacturer of the piezoelectric rings (Figure 5.2). The expected behavior of the rings can be observed, the minimum peak of the absolute impedance correlates with the resonance frequency of the transducer, while the sharp peak after the resonance frequency corresponds with the antiresonance frequency.

The impedance and phase of a few selected piezoelectic rings are shown in Figure 5.3. The labels of the rings are listed in Table 4.1. The rest of the rings on this device have an impedance in the range of kOhm according to the impedance measurement, suggesting that they are not properly connected or encapsulated, leading to short circuits, thus not presented. Piezoelectric rings p25 and p29 present clear distinguished peaks in impedance, suggesting that they will operate properly. Their resonance frequency decreased to approximately 3.8 MHz, which is normal behavior due to manual assembly [12]. Ring p30 presents less distinguished peaks in impedance, which suggests that further measurements are needed to evaluate if the ring would operate as expected. Ring p35 presents a proper connection,

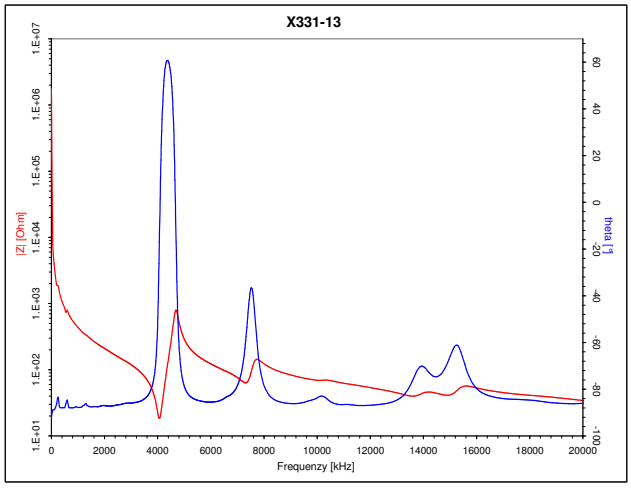

Figure 5.2: Impedance and phase of one piezoelectric ring as an example, provided by the manufacturer.

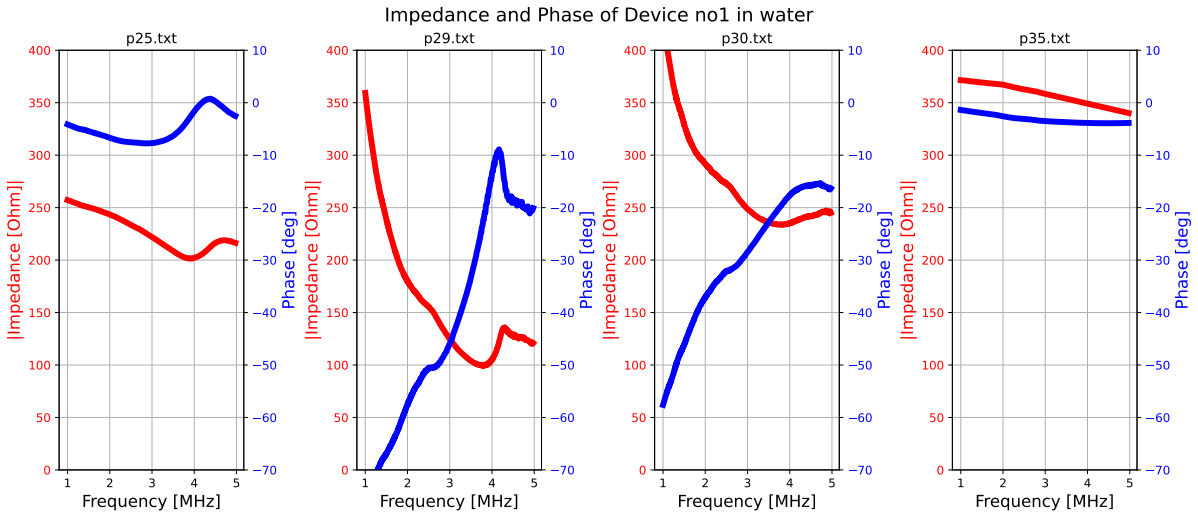

Figure 5.3: Impedance and phase of Device number one.

however, the piezoelectric behavior is not observable. This suggests that the ring might have lost its piezoelectric property during assembly.

The impedance and phase of Device number 2 are presented in Figure 5.4. The labels of the rings are listed in Table 4.2. It can be seen that only a few piezoelectric rings present the expected behavior. Piezoelectric rings p13 and p16 present a distinguished peak in phase and impedance, suggesting that they will operate as expected. It can be seen that the resonance for both of these rings increased to approximately 4.1 MHz, which is normal behavior as the resonance frequency can change due to load on the transducer [12]. Piezoelectric rings p21 and p24 have an impedance in the order of kOhms, thus not presented on this axis. This suggests that they are not properly connected or the encapsulation with the parylene was insufficient and the transducer got shorted via the water. The rest of the rings on this device have an impedance in the range of a few hundred Ohm, suggesting that the connection is proper, however, they do not present a distinguished peak in the range of the examined frequencies. This might be explained by the fact that in some cases the resonance frequency increases significantly after manual assembly [12]. The behavior of the phase correlates with this theory. The impedance and phase measurements were useful to obtain an initial insight into the proper functionality of the piezoelectric rings. In order to evaluate the device for its designed functionality, further measurements are needed.

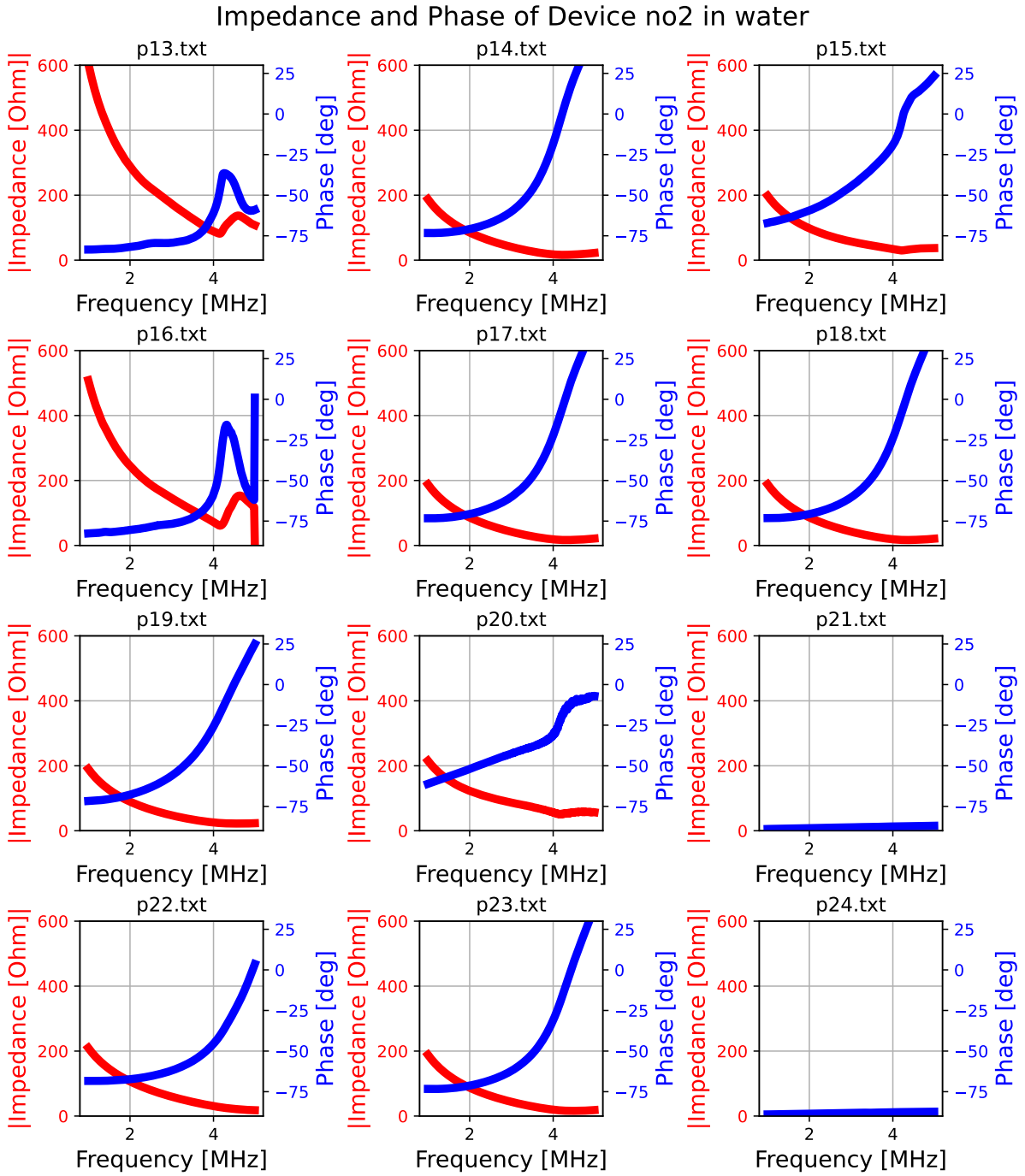

Figure 5.4: Impedance and phase of Device number two. The clear distingushed peaks in impedanace can be observed in piezoleoectric rings number p13, p16. Piezoelectric rings number p21 and p24 have an impedance in the range of kOhms, most likely due to not being properly connected or insufficient encapsulation which lead to short circuit via the deionized water.

5.1.2. Pressure Field Measurement

To test the functionality of the piezoelectric transducers, measurements in the watertank have been conducted. The measurement setup can be seen in Figure 5.5. A function generator (RIGOL DG4202) serves as the acoustic source, which is connected to the custom-made PCB as an interface for connecting to the ultrasound transducer. The device is fixed on a custom-made holder, and deployed in deionized water, which serves as a media for the pressure field measurements. As there were several challenges with the parylene encapsulation, an ultrasound transparent membrane was used to protect the device and ensure water-tightness. A 10um Fibre-optic hydrophone (Precision Acoustics) is employed for ultrasound reception, which is connected to an oscilloscope. The hydrophone has different sensitivities for different frequencies, thus it had to be set correctly. The function generator and the oscilloscope are connected to a computer, from where both devices can be controlled through a MATLAB software developed by our research group. The schematics of the coordinate system of the hydrophone are shown in Figure 5.6.

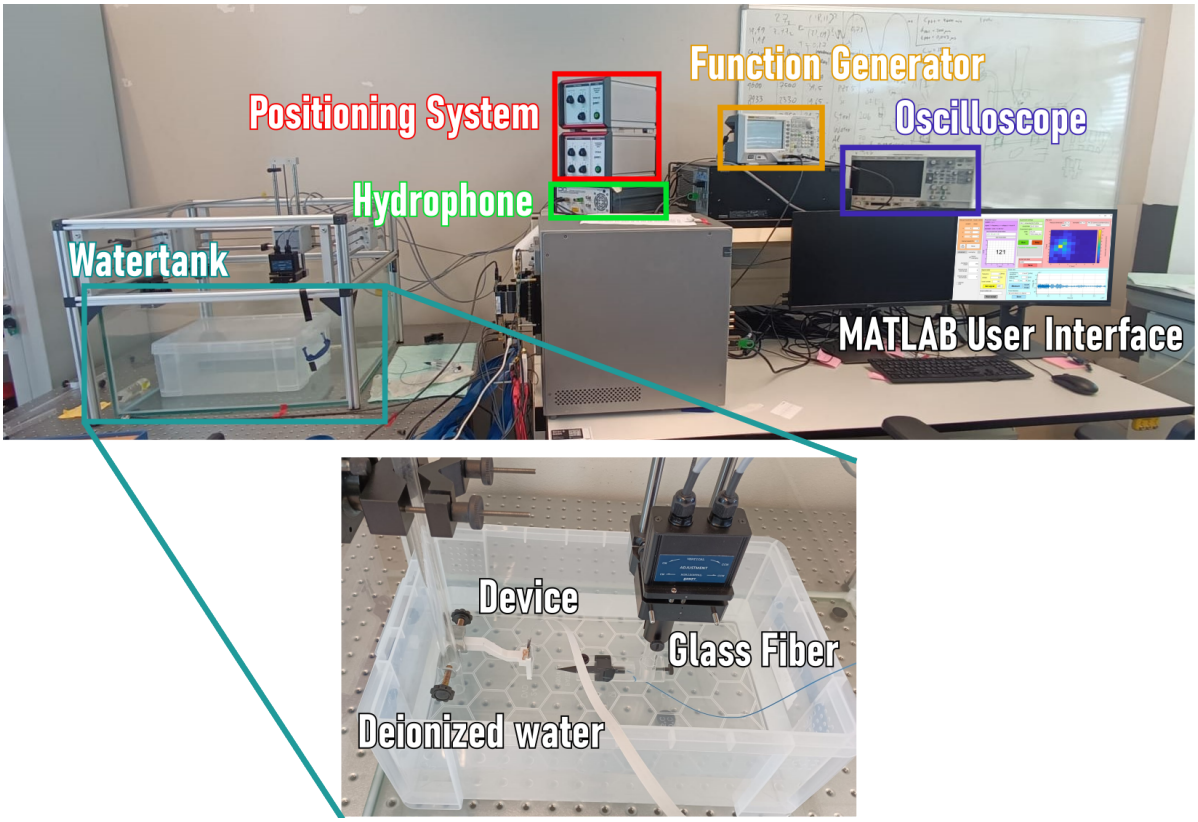

Figure 5.5: The measurement setup presenting the device in the watertank.

Different measurements have been conducted to characterize the ultrasound transducer with and without the electrode array fixed on it. First, it needed to be determined if the examined piezoelectric transducer was functioning as expected. The transducers were excited with a 10 Vpp 4 MHz signal consisting of 2 pulses with a 50% duty cycle, while the hydrophone was positioned approximately in the middle of the transducer 5 mm away from it. It was found that one pulse is not sufficient for the transducers to vibrate. Figure 5.7 presents an example of data collected by the oscilloscope of the desired ultrasound signal. The initial microsecond of the signal appears to be electrical interference, likely originating from the measurement setup. The sinusoidal waves observed around 5-6 μs correspond to the ultrasound signals detected by the hydrophone. The remaining portion of the signal predominantly consists of noise from the oscilloscope. Several piezoelectric rings have been examined in order to evaluate them. It has been found that the rings for which an impedance in the range of kOhms have been measured during the impedance analysis cannot produce ultrasound, and the rings that have an impedance in the range of a hundred Ohms but did not have a clearly distinguished peak in impedance at the resonance and antiresonance frequency also did not produce ultrasound with the current set-

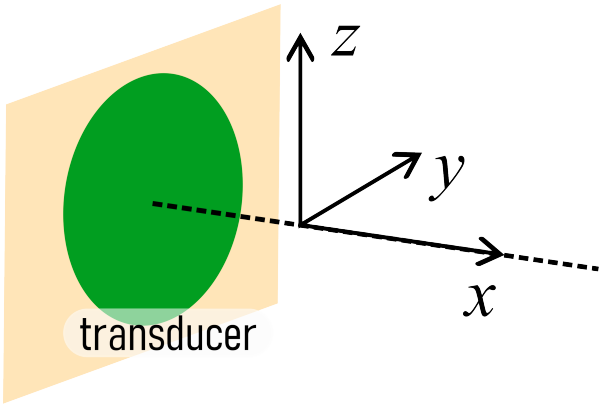

Figure 5.6: The schematics of the coordinate system of the hydrophone for scanning.

tings. This leaves five piezoelectric rings in total (p13, p16, p25, p29, and p30), of which three have been chosen to be characterized fully in accordance with Table 4.1, Table 4.2 and Figure 4.23 (p13 - ultrasound channel number 3 on Device number 2, p16 - ultrasound channel number 4 on Device number 2, p25 - ultrasound channel number 3 on Device number 1). On Figures 5.8, 5.9, 5.10, 5.11, 5.12 subfigures a) and b) present the data collected on ultrasound channel number 3 of Device number 1. subfigures a) and b) present the data collected on ultrasound channel number 3 of Device number 1. Subfigures c) and d) present the data collected on ultrasound channel number 3 of Device number 2. Subfigures e) and f) present the data collected on ultrasound channel number 4 of Device number 2. Subfigues a), c), e) present the data collected with an electrode array fixed on the top of the transducer, while Subfigures b), d), f) present the data collected from the transducer on its own.

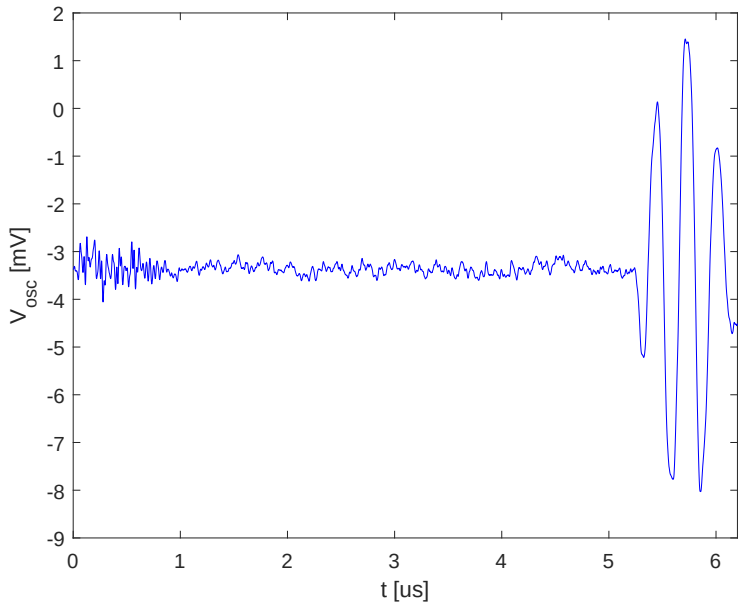

Figure 5.7: The pressure recorded by the hydrophone, displayed by the oscilloscope for Device number 1, ultrasound channel 3, for a 2 pulse excitation with 4 HMz 10 V.

The results are presented in Figure 5.8 of voltages corresponding to the pressure field in the center of the transducer 5 mm away from it for the selected piezoelectric transducers with an excitation of 4 MHz with an amplitude of 10 V, 2 pulses. The pulses highlighted in red are the desired ultrasound pulses as they are sinusoidal and they correlate with the 2 pulses of excitation. The signals following the ultrasound pulse signals are most likely echoes from the surface of the water or the wall of the watertank. It can be concluded that two pulses are sufficient for the ultrasound transducer to vibrate.

It is suggested that without the electrode array, the received signals are stronger as the signals have a higher amplitude in general. However, the ratio between the signals with and without the electrode array is not consistent, suggesting that the addition of the electrode array to the ultrasound array does not produce predictable pressure fields, thus needing individual characterization.

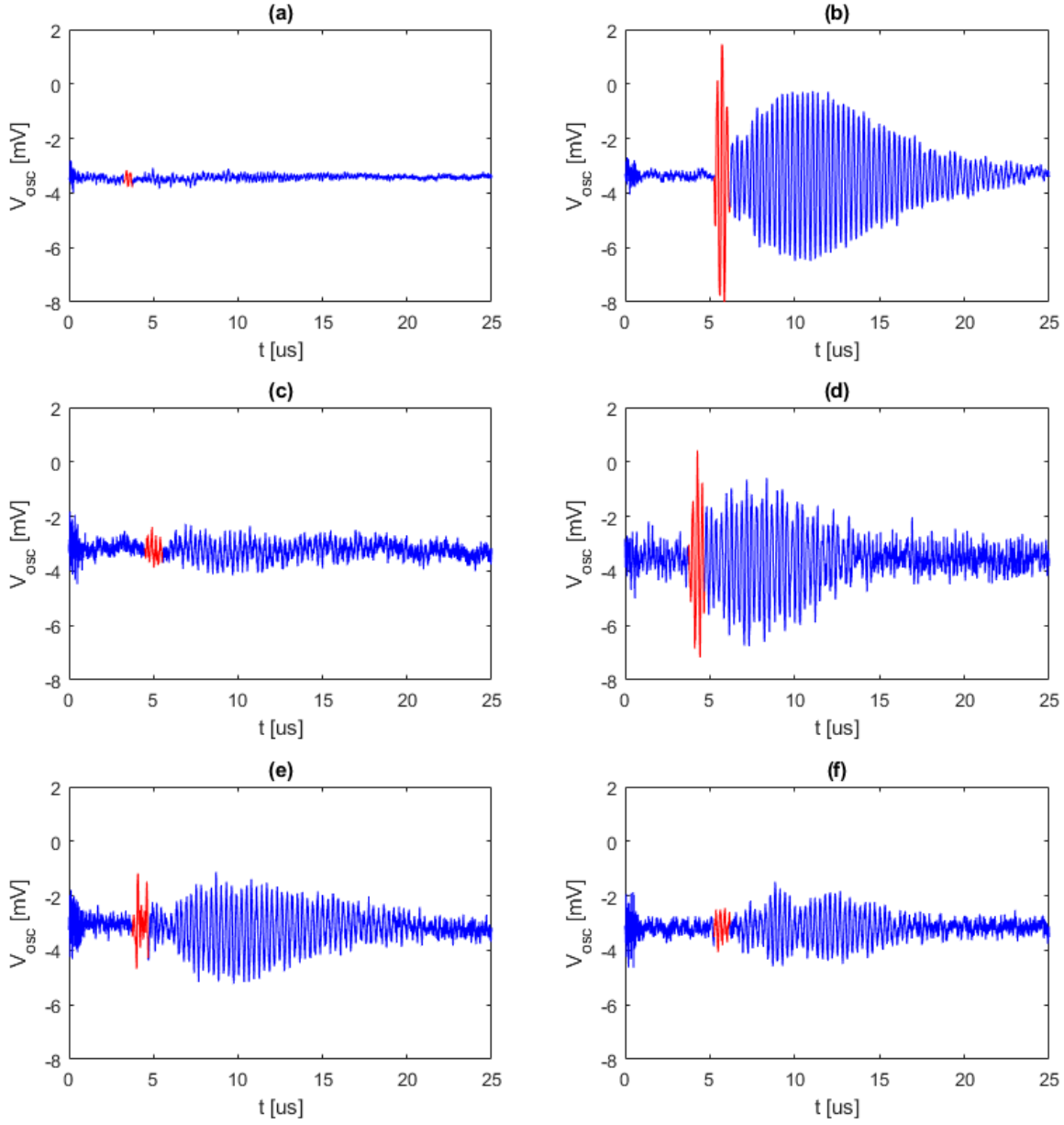

Figure 5.8: The voltage corresponding to the pressure field in the location of the highest pressure values for different piezoelectric transducers with an excitation of 4 MHz with an amplitude of 10 V, 2 pulses. subfigures a) and b) present the data collected on ultrasound channel number 3 of Device number 1. Subfigures c) and d) present the data collected on ultrasound channel number 3 of Device number 2. Subfigures e) and f) present the data collected on ultrasound channel number 4 of Device number 2. Subfigues a), c), e) present the data collected with an electrode array fixed on the top of the transducer, while Subfigures b), d), f) present the data collected from the transducer on its own. The pulses highlighted in red are the desired ultrasound pulses, and the signals following are most likely echoes.

To evaluate the quality of the pressure field and the lobe of the transducer further measurements were conducted with the same measurement setup. The piezoelectric transducers were excited with a 10 Vpp 4 MHz signal consisting of 100 pulses with a 50% duty cycle to obtain high contrast pressure fields. First, to find the location of the highest intensity, the center of the beam, low-resolution scans were done in the yz plane. After it had been localized, a high resolution, 5 x 5 mm wide scan was done in the yz plane approximately 7 mm away from the transducer with a $250\mu m$ step around the center of the beam for all examined transducers with and without electrode array. The results are presented in Figure 5.9. It can be observed that in most cases it was possible to achieve 30 - 40 kPa pressure with the current settings. Examining the chosen transducers, it can be seen that there is no clear correlation between the changes in the pressure field in the presence of the electrode array.

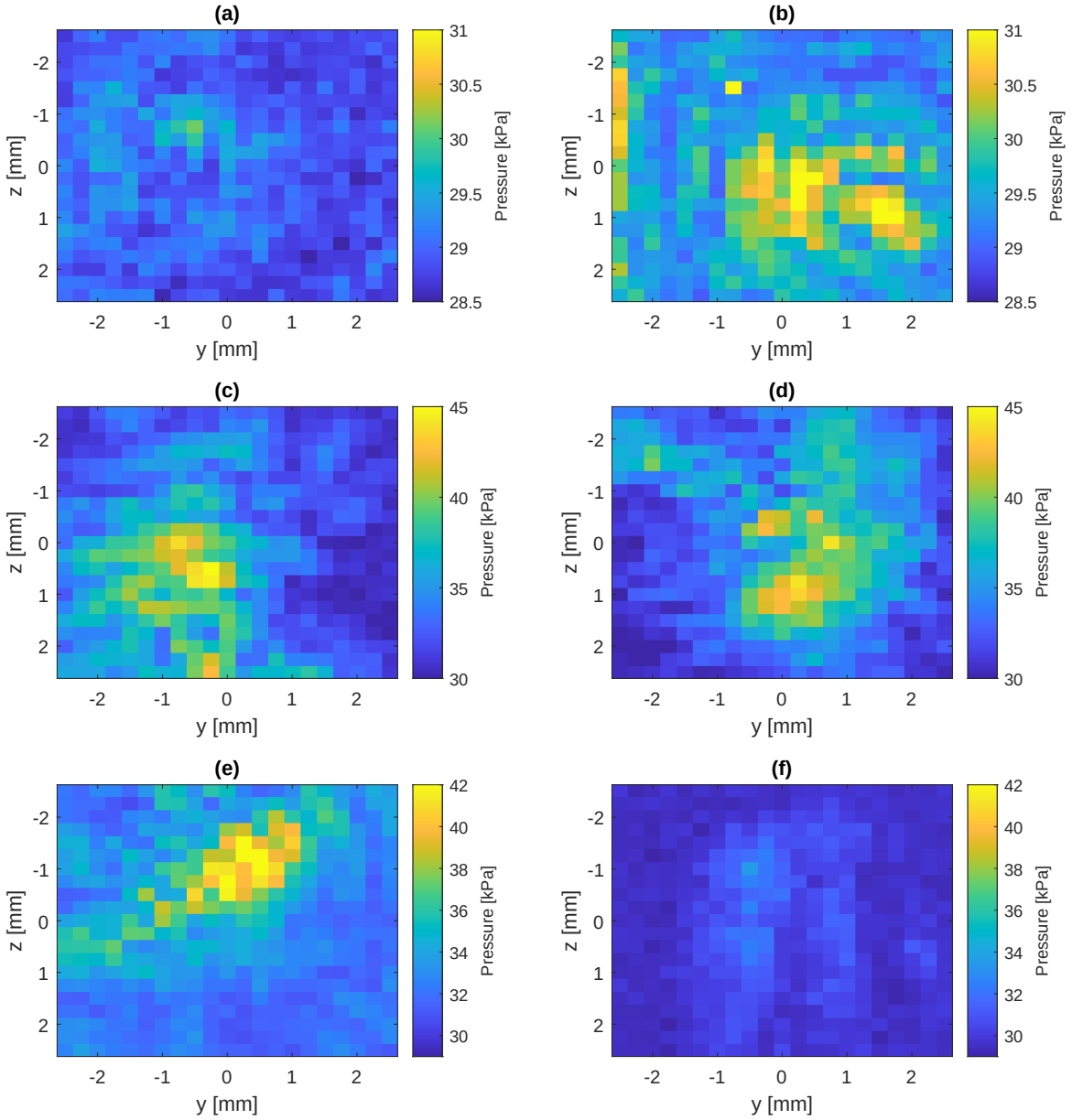

Figure 5.9: The pressure field in the yz plane for all the examined transducers. a) and b) present the data collected on ultrasound channel number 3 of Device number 1. c) and d) present the data collected on ultrasound channel number 3 of Device number 2. e) and f) present the data collected on ultrasound channel number 4 of Device number 2. a), c), e) present the data collected with an electrode array fixed on the top of the transducer, while b), d), f) present the data collected from the transducer on its own.

For examining the shape of the lobe, the normalized pressure field of the yz scans are presented in Figure 5.10. It can be seen that most lobes have a diameter of 2-3 mm, and the presence of the electrode array does not seem to affect it significantly. Moreover, the shape of the pressure field of ultrasound channel number three of device one is a concentric ring, as the pressure field for these transducers should be. The other transducers do not present this behavior, however, that might be due to not perfect positioning as it was done manually.

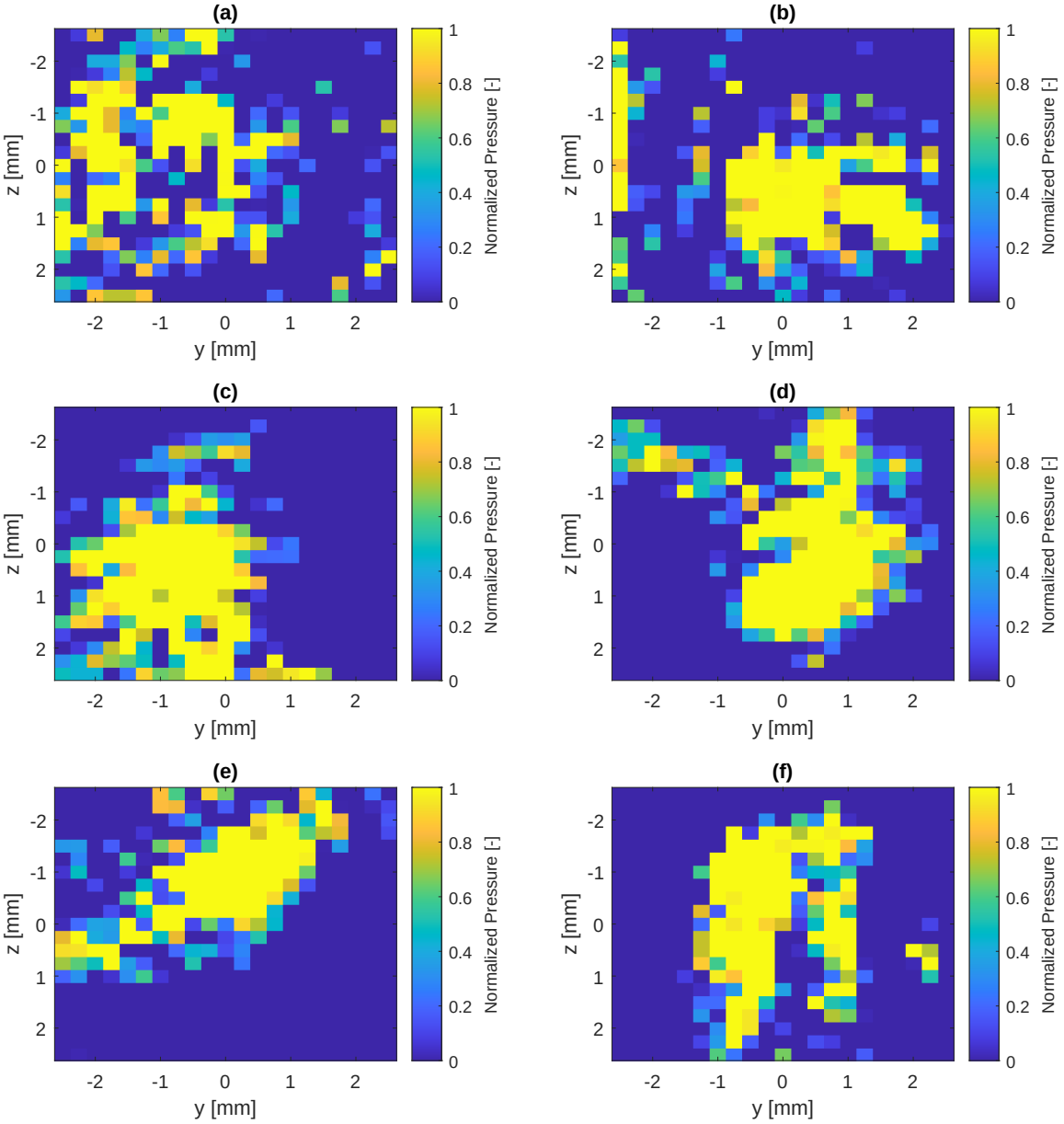

Figure 5.10: The normalized pressure field in the yz plane for all the examined transducers. Subfigures a) and b) present the data collected on ultrasound channel number 3 of Device number 1. Subfigures c) and d) present the data collected on ultrasound channel number 3 of Device number 2. Subfigures e) and f) present the data collected on ultrasound channel number 4 of Device number 2. Subfigues a), c), e) present the data collected with an electrode array fixed on the top of the transducer, while Subfigures b), d), f) present the data collected from the transducer on its own.

Afterward, a high-resolution 10 x 5 mm scan in the xy plane was conducted at z being fixed at the center of the lobe with a $250\mu m$ step to examine the lobe from the side view with and without the electrode array. The results are shown in Figure 5.11. It can be observed that generally, the lobe has an oval shape as expected, while the maximum pressure values correlate with the yz scan except for d2 us3. Similarly to the yz scan, the presence of an electrode array does not seem to have a well-defined effect on the pressure field. It can be observed that the pressure values do not change significantly up until 8 mm away from the transducer.

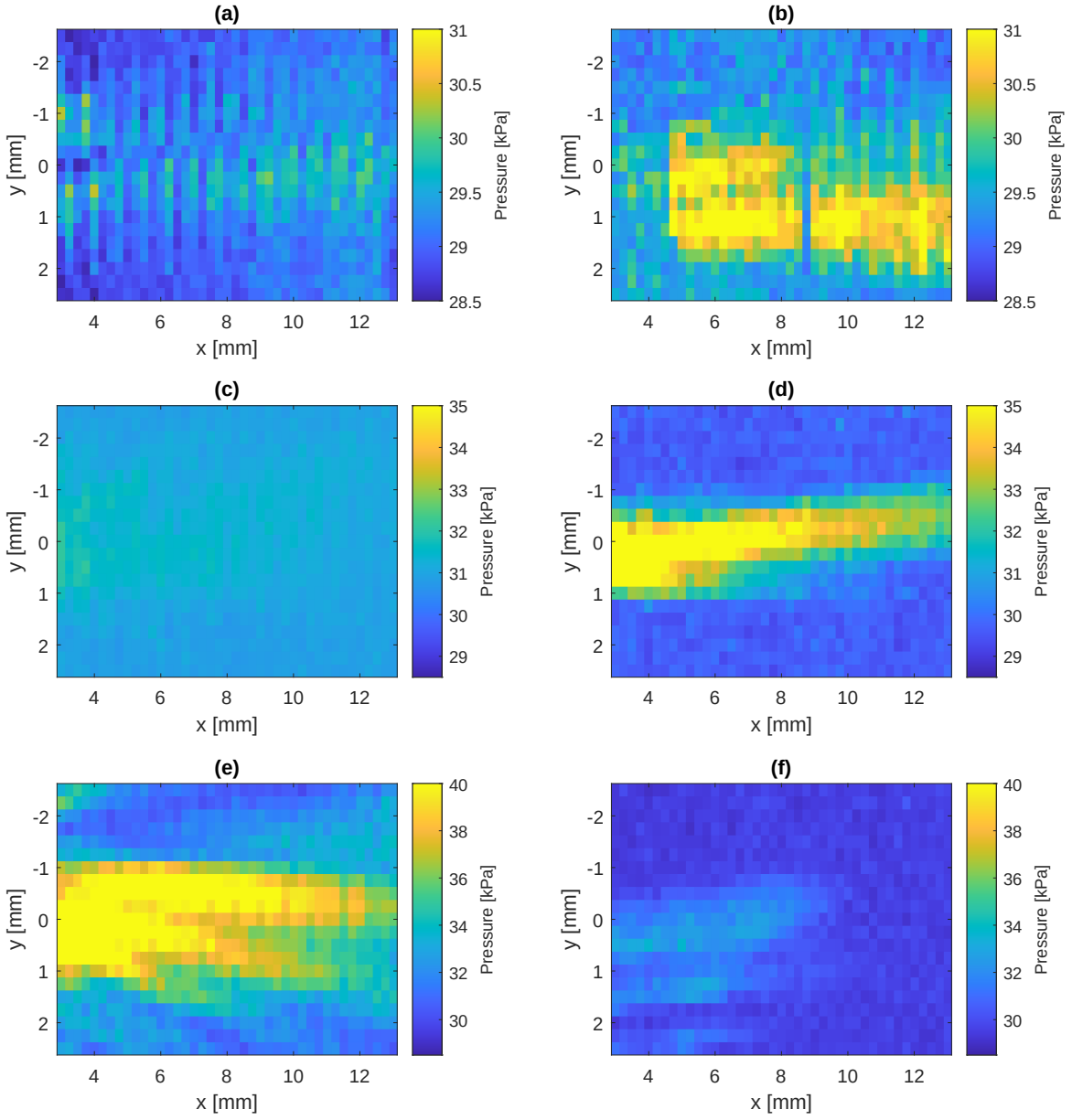

Figure 5.11: The pressure field in the xy plane for all the examined transducers. Subfigures a) and b) present the data collected on ultrasound channel number 3 of Device number 1. Subfigures c) and d) present the data collected on ultrasound channel number 3 of Device number 2. Subfigures e) and f) present the data collected on ultrasound channel number 4 of Device number 2. Subfigues a), c), e) present the data collected with an electrode array fixed on the top of the transducer, while Subfigures b), d), f) present the data collected from the transducer on its own.

For examining the shape of the lobe, the normalized pressure fields of the xy scans are presented in Figure 5.12. It can be seen that the lobe is 2-3 mm wide in the near-field. The shape of the lobe of ultrasound channel number 3 of Device number two looks perfectly aligned with the scanning plane, thus presenting coherent behavior.

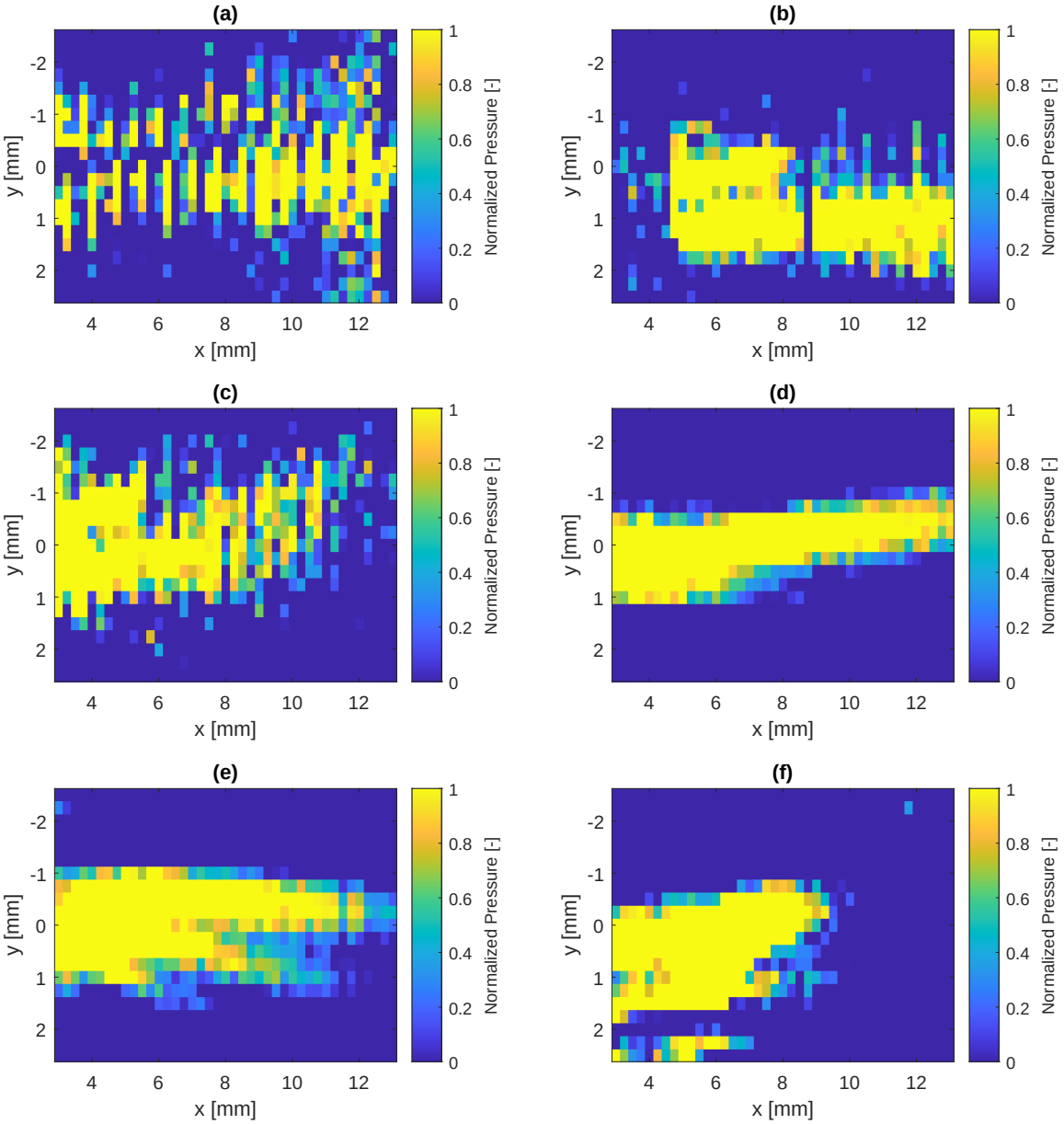

Figure 5.12: The normalized pressure field in the xy plane for all the examined transducers. Subfigures a) and b) present the data collected on ultrasound channel number 3 of Device number 1. Subfigures c) and d) present the data collected on ultrasound channel number 3 of Device number 2. Subfigures e) and f) present the data collected on ultrasound channel number 4 of Device number 2. Subfigues a), c), e) present the data collected with an electrode array fixed on the top of the transducer, while Subfigures b), d), f) present the data collected from the transducer on its own.

Afterward, a frequency sweep between 2 and 5 MHz was conducted in the center of the beam, 5 mm away from the transducer with a step of 100 kHz. The sensitivity-corrected results are shown in Figure 5.13 a). It can be seen that there is a peak in pressure around 3.5 MHz for all transducers, suggesting that the resonance frequency decreased. Lastly, a voltage sweep was conducted between 1 and 10 V in the center of the beam, 5 mm away from the transducer with the corrected resonance frequency for all transducers with and without electrode array. The results are presented in Figure 5.13 b). It can be seen that generally, the transducers produced more pressure without the electrode array.

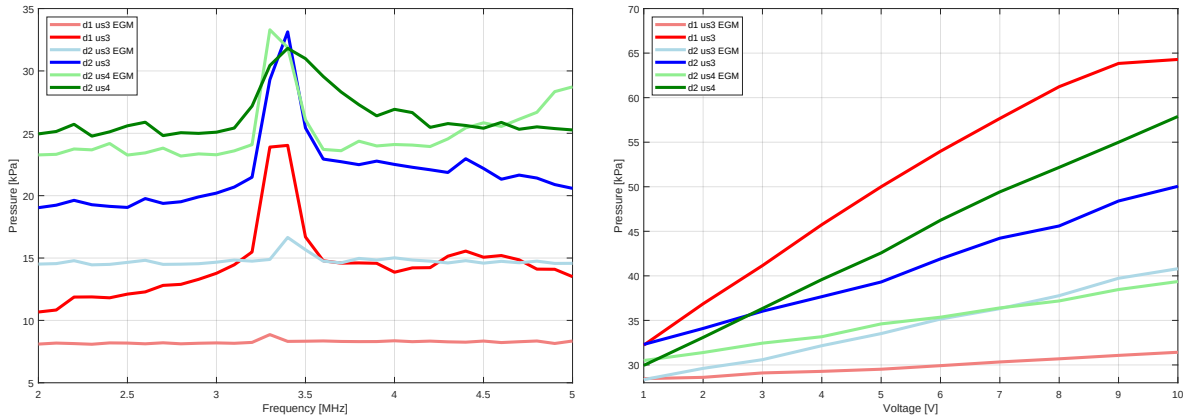

(a) The sensitivity corrected pressure values for different frequencies collected in the center of the beam, 5 mm away from the transducer for all examined transducers.

(b) The pressure values for different voltages collected in the center of the beam, 5 mm away from the transducer for all examined transducers.

Figure 5.13: Voltage and frequency sweep for the examined transducers. EGM means that the electrode array was mounted on the ultrasound transducer.

5.1.3. Pulse - Echo Measurement

Figure 5.14: The measurement setup for the pulse-echo measurements with the Verasonics ultrasound machine.

Preliminary measurements have been conducted to observe the pulse-echo response of the ultrasound transducers with the electrode array. The measurement setup can be observed in Figure 5.14.

The Device has been put into a beaker containing deionized water, and connected to the Verasonics Ultrasound Machine with the custom PCB while being encapsulated by an ultrasound transparent membrane. Twelve analog channels (CH81, CH85, CH86, CH87, CH88, CH89, CH90, CH91, CH92, CH93, CH94, CH95) were used to connect all of the transducers to the Ultrasound Machine in accordance with Table 4.1 and Table 4.2. The Verasonics Ultrasound Machine can be programmed in MATLAB. A custom program has been made in order to test the pulse-echo response of the transducers. The program consisted of exciting the selected transducer with two 4MHz pulses with 10 V amplitude and then receiving with all of the transducer. The echoes are expected from the side of the beaker. After starting the measurement, the beaker has been moved away relative to the transducer. As this measurement is preliminary, the transmit function of only one transducer have been tested, ultrasound channel number 3 of Device number one.

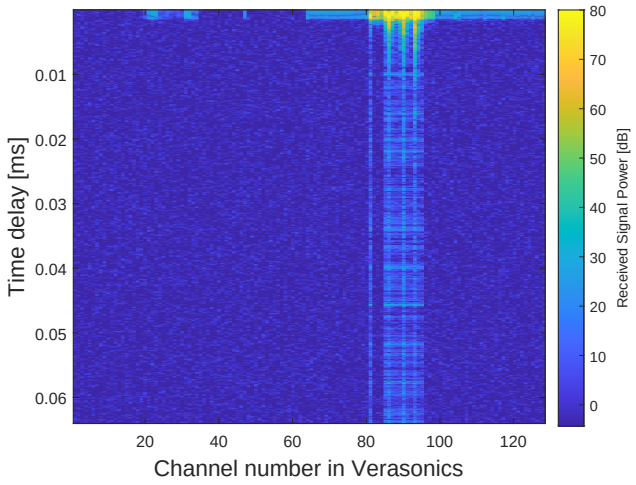

Figure 5.15: The recorded signals of all of the channels of the Verasonics Ultrasound Machine.

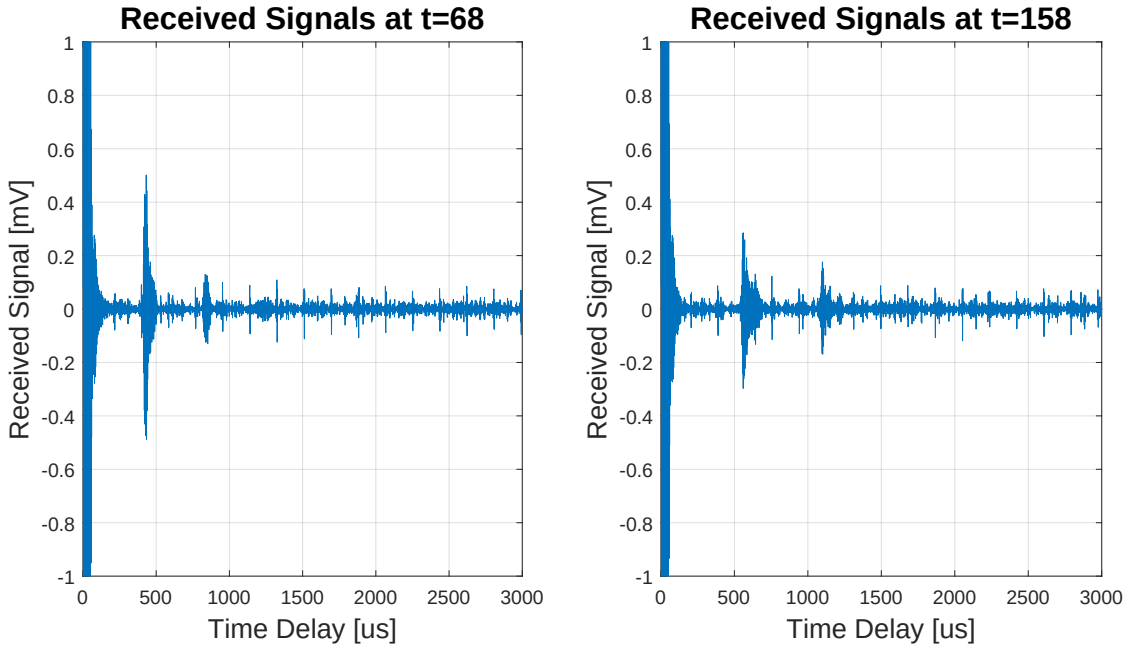

Figure 5.16: The recorded signals of the ultrasound channel number 3 of Device number 1 by the Verasonics Ultrasound Machine.

First, the received data from all piezoelectric transducers have been analyzed while the chosen transducer was transmitting. Figure 5.15 presents the recorded signals in all of the 128 channels of the Verasonics. It can be seen that all of the channels that are connected to the transducers do receive strong signals from a close distance with a time delay below 0.005 ms, and weaker signals from further away with a time delay above 0.005 ms. The former is suggested to be the interference from the excitation of the active transducer, while the latter is suggested to be noise. This indicates that all of the transducers of Device number 1 are capable of receiving ultrasound signals. The received signals in the time domain are shown in Figure 5.16 as an example in two different times. It can be seen that in the first few microseconds, the received signals are saturated, these signals are the voltage applied on the transducer for transmission. In both subfigures it can be observed that there are some significant peaks in the signal, with a higher time delay later on, suggesting that the object of which these echoes occurred moved away. This suggests that these echoes are from the side of the beaker as there was nothing else in the water and the beaker was moved away from the transducer. The full video can be found at [40].

5.2. Electrode Array Characterization

5.2.1. Impedance Measurement

A preliminary measurement has been conducted to evaluate the fabricated electrode array with electrochemical impedance spectroscopy and to analyze if the holes in the polyimide have an effect on the electrode quality [25]. The measurement setup is presented in Figure 5.17. The electrodes were put in a phosphate-buffed saline (PBS) medium, which is a standard conductive medium for spectroscopy. The electrode array was connected to a custom-made PCB, which can be used for electrode characterization and connecting the electrodes to the TDT Electrophysiology workstation. A PalmSense 4 potentiostat was used to collect the data. A frequency sweep between 1 Hz and 1 MHz has been conducted, while the impedance of the electrodes has been measured individually. Every electrode of an electrode array has been measured.

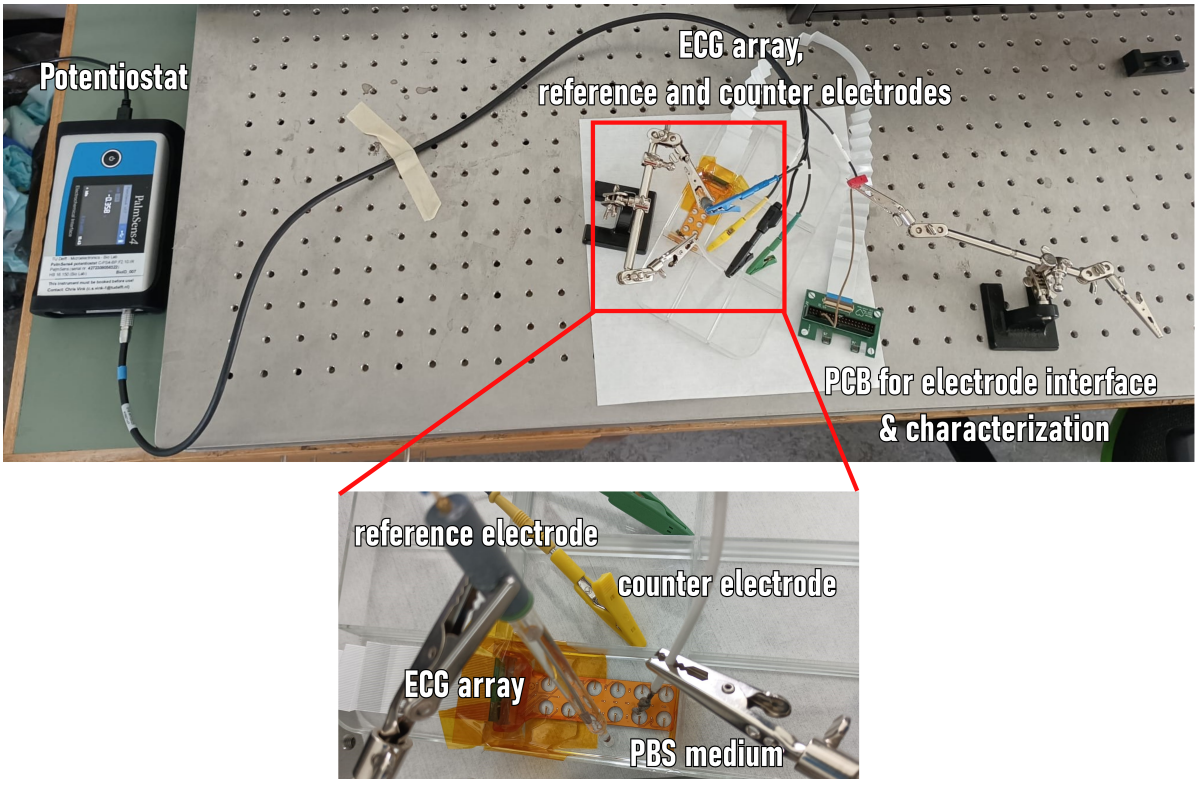

Figure 5.17: The measurement setup for electrochemical impedance spectroscopy to measure the impedance of the electrodes of the electrode array.

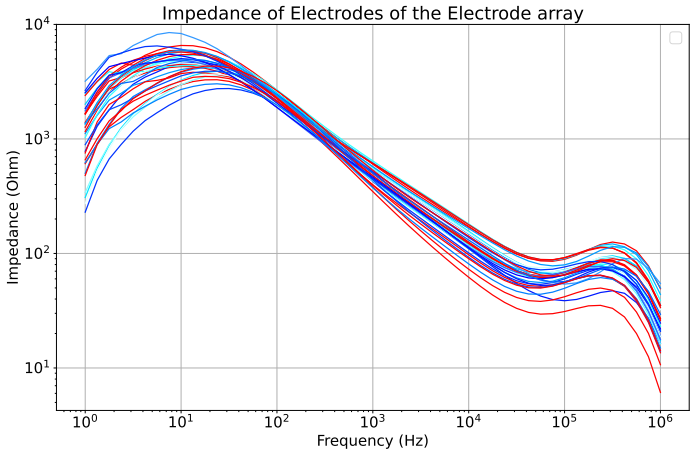

Figure 5.18: The measured impedance for all 32 electrodes of one electrode array for the chosen frequency range to analyze if the holes affect the quality of the electrodes. The red lines represent the electrodes with a hole around them, while the blue lines represent the rest of the electrodes.

The results of the measurements are presented in Figure 5.18. The impedance of the different electrodes of the electrode array is displayed over frequencies between 1 Hz and 1 MHz. It can be seen that the impedance ranges from 10 Ohm to 10 kOhm. The range of interest is between 1 Hz and 400 Hz as the electrograms collected on the surface of the heart are in that range, where the impedance is in the range of kOhms [53]. All electrodes have the same range of impedance, suggesting that there is no significant difference in impedance between the electrodes which have holes around them.

6 Discussion

First, this Chapter will discuss the relevance of the current study. Afterward, the observed results and challenges are discussed, and recommendations are presented. Lastly, the limitations of the study are detailed.

6.1. Relevance

The underlying causes of Arrhythmia, one of the most common heart diseases are still not yet fully understood, thus the treatment is limited. Currently, the electrical activity of the heart tissue of patients with Arrhythmia is researched, gaining more insight into the nature of the disease [67]. Due to a natural phenomenon, the so-called electro-mechanical coupling the behavior of the electrical and mechanical activity of the heart are closely linked together [19]. Thus it would be beneficial to simultaneously obtain data on the electrical and mechanical properties of the same area of the heart tissue, which topic has not been studied before. Thus it would be valuable to develop a device that is able to do so as no previous works targeted this specific problem. The aim of this study is to explore possible solutions, develop a prototype, and evaluate it.

6.2. Results

A device in which ultrasound transducers and an electrode array have been integrated was designed and fabricated as a first prototype following the observations in the literature. In order to evaluate the functionality of the device measurements were conducted to analyze the impedance of the ultrasound transducers, and the electrode array individually. It can be concluded from the results of the impedance analysis of the ultrasound transducers presented in Figure 5.3 and Figure 5.4 that there were five piezoelectric rings, which presented the expected behavior with sharp distinguished peaks in impednace, suggesting that the proposed prototype can fulfill its purpose. While there were several rings that presented optimal impedance and phase values, but not a distinguished peak, which might be a consequence of manual assembly. Lastly, there are a few rings, which have an impedance in the range of kOhms, suggesting that the transducers are not connected properly or that not encapsulated properly, thus short circuited due to the water. The impedance measurements of the electrode array presented in Figure 5.18 showed that there is no significant difference in impedance in electrodes with and without holes around them, suggesting that the presence of the holes does not affect the quality of the electrode.

Further measurements were conducted to analyze the pressure field created by the ultrasound transducers with and without the electrode array integration. The aim of these measurements was to prove that the device is able to fulfill its purpose by creating sufficient pressure fields with the electrode array integrated. Three transducers have been chosen randomly for characterization. It can be concluded that the shape of the lobe and the length of the near-field correlates with the COMSOL simulation results (Figure 4.10 b and Figure 5.11 - Figure 5.12). Moreover, the obtained pressure values are in the range of 30 - 40 kPa, which suggests that even with a 10 V amplitude excitation the transducers are able to produce enough pressure for sufficient pulse-echo response [24]. The acoustically measured

resonance frequencies are lower than the resonance frequencies measured with the Impedance Analyzer (Figure 5.3 and Figure 5.4), which might be due to the ultrasound transparent membrane applied on the transducers for the acoustic measurements. The effect of the integration of the electrode array on the acoustic qualities has been explored. Evaluating the results of the voltage and the frequency sweep (Figure 5.13), it can be observed that the obtained pressure was lower in the presence of the electrode array. However, other measurement results do not support this statement, suggesting that further measurements would be needed to individually evaluate the transdcuers.

Lastly, preliminary measurements have been conducted to evaluate the pulse-echo response of one transducer with the electrode array as a proof-of-concept with the use of the Verasonics Ultrasound Machine. It has been demonstrated that the device is capable of obtaining echoes of the glass beaker while the excitation was 10 V 4 MHz with 2 pulses (Figure 5.16), suggesting that it might be sufficient for measuring the thickness of the atria. Moreover, it is suggested that all transducers are capable of receiving (Figure 5.15), which does not correlate with the results of the impedance analysis (Figure 5.3 and Figure 5.4). The difference can be explained by the fact that for the impedance analysis Device number 1 was only encapsulated with parylene, which might not have been sufficient, thus the transducers might have gotten shorted not presenting the expected behavior, while for the pulse-echo measurements, they were properly encapsulated by the ultrasound transparent membrane. The suggestion of all transducers of Device number one receiving echoes does not seem to correlate with the findings of the pressure field measurements, namely that only a few rings demonstrate piezoelectric properties, however the intrinsic noise levels of the Verasonics Ultrasound Machine and the hydrophone and oscilloscope are different, thus it could be the case that that the pulse signals collected by the oscilloscope are below the noise level of the system, while the Verasonics is still able to capture the echo signals. Future measurements would be needed to evaluate the axial resolution of the device.

6.3. Challenges and Recommendations

During the assembly process, several challenges had to be overcome. One of the main challenges of the assembly was to ensure proper connections with the epoxy for the connector. The conductivity of the epoxy was lower than expected and handling the epoxy required precise manual skills. It is recommended to ask for assembly for the connector from the manufacturer, thus saving time and lowering the risk of improper connections. If that is not feasible, the use of solder paste is recommended to mount the connector on the flexible PCB. Moreover, mounting the ground wire with epoxy on the aluminum foil and the flexible PCB was challenging due to the lower-than-expected conductivity of the epoxy. It is recommended to solder the wire onto the PCB before mounting the piezoelectric rings and use silver paint to mount the wire to the aluminum foil.

Another challenge was to find the optimal amount of epoxy for the transducers to ensure that the surface was properly coated with a thin uniform layer without overflow. It is important to create a thin uniform surface for the ideal electric field and in order for the different piezoelectric rings to be at the same height. However, an overflow of epoxy can cause shorts and alter the electric field in an undesired way. It is recommended to use as little as possible, distributing it equally (Figure 6.1 a)). Furthermore, epoxy could be used as a backing layer with sufficient thickness due to its material properties, and the air bubbles which can be formed in it. While generally the presence of a backing layer is desired, it is hard to control the bubbles and thickness in this specific methodology, thus the outcome is not predictable, making it an unfavorable solution. An alternative to epoxy is to use silverpaint on both sides of the piezoelectric rings. It is desired to make the connection between the aluminum foil and the piezoelectric rings as tight as possible, thus minimal silverpaint and curing under pressure were used to achieve this. However, as one aluminum foil was used for all 12 piezoelectric rings, it is not possible to achieve perfect connections with this method, as the rings might be at slightly different heights, and using one block to create the pressure on them cannot provide perfectly equal pressure distribution. It is suggested to put pressure on the rings individually. Furthermore, bubbles have been found between the aluminum foil and the piezoelectric rings despite careful handling (Figure 6.1 b)). As that is the desired side of transmitting ultrasound, air gaps can cause disruptions in that goal. To resolve this, a small hole was made in the aluminum foil, and the air was carefully squeezed out.

Lastly, the parylene coating entailed several challenges, as the pads of connector needed to be properly covered in order for the parylene not to get onto the connections, while the legs of the connector

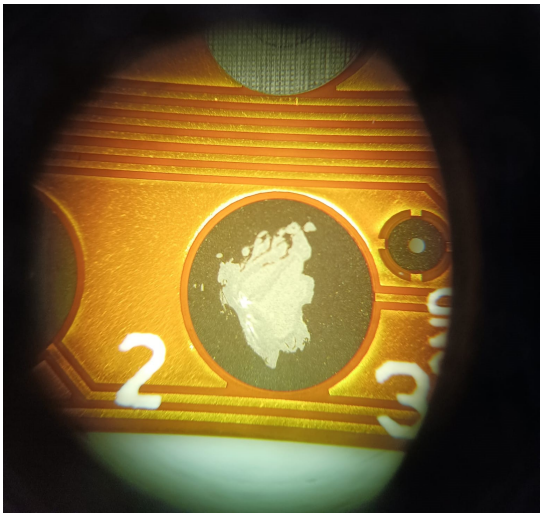

(a) Ideal amount of epoxy for mounting the piezoelectric rings. After applying gentle pressure on the ring and turning it slowly, the epoxy will be distributed equally.

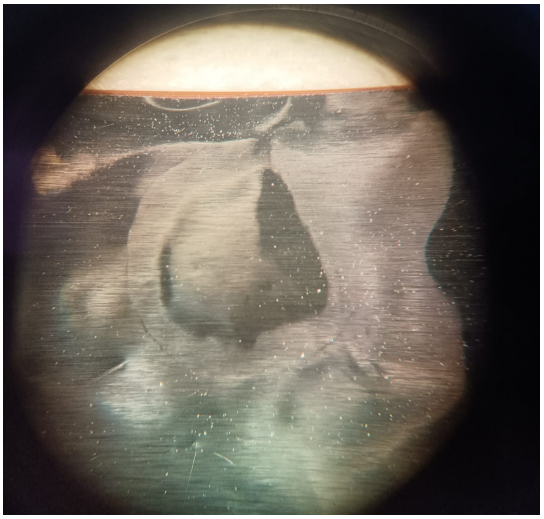

(b) A bubble found between the aluminum foil and the piezoelectric rings despite careful handling

Figure 6.1

should be sufficiently covered. For the first prototype only the pads were covered as shown in Figure 6.2, however, ensuring proper covering was more challenging than expected and parylene needed to be removed from the pads. As it is favorable to access the pads during debugging measurement and testing, the second prototype did not receive parylene coating on the connector at all. This allows for easy access for the pads during measurement debugging, however, for the final tests it is required to fully coat the device.

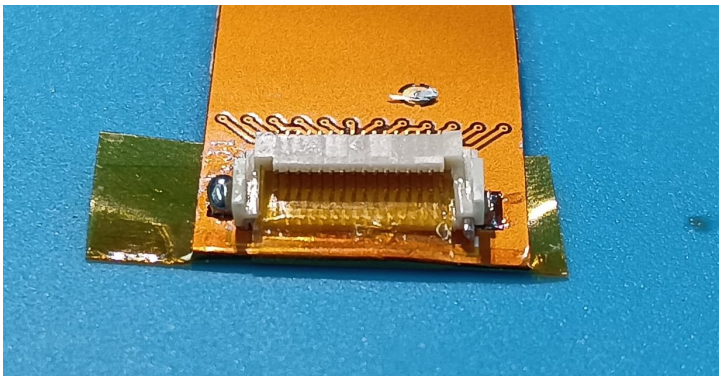

Figure 6.2: Polyimide tape used for covering the pads of the connector where the cable is to be inserted, in order to for it to not be covered in parylene.

6.4. Limitations

There are a few limitations of the thesis as it is a preliminary study. First, the budget limitations have an effect on the size of the device. It would have been preferred to have a longer flexible PCB with the same active area as the proposed prototype so that the connectors are further away from the transducers and the electrode array. This would have allowed an easier assembly and eliminated the need to encapsulate the connector, decreasing the challenges of the assembly. Some degradation of the connector has been observed after the watertank measurements as presented on Figure 6.3, suggesting that it is not advised to have the connector in contact with the water or ultrasound gel. Moreover, for the final application having the connector close to the heart would increase risks. As

this thesis is a preliminary study with the first prototype, it is suggested to design devices with the same active area but with higher spacing between the connector and the electrodes and ultrasound transducers.

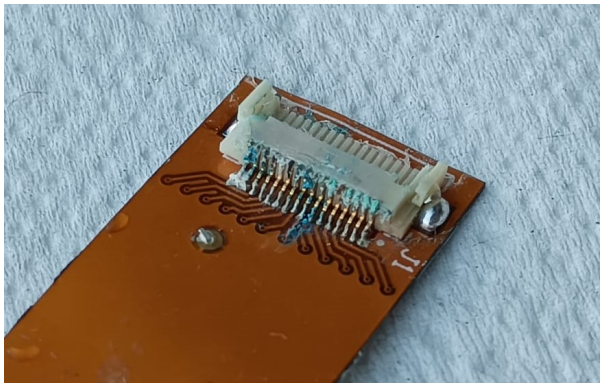

Figure 6.3: Degradation of the connector on Device number one. Might be copper sulfate due to the degradation of the bronze connector by applying voltage on it while being in the deionized water.

The manual assembly is a huge limitation of the study as it leaves a lot of room for human mistakes. Furthermore, the repeatability and quality are less controllable. It is advised to eliminate manual assembly as much as possible in the future. There are several limitations regarding the measurements of the study due to time constraints. Not all of the transducers have been characterized, limiting the sample size of the study. Moreover, the excitation voltage was only 10 V, which is advised to be increased for higher pressure values if needed. As the noise from the measurement setup is higher than expected (Figure 5.7), it would be favorable to increase the excitation voltage to obtain pressure fields with higher contrast. Moreover, only the nominal resonance frequency has been examined for this work due to time constraints. It is advised to conduct measurements with the corrected resonance frequency. Furthermore, air bubbles affect the quality of the ultrasound beam as they attenuate ultrasound drastically, thus their presence should be minimized. Despite the careful handling, there might have been some air bubbles in the silver paint between the piezoelectric rings and the aluminum foil, or in the ultrasound gel applied on the aluminum foil to ensure the connection between the device and the ultrasound transparent membrane. Wrinkles in the ultrasound transparent membrane can have a negative impact on the beam quality and thus should be avoided. However, an inevitable wrinkle at the side of the transducer might have migrated towards the transducer despite the careful handling. It would be advised to find a differently shaped membrane to minimize the wrinkles. Moreover, as the ultrasound transparent membrane needed to be applied again on the device when preparing the measurement with the electrode array, there was a risk of having a different amount of ultrasound gel on the surface or that inevitable wrinkles were positioned on the side of the transducer differently. Lastly, the impedance analyzer used to characterize the transducers is only able to collect data up to 5 MHz, while it would be favorable to investigate higher frequencies.

7 Conclusion

The aim of this thesis was to develop a device that is able to simultaneously record electrical and mechanical signals of the heart tissue during open heart surgery, thus allowing to gain a better understanding of the underlying causes in patients with Arrytmia. After carefully studying the literature, three concepts consisting of a device in which an electrode array and ultrasound transducers are integrated have been proposed based on the limitations of the environment and the conducted finite element simulations. One of the concepts was executed by designing, assembling, and evaluating a prototype. The key results of this work are listed below.

7.1. Key Results

Concept and Configuration Three concepts for the integration of an ultrasound transducer and electrode array presented in this work considered the limitations of the environment. One of the concepts was designed and the first prototype has been created. This concept consists of two devices, a flexible electrode array with 32 gold electrodes of which 12 have holes around them, and a device for the ultrasound transducers, which consist of 12 piezoelectric rings made out of 1-3 piezocomposite for optimal acoustic matching to the atrial tissue. The parameters of the transducer have been chosen to image the atrial tissue. The two devices are mounted on top of each other in a way that the electrodes can be in contact with the tissue and the ultrasound does not attenuate as there are holes in the polyimide of the electrode array. The intended usage is detailed in Figure 4.21.

Prototyping A prototype has been created for the chosen concept. Two flexible PCBs have been designed for this prototype, one for the ultrasound transducer allowing 12 piezoelectric rings with a diameter of 5 mm to be attached and another for the 36 electrodes of the electrode array. The prototypes have been assembled.

Measurements Impedance measurements have been conducted to evaluate the electrodes individually. The results imply that the presence of the holes does not have an impact on the fabricated electrode array. Measurements were conducted to analyze the pulse-echo response and the pressure field created by the transducer while the electrode array was mounted on it. The obtained pressure values are in the range of 30 - 40 kPa, which suggests that even with a 10 V amplitude excitation the transducers are able to produce enough pressure for sufficient pulse-echo response with the electrode array mounted on top. This suggests that the ultrasound transducer with the electrode array is suitable for the designed purpose. Based on the preliminary pulse-echo measurements results, it is suggested that the ultrasound transducer with the electrode array integrated into it is sufficient for obtaining a pulse-echo response from the field of interest.

7.2. Future work

For further evaluation, it is suggested to conduct more extensive pulse-echo measurements, for example with a thin wire as a target. Moreover, it would be favorable to investigate the performance of the electrode array with the ultrasound transducer with the TDT system with a phantom atrial tissue in order to evaluate how transmit and receive affect the electrograms. Furthermore, it would be beneficial to test this prototype on an ex vivo pig heart, demonstrating the intended usage (Figure 4.21). It would be benefitial to examine if the designed device is able to derive detailed information about the of the tissue apart from thickness of the atria, such as collagen content or fiber directions. To further improve this prototype, it is suggested to make certain alternations to the currently presented method as presented in 6. Future work should entail improving the axial resolution and the field of view of the two devices. The former can be achieved by using higher frequencies for the ultrasound transducers thus allowing for shorter pulses, which result in more details in the received data. It is suggested to investigate focused ultrasound transducers, for example by adding an acoustic lens to the presented device to further improve the imaging quality. Furthermore, it would be beneficial to explore the integration of an ultrasound array instead of a single element for future prototypes, as then more information could be obtained from the mechanical structure of the atrial tissue due to the option of B-mode imaging and broader field of view. Lastly, it is suggested to increase the number of electrodes as much as the ultrasound transducer allows in order to obtain more detailed information about the electrical activity.

References

[1] Bahareh Abdi. “Atrial fibrillation fingerprinting”. PhD thesis. Delft University of Technology, 2021.

[2] Ziti Fariha Mohd Apandi, Ryojun Ikeura, and Soichiro Hayakawa. “Arrhythmia Detection Using MIT-BIH Dataset: A Review”. In: *2018 International Conference on Computational Approach in Smart Systems Design and Applications (ICASSDA)*. 2018 International Conference on Computational Approach in Smart Systems Design and Applications (ICASSDA). 2018, pp. 1–5. DOI: 10.1109/ICASSDA.2018.8477620.

[3] Jurgen Oude Booijink. *Innovations of the High Resolution Epicardial Mapping System*. 2014.

[4] A. Botter et al. “A Novel System of Electrodes Transparent to Ultrasound for Simultaneous Detection of Myoelectric Activity and B-mode Ultrasound Images of Skeletal Muscles Innovative Methodology”. In: URL: https://www.semanticscholar.org/paper/A-Novel-System-of-Electrodes-Transparent-to-for-of-Botter-Vieira/ea60393f4b40f49ee595e8cd7a988cd4f3b9f4e5 (visited on 08/14/2024).

[5] Adomas Bunevicius, Nathan Judson McDannold, and Alexandra J Golby. “Focused Ultrasound Strategies for Brain Tumor Therapy”. In: *Operative Neurosurgery* 19.1 (July 2020), pp. 9–18. ISSN: 2332-4252. DOI: 10.1093/ons/opz374. URL: https://www.ncbi.nlm.nih.gov/pmc/articles/PMC7293897/ (visited on 06/27/2023).

[6] H.L.W. Chan and J. Unsworth. “Properties of 1-3 PZT/Epoxy Composites for Ultrasonic Transducer Applications”. In: *Sixth IEEE International Symposium on Applications of Ferroelectrics* (1986). Conference Name: Sixth IEEE International Symposium on Applications of Ferroelectrics Publisher: IEEE, pp. 277–280. DOI: 10.1109/ISAF.1986.201141. URL: http://ieeexplore.ieee.org/document/1538081/ (visited on 12/11/2023).

[7] S. Cochran. “1 - Piezoelectricity and basic configurations for piezoelectric ultrasonic transducers”. In: *Ultrasonic Transducers*. Ed. by K. Nakamura. Woodhead Publishing Series in Electronic and Optical Materials. Woodhead Publishing, Jan. 1, 2012, pp. 3–35. ISBN: 978-1-84569-989-5. DOI: 10.1533/9780857096302.1.3. URL: https://www.sciencedirect.com/science/article/pii/B9781845699895500012 (visited on 10/06/2023).

[8] James L. Cox et al. “The surgical treatment of atrial fibrillation: II. Intraoperative electrophysiologic mapping and description of the electrophysiologic basis of atrial flutter and atrial fibrillation”. In: *The Journal of Thoracic and Cardiovascular Surgery* 101.3 (Mar. 1, 1991), pp. 406–426. ISSN: 0022-5223. DOI: 10.1016/S0022-5223(19)36723-6. URL: https://www.sciencedirect.com/science/article/pii/S0022522319367236 (visited on 05/11/2023).

[9] Vitantonio Di Bello et al. “Increased echodensity of myocardial wall in the diabetic heart: An ultrasound tissue characterization study”. In: *Journal of the American College of Cardiology* 25.6 (May 1, 1995), pp. 1408–1415. ISSN: 0735-1097. DOI: 10.1016/0735-1097(95)00026-Z. URL: https://www.sciencedirect.com/science/article/pii/073510979500026Z (visited on 06/27/2023).

[10] Danny Eytan et al. “Dopamine-Induced Dispersion of Correlations Between Action Potentials in Networks of Cortical Neurons”. In: *Journal of Neurophysiology* 92.3 (Sept. 2004). Publisher: American Physiological Society, pp. 1817–1824. ISSN: 0022-3077. DOI: 10.1152/jn.00202.2004. URL: https://journals.physiology.org/doi/full/10.1152/jn.00202.2004 (visited on 06/26/2023).

[11] J.O. Fiering et al. “High-density flexible interconnect for two-dimensional ultrasound arrays”. In: *IEEE Transactions on Ultrasonics, Ferroelectrics, and Frequency Control* 47.3 (2000). Conference Name: IEEE Transactions on Ultrasonics, Ferroelectrics, and Frequency Control, pp. 764–770. ISSN: 1525-8955. DOI: 10.1109/58.842067.

[12] Niharika Gogoi et al. “Dependence of Piezoelectric Discs Electrical Impedance on Mechanical Loading Condition”. In: *Sensors* 22.5 (Feb. 22, 2022), p. 1710. ISSN: 1424-8220. DOI: 10.3390/s22051710. URL: https://www.mdpi.com/1424-8220/22/5/1710 (visited on 08/08/2024).

[13] Philipp Görtz et al. “Multielectrode array analysis of cerebrospinal fluid in Alzheimer’s disease versus mild cognitive impairment: A potential diagnostic and treatment biomarker”. In: *Biochemical and Biophysical Research Communications* 434.2 (May 3, 2013), pp. 293–297. ISSN: 0006-291X. DOI: 10.1016/j.bbrc.2013.02.121. URL: https://www.sciencedirect.com/science/article/pii/S0006291X13004774 (visited on 06/26/2023).

[14] S.A. Goss and F.J. Fry. “Nonlinear Acoustic Behavior in Focused Ultrasonic Fields: Observations of Intensity Dependent Absorption in Biological Tissue”. In: *IEEE Transactions on Sonics and Ultrasonics* 28.1 (Jan. 1981), pp. 21–25. ISSN: 0018-9537. DOI: 10.1109/T-SU.1981.31213. URL: http://ieeexplore.ieee.org/document/1539289/ (visited on 08/16/2024).

[15] J. J. Green and J. C. Hobbins. “Abdominal ultrasound examination of the first-trimester fetus”. In: *American Journal of Obstetrics and Gynecology* 159.1 (July 1, 1988), pp. 165–175. ISSN: 0002-9378. DOI: 10.1016/0002-9378(88)90515-7. URL: https://www.sciencedirect.com/science/article/pii/0002937888905157 (visited on 06/27/2023).

[16] Zhile Han et al. “Phased-Array Transducer for Intracardiac Echocardiography Based on 1–3 Piezocomposite”. In: *Frontiers in Materials* 8 (2021). ISSN: 2296-8016. URL: https://www.frontiersin.org/articles/10.3389/fmats.2021.663926 (visited on 08/04/2023).

[17] Bence Hegyi et al. “Mechanoelectric coupling and arrhythmogenesis in cardiomyocytes contracting under mechanical afterload in a 3D viscoelastic hydrogel”. In: *Proceedings of the National Academy of Sciences* 118.31 (Aug. 3, 2021). Publisher: Proceedings of the National Academy of Sciences, e2108484118. DOI: 10.1073/pnas.2108484118. URL: https://www.pnas.org/doi/10.1073/pnas.2108484118 (visited on 01/14/2023).

[18] Hongjie Hu et al. “Stretchable ultrasonic transducer arrays for three-dimensional imaging on complex surfaces”. In: *Science Advances* 4.3 (Mar. 23, 2018). Publisher: American Association for the Advancement of Science, eaar3979. DOI: 10.1126/sciadv.aar3979. URL: https://www.science.org/doi/10.1126/sciadv.aar3979 (visited on 01/09/2024).

[19] Matthias Imboden et al. “High-speed mechano-active multielectrode array for investigating rapid stretch effects on cardiac tissue”. In: *Nature Communications* 10.1 (Feb. 19, 2019). Number: 1 Publisher: Nature Publishing Group, p. 834. ISSN: 2041-1723. DOI: 10.1038/s41467-019-08757-2. URL: https://www.nature.com/articles/s41467-019-08757-2 (visited on 11/28/2022).

[20] *ISO 11135:2014*. URL: https://www.iso.org/standard/56137.html (visited on 10/02/2023).

[21] Radovan Jiˇrık, Torfinn Taxt, and Jiˇrı Jan. “ULTRASOUND ATTENUATION IMAGING”. In: 55.7 (2004).

[22] Peter Kohl, Frederick Sachs, and Michael R. Franz. *Cardiac Mechano-Electric Coupling and Arrhythmias*. Google-Books-ID: CBV4Jq6YWgsC. OUP Oxford, Aug. 25, 2011. 508 pp. ISBN: 978-0-19-163623-3.

[23] Sophie Kussauer, Robert David, and Heiko Lemcke. “hiPSCs Derived Cardiac Cells for Drug and Toxicity Screening and Disease Modeling: What Micro- Electrode-Array Analyses Can Tell Us”. In: *Cells* 8.11 (Nov. 2019). Number: 11 Publisher: Multidisciplinary Digital Publishing Institute, p. 1331. ISSN: 2073-4409. DOI: 10.3390/cells8111331. URL: https://www.mdpi.com/2073-4409/8/11/1331 (visited on 06/26/2023).

[24] Thanh Giang La et al. “Investigating Transducer–Tissue Interface Pressure for Soft Tissue Stress–Strain Behavior and the Effects on Echoic Intensities in Ultrasound Imaging of Periodontium”. In: *Advanced Materials Technologies* 9.8 (Apr. 2024), p. 2301732. ISSN: 2365-709X, 2365-709X. DOI: 10.1002/admt.202301732. URL: https://onlinelibrary.wiley.com/doi/10.1002/admt.202301732 (visited on 08/08/2024).

[25] Alexandros Ch. Lazanas and Mamas I. Prodromidis. “Electrochemical Impedance Spectroscopy—A Tutorial”. In: *ACS Measurement Science Au* 3.3 (June 21, 2023). Publisher: American Chemical Society, pp. 162–193. DOI: 10.1021/acsmeasuresciau.2c00070. URL: https://doi.org/10.1021/acsmeasuresciau.2c00070 (visited on 06/27/2024).

[26] Wonryung Lee and Takao Someya. “Emerging Trends in Flexible Active Multielectrode Arrays”. In: *Chemistry of Materials* 31.17 (Sept. 10, 2019). Publisher: American Chemical Society, pp. 6347–6358. ISSN: 0897-4756. DOI: 10.1021/acs.chemmater.9b00165. URL: https://doi.org/10.1021/acs.chemmater.9b00165 (visited on 05/23/2023).

[27] Wonryung Lee et al. “Nonthrombogenic, stretchable, active multielectrode array for electroanatomical mapping”. In: *Science Advances* 4.10 (Oct. 19, 2018). Publisher: American Association for the Advancement of Science, eaau2426. DOI: 10.1126/sciadv.aau2426. URL: https://www.science.org/doi/full/10.1126/sciadv.aau2426 (visited on 05/23/2023).

[28] Thomas Lekscha. *Ultrasound for medical therapy devices*. Sept. 23, 2010. ISBN: 978-3-640-74475-6 978-3-640-74520-3. URL: https://www.grin.com/document/158611 (visited on 01/18/2023).

[29] Yi-Chen Ethan Li and I.-Chi Lee. “The Current Trends of Biosensors in Tissue Engineering”. In: *Biosensors* 10.8 (Aug. 2020). Number: 8 Publisher: Multidisciplinary Digital Publishing Institute, p. 88. ISSN: 2079-6374. DOI: 10.3390/bios10080088. URL: https://www.mdpi.com/2079-6374/10/8/88 (visited on 06/26/2023).

[30] Jiapu Li et al. “Recent Advancements in Ultrasound Transducer: From Material Strategies to Biomedical Applications”. In: *BME Frontiers* 2022 (May 12, 2022). Publisher: Science Partner Journal. DOI: 10.34133/2022/9764501. URL: https://spj.sciencemag.org/journals/bmef/2022/9764501/ (visited on 11/28/2022).

[31] Zhangjian Li et al. “Parylene coating for 13 MHz 1-3 composite transducer performance enhancement”. In: *Applied Acoustics* 174 (Mar. 2021), p. 107696. ISSN: 0003682X. DOI: 10.1016/j.apacoust.2020.107696. URL: https://linkinghub.elsevier.com/retrieve/pii/S0003682X20308008 (visited on 08/08/2024).

[32] E. D. Light et al. “Real-time three-dimensional intracardiac echocardiography”. In: *Ultrasound in Medicine & Biology* 27.9 (Sept. 2001), pp. 1177–1183. ISSN: 0301-5629. DOI: 10.1016/s0301-5629(01)00421-5.

[33] E.D. Light et al. “Two dimensional arrays for real time volumetric and intracardiac imaging with simultaneous electrocardiogram”. In: *2000 IEEE Ultrasonics Symposium. Proceedings. An International Symposium (Cat. No.00CH37121)*. 2000 IEEE Ultrasonics Symposium. Proceedings. An International Symposium (Cat. No.00CH37121). Vol. 2. ISSN: 1051-0117. 2000, 1195–1198 vol.2. DOI: 10.1109/ULTSYM.2000.921537. URL: https://ieeexplore.ieee.org/abstract/document/921537 (visited on 01/16/2024).

[34] Jia Liu et al. “Intrinsically stretchable electrode array enabled in vivo electrophysiological mapping of atrial fibrillation at cellular resolution”. In: *Proceedings of the National Academy of Sciences* 117.26 (June 30, 2020). Publisher: Proceedings of the National Academy of Sciences, pp. 14769–14778. DOI: 10.1073/pnas.2000207117. URL: https://www.pnas.org/doi/full/10.1073/pnas.2000207117 (visited on 11/28/2022).

[35] Rafik Mebarki, Alexandre Krupa, and François Chaumette. “2-D Ultrasound Probe Complete Guidance by Visual Servoing Using Image Moments”. In: *IEEE Transactions on Robotics* 26.2 (Apr. 2010). Conference Name: IEEE Transactions on Robotics, pp. 296–306. ISSN: 1941-0468. DOI: 10.1109/TRO.2010.2042533.

[36] *METC Erasmus MC - Erasmus MC*. URL: https://www.erasmusmc.nl/nl-nl/pages/metc (visited on 09/28/2023).

[37] Beatrice Miccoli et al. “High-Density Electrical Recording and Impedance Imaging With a Multi-Modal CMOS Multi-Electrode Array Chip”. In: *Frontiers in Neuroscience* 13 (2019). ISSN: 1662-453X. URL: https://www.frontiersin.org/articles/10.3389/fnins.2019.00641 (visited on 06/26/2023).

[38] T. Misaridis and J.A. Jensen. “Use of modulated excitation signals in medical ultrasound. Part II: design and performance for medical imaging applications”. In: *IEEE Transactions on Ultrasonics, Ferroelectrics and Frequency Control* 52.2 (Feb. 2005), pp. 192–207. ISSN: 0885-3010. DOI: 10.1109/TUFFC.2005.1406546. URL: http://ieeexplore.ieee.org/document/1406546/ (visited on 02/12/2024).

[39] Alexandru Corneliu Moldovan. “Development of a 1D phased ultrasonic array for intravascular sonoporation”. In: (2020).

[40] Cecília Molnár. *Preliminary Pulse-Echo Measurement Results*. URL: https://youtu.be/xv7srsQfkA8.

[41] Cecília Molnár. *Visualization of atrial tissue during atrial mapping*. Internship report. Oct. 27, 2023.

[42] Valéria Nascimento et al. “Influence of backing and matching layers in ultrasound transducer performance”. In: 5035 (May 23, 2003). DOI: 10.1117/12.479924.

[43] Paul L. M. J. van Neer et al. “Flexible large-area ultrasound arrays for medical applications made using embossed polymer structures”. In: *Nature Communications* 15.1 (Mar. 30, 2024). Publisher: Nature Publishing Group, p. 2802. ISSN: 2041-1723. DOI: 10.1038/s41467-024-47074-1. URL: https://www.nature.com/articles/s41467-024-47074-1 (visited on 06/28/2024).

[44] *NEN-EN-IEC 60601-1:2006 en*. URL: https://www.nen.nl/nen-en-iec-60601-1-2006-en-113508 (visited on 10/02/2023).

[45] Manuel Ochoa et al. “A hybrid PDMS-Parylene subdural multi-electrode array”. In: *Biomedical Microdevices* 15.3 (June 1, 2013), pp. 437–443. ISSN: 1572-8781. DOI: 10.1007/s10544-013-9743-2. URL: https://doi.org/10.1007/s10544-013-9743-2 (visited on 06/26/2023).

[46] Pierpaolo Pellicori et al. “Ultrasound imaging of congestion in heart failure: examinations beyond the heart”. In: *European Journal of Heart Failure* 23.5 (2021). _eprint: https://onlinelibrary.wiley.com/doi/pdf/10.1002 pp. 703–712. ISSN: 1879-0844. DOI: 10.1002/ejhf.2032. URL: https://onlinelibrary.wiley.com/doi/abs/10.1002/ejhf.2032 (visited on 06/27/2023).

[47] Chang Peng et al. “Recent Advances in Transducers for Intravascular Ultrasound (IVUS) Imaging”. In: *Sensors (Basel, Switzerland)* 21.10 (May 19, 2021), p. 3540. ISSN: 1424-8220. DOI: 10.3390/s21103540. URL: https://www.ncbi.nlm.nih.gov/pmc/articles/PMC8160965/ (visited on 08/29/2023).

[48] P. J. Porte. *Simultaneous recordings of epicardial mappings and ultrasound imgaes of the atria*. 2014.

[49] D.J. Powell and G. Hayward. “Flexible ultrasonic transducer arrays for nondestructive evaluation applications. I. The theoretical modeling approach”. In: *IEEE Transactions on Ultrasonics, Ferroelectrics, and Frequency Control* 43.3 (1996). Conference Name: IEEE Transactions on Ultrasonics, Ferroelectrics, and Frequency Control, pp. 385–392. ISSN: 1525-8955. DOI: 10.1109/58.489395.

[50] D.J. Powell and G. Hayward. “Flexible ultrasonic transducer arrays for nondestructive evaluation applications. II. Performance assessment of different array configurations”. In: *IEEE Transactions on Ultrasonics, Ferroelectrics, and Frequency Control* 43.3 (1996). Conference Name: IEEE Transactions on Ultrasonics, Ferroelectrics, and Frequency Control, pp. 393–402. ISSN: 1525-8955. DOI: 10.1109/58.489396.

[51] S. Rhee et al. “Materials for acoustic matching in ultrasound transducers”. In: *2001 IEEE Ultrasonics Symposium. Proceedings. An International Symposium (Cat. No.01CH37263)*. 2001 IEEE Ultrasonics Symposium. Proceedings. An International Symposium (Cat. No.01CH37263). Vol. 2. Oct. 2001, 1051–1055 vol.2. DOI: 10.1109/ULTSYM.2001.991900.

[52] R. Segev and I. I. Berry. “MJ (2003). Recording from all of the ganglion cells in the retina”. In: *Soc Neurosci Abstr*. Vol. 264. Issue: 11.

[53] Erkin Seker et al. “The fabrication of low-impedance nanoporous gold multiple-electrode arrays for neural electrophysiology studies”. In: *Nanotechnology* 21.12 (Mar. 26, 2010), p. 125504. ISSN: 0957-4484, 1361-6528. DOI: 10.1088/0957-4484/21/12/125504. URL: https://iopscience.iop.org/article/10.1088/0957-4484/21/12/125504 (visited on 08/08/2024).

[54] Chris Sekirnjak et al. “Electrical Stimulation of Mammalian Retinal Ganglion Cells With Multielectrode Arrays”. In: *Journal of Neurophysiology* 95.6 (June 2006). Publisher: American Physiological Society, pp. 3311–3327. ISSN: 0022-3077. DOI: 10.1152/jn.01168.2005. URL: https://journals.physiology.org/doi/full/10.1152/jn.01168.2005 (visited on 06/26/2023).

[55] Charles A. Sennoga. “Chapter 2.2 - Ultrasound imaging”. In: *Bioengineering Innovative Solutions for Cancer*. Ed. by Sylvain Ladame and Jason Y. H. Chang. Academic Press, Jan. 1, 2020, pp. 123–161. ISBN: 978-0-12-813886-1. DOI: 10.1016/B978-0-12-813886-1.00007-3. URL: https://www.sciencedirect.com/science/article/pii/B9780128138861000073 (visited on 08/15/2024).

[56] Ronald H. Silverman. “Focused ultrasound in ophthalmology”. In: *Clinical Ophthalmology (Auckland, N.Z.)* 10 (2016), pp. 1865–1875. ISSN: 1177-5467. DOI: 10.2147/OPTH.S99535.

[57] R. S. Singh et al. “Conformal Ultrasound Imaging System”. In: *Acoustical Imaging*. Ed. by Michael P. André, Joie P. Jones, and Hua Lee. Acoustical Imaging. Dordrecht: Springer Netherlands, 2011, pp. 211–222. ISBN: 978-90-481-3255-3. DOI: 10.1007/978-90-481-3255-3_25.

[58] Rahul S. Singh et al. “Development of an ultrasound imaging system for needle guidance”. In: *2009 IEEE International Ultrasonics Symposium*. 2009 IEEE International Ultrasonics Symposium. ISSN: 1948-5727. Sept. 2009, pp. 1852–1855. DOI: 10.1109/ULTSYM.2009.5441829.

[59] Micha E. Spira and Aviad Hai. “Multi-electrode array technologies for neuroscience and cardiology”. In: *Nature Nanotechnology* 8.2 (Feb. 2013). Number: 2 Publisher: Nature Publishing Group, pp. 83–94. ISSN: 1748-3395. DOI: 10.1038/nnano.2012.265. URL: https://www.nature.com/articles/nnano.2012.265 (visited on 06/26/2023).

[60] Alfred Stett et al. “Biological application of microelectrode arrays in drug discovery and basic research”. In: *Analytical and Bioanalytical Chemistry* 377.3 (Oct. 1, 2003), pp. 486–495. ISSN: 1618-2650. DOI: 10.1007/s00216-003-2149-x. URL: https://doi.org/10.1007/s00216-003-2149-x (visited on 06/26/2023).

[61] K. A. Streeter et al. “Coupling multielectrode array recordings with silver labeling of recording sites to study cervical spinal network connectivity”. In: *Journal of Neurophysiology* 117.3 (Mar. 2017). Publisher: American Physiological Society, pp. 1014–1029. ISSN: 0022-3077. DOI: 10.1152/jn.00638.2016. URL: https://journals.physiology.org/doi/full/10.1152/jn.00638.2016 (visited on 06/26/2023).

[62] Jin Ho Sung and Jong Seob Jeong. “Development of High-Frequency (>60 MHz) Intravascular Ultrasound (IVUS) Transducer by Using Asymmetric Electrodes for Improved Beam Profile”. In: *Sensors (Basel, Switzerland)* 18.12 (Dec. 13, 2018), p. 4414. ISSN: 1424-8220. DOI: 10.3390/s18124414. URL: https://www.ncbi.nlm.nih.gov/pmc/articles/PMC6308511/ (visited on 04/12/2023).

[63] Makoto Taketani and M. Baudry, eds. *Advances in network electrophysiology: using multi-electrode arrays*. New York, NY: Springer, 2006. 478 pp. ISBN: 978-0-387-25857-7.

[64] Chonghe Wang et al. “Monitoring of the central blood pressure waveform via a conformal ultrasonic device”. In: *Nature Biomedical Engineering* 2.9 (Sept. 2018). Number: 9 Publisher: Nature Publishing Group, pp. 687–695. ISSN: 2157-846X. DOI: 10.1038/s41551-018-0287-x. URL: https://www.nature.com/articles/s41551-018-0287-x (visited on 01/09/2024).

[65] Fengle Wang et al. “Flexible Doppler ultrasound device for the monitoring of blood flow velocity”. In: *Science Advances* 7.44 (Oct. 27, 2021). Publisher: American Association for the Advancement of Science, eabi9283. DOI: 10.1126/sciadv.abi9283. URL: https://www.science.org/doi/10.1126/sciadv.abi9283 (visited on 01/09/2024).

[66] Zhe Wang et al. “A flexible ultrasound transducer array with micro-machined bulk PZT”. In: *Sensors* 15.2 (2015). Publisher: Multidisciplinary Digital Publishing Institute, pp. 2538–2547.

[67] Ameeta Yaksh et al. “A novel intra-operative, high-resolution atrial mapping approach”. In: *Journal of Interventional Cardiac Electrophysiology* 44.3 (2015). Publisher: Springer, pp. 221–225.

[68] Xuefeng Zhuang et al. “Flexible transducer arrays with through-wafer electrical interconnects based on trench refilling with PDMS”. In: *2007 IEEE 20th International Conference on Micro Electro Mechanical Systems (MEMS)*. 2007 IEEE 20th International Conference on Micro Electro Mechanical Systems (MEMS). ISSN: 1084-6999. 2007, pp. 73–76. DOI: 10.1109/MEMSYS.2007.4433016.